



PAPER



Cite this: *J. Anal. At. Spectrom.*, 2020, 35, 993

Atomic fluorescence spectrometry for ultrasensitive determination of bismuth based on hydride generation – the role of excitation source, interference filter and flame atomizers†

Barbora Štádlarová,¹  ^{ab} Marta Kolrosová,²  ^{ab} Jiří Dědina  ^a and Stanislav Musil  ^a

A method of highly sensitive bismuth determination by hydride generation coupled with in-house assembled non-dispersive atomic fluorescence spectrometry was developed. Bismuthane was generated by the reaction with NaBH₄ in HCl medium in a flow injection arrangement and directed by a stream of carrier gas and hydrogen to an atomizer. A detailed optimization of the optical path of the spectrometer (electrodeless discharge lamp, lenses and interference filter) and atomization parameters in two flame atomizers – miniature diffusion flame and flame-in-gas-shield atomizer – was performed. An excellent repeatability below 1% and extremely low limits of detection were achieved, namely 1.8 ng L⁻¹ with the miniature diffusion flame atomizer and 0.9 ng L⁻¹ with the flame-in-gas-shield atomizer and 307.1 nm interference filter. Interferences of other hydride forming elements were investigated. The developed ultrasensitive methodology was successfully verified by Bi determination in certified reference materials of (sea)water and of hair and blood after microwave assisted digestion.

Received 8th February 2020
Accepted 7th April 2020

DOI: 10.1039/d0ja00043d

rsc.li/jaas

1 Introduction

Bismuth is introduced into the atmosphere and oceans primarily from volcanoes and human activities, such as mining and smelting, and can be thus investigated as a useful tracer of anthropogenic activity and volcanic emissions in environmental samples.^{1,2} However, the concentration of Bi in environmental samples is usually at trace or ultratrace levels and therefore highly sensitive methods need to be employed for Bi determination. In addition to the most commonly used approach that lies in conventional solution nebulization and inductively coupled plasma mass spectrometry (ICPMS), hydride generation (HG) with atomic fluorescence spectrometry (AFS)³ can also offer the desired sensitivity for such analyses.

In AFS, the use of high intensity line radiation sources is required in order to achieve desired sensitivity and therefore the boosted-discharge hollow cathode lamps (BDHCLs)⁴ and the electrodeless discharge lamps (EDLs)⁵ became the radiation sources of choice. In the case of EDLs, bismuth⁶ or even iodine^{6,7} laboratory made sources, exciting Bi free atoms with a coinciding non-resonance line at 206.1 nm, were initially employed for Bi determination. Kobayashi *et al.*⁸ first reported

the determination of Bi by AFS coupled with HG which remarkably improved the limits of detection (LODs) by eliminating the scattered radiation caused by non-volatilized aerosol particles when direct solution nebulization was used. Nowadays, a HG unit is a common component of commercial AFS instruments.⁴ An argon–hydrogen flame supported on a conventional slot burner employing high flow rates, which caused dilution of the analyte and thus poor detection limits, was used by Kobayashi *et al.*⁸ in the early days. Ebdon *et al.*⁹ introduced a very simple design of the argon–hydrogen flame, a borosilicate glass tube with inverted “Y” side-arms to act as gas inlets employing relatively low gas flow rate, bringing forth the version as we know it today – the miniature diffusion flame (MDF). Although several new atomizers of hydrides for AFS have been developed since that time, such as dielectric barrier discharge,¹⁰ the MDF or its modified versions remain the most frequently used atomizers due to their simplicity, easy operation, robustness and efficiency of atomization.¹¹

The MDF is a standard hydride atomizer for AFS in commercial⁴ as well as laboratory made spectrometers. The design of MDF is very simple, it consists of a vertical support tube into which an argon–hydrogen mixture with the analyte hydride is introduced.¹² Hydrogen burns in the ambient atmosphere forming the diffusion flame at the top of this tube. Hydrogen radicals are formed in the outer zone of the flame by reactions between hydrogen and ambient oxygen and diffuse into the inner volume of the flame where the analyte hydride is fully atomized. The outer hot shell of the flame acts as an

^aInstitute of Analytical Chemistry of the Czech Academy of Sciences, Veveří 97, 602 00 Brno, Czech Republic. E-mail: stadlerova@iach.cz

^bCharles University, Department of Analytical Chemistry, Hlavova 8, 128 43 Prague, Czech Republic

† Electronic supplementary information (ESI) available. See DOI: 10.1039/d0ja00043d

efficient shield preventing the decay of H radicals and free atoms of the analyte in the inner volume of the flame by reactions with components from ambient atmosphere. The sensitivity of MDF is mainly controlled by the total flow rate of flame gases and the composition of the argon–hydrogen mixture.¹¹

A modified version of MDF was developed to be employed as the atomizer in AFS – a flame-in-gas-shield atomizer (FIGS).¹³ It involves the same vertical tube (with the inlet of Ar, H₂ and hydride) but there is also a centred capillary for oxygen delivery. Oxygen burns at the top of the capillary in an excess of hydrogen forming a highly fuel-rich oxygen–hydrogen microflame.¹³ In the microflame, an inhomogeneous cloud of H radicals is formed where the analyte hydride is fully atomized. High flow rates of shielding argon are employed to protect H radicals and free atoms of the analyte from a decay by reactions with atmospheric components and also to prevent an ignition of a diffusion flame at the top of the support tube.

The fundamental processes, *i.e.*, production of H radicals, protection of free atoms from ambient atmosphere and dilution of analyte in the observation volume of the flame, are all controlled by the composition and the flow rate of the argon–hydrogen mixture when MDF is employed. In FIGS, each of the three processes is controlled independently, which ought to be its most important asset. Since there is always an excess of hydrogen compared to oxygen, the production of H radicals, as well as the temperature, is controlled by the flow rate of oxygen; the flow rate of shielding argon controls the isolation of free atoms from molecular oxygen (present in ambient atmosphere) and the dilution of analyte is regulated by the total gas flow rate of flame gases.^{11,13,14}

The general aim of this work was to optimize a HG-AFS method to reach as low LOD as possible, which would enable Bi determination at ultratrace levels without any preconcentration step. A non-dispersive spectrometer developed at our laboratory¹⁵ employing commercially available electrodeless discharge lamps (EDLs) hitherto applied only to sensitive determination of arsenic¹⁶ and to As speciation studies,^{15,17,18} was adjusted. The main individual tasks lay in optimization and focusing of the EDL source, search for a suitable interference filter and optimization of the conditions of atomization in two flame atomizers, MDF and FIGS. The most promising configurations (interference filter and atomizer) were examined with respect to measured sensitivity, repeatability, resistance towards interferences from other hydride forming elements and accuracy of the results obtained with analysis of several available certified reference materials.

2 Experimental

2.1 Spectrometers

An in-house assembled non-dispersive atomic fluorescence spectrometer¹⁵ was used as a detector. This spectrometer of a simple design (see Fig. 1) consists of three main components – radiation source, atomizer and photomultiplier tube (PMT).

A Bi EDL (PerkinElmer, System 2) was used as a radiation source with feeding current square-wave modulated at frequency of 40 Hz and with 52% duty cycle (13 ms lamp on, 12 ms lamp off). The operating current for EDL was 400 mA, unless stated

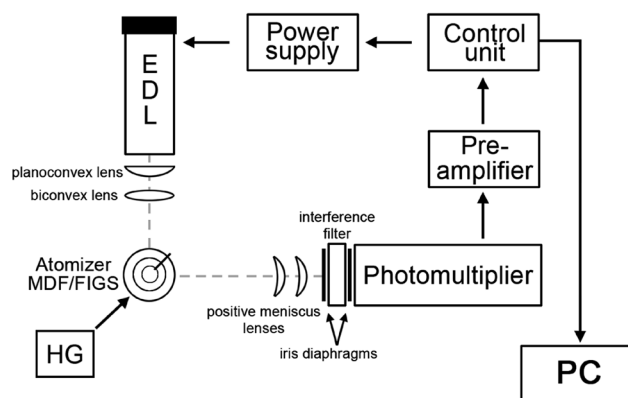


Fig. 1 Scheme of non-dispersive atomic fluorescence spectrometer.

otherwise. The radiation beam from the source was focused above the atomizer using two UV fused silica lenses. A planoconvex lens ($d = 25$ mm, 40 mm focal length) was inserted into the exit orifice of the cavity containing the EDL bulb and a doubleconvex lens ($d = 22$ mm, 45 mm focal length) was attached, in a lens holder, to the rim of the EDL. A PMT was placed perpendicularly to the EDL to collect the produced fluorescence radiation. A combination of two positive meniscus UV fused silica lenses ($d = 17$ and 22 mm; 21 mm focal length) was used to focus the produced radiation onto the interference filter, which was used for wavelength selection. Several broadband interference filters with various central wavelengths were tested, namely at 193.2 nm (full width at half maximum 20 nm and peak transmittance 17%, Melles Griot); 202.1 nm (10 nm and 15%, Melles Griot), 222.63 nm (10 nm and 18%, Melles Griot) and 307.1 nm (10 nm and 17%, Edmund Optics). These filters are denoted thereafter as 193, 202, 223 and 307 nm filters for simplicity. A solar-blind PMT (165–320 nm, MH 1922, PerkinElmer, Germany) supplied with negative voltage was used as detector.

The AFS instrument was placed inside a fume hood. The door was covered with a black curtain during all the measurements to avoid contribution of any parasitic radiation from the laboratory environment to the measured signal, especially when no or the 307 nm filter was used.

A miniature fibre optics UV-vis spectrometer, model BLACK-Comet C (StellarNet Inc., USA) equipped with a concave grating covering a range of 190–850 nm and armoured solarization resistant 1000 μ m fibre optic cable (F1000-UVVIS-SR-1), was employed to acquire the emission spectrum of the Bi EDL. Due to the insufficient resolution of this spectrometer, the individual emission lines were identified with the use of a high resolution atomic absorption spectrometer – ContraAA 300 (Analytik Jena, Germany) in emission mode. The Bi EDL was placed in the optical path of the spectrometer and each specific line was scanned. The individual lines were identified, if possible, directly by the operating software (ASpect CS 2.1.2.0) and then confirmed using the NIST Atomic spectra database.¹⁹

2.2 Standards, reagents and reference materials

Deionized water (DIW, Ultrapur, Watrex, USA) was used for the preparation of all solutions. A 0.5% (m/v) NaBH₄ (Sigma-

Aldrich, Germany) in 0.4% (m/v) KOH (Lach-Ner, Czech Republic) was used as a reductant. A stock solution of 1 mol L^{-1} HCl was prepared from 37% HCl (Merck, Germany) and used as a carrier and blank. Working Bi solutions were prepared by serial dilution of 1000 mg L^{-1} Bi standard for AAS (Sigma-Aldrich, Germany). A concentrated HNO_3 (65%, semiconductor grade, Honeywell, Germany) was used for the microwave assisted digestion of the samples.

Stock solutions of 1000 mg L^{-1} of elements for an interference study were sourced as follows: Pb^{II} and Hg^{II} from Analytika (Czech Republic), Sb^{III} from Fluka (Germany), Sn^{IV} and Se^{IV} from Sigma-Aldrich (Germany). Solution of 1000 mg L^{-1} of As^{III} was prepared by dissolving solid As_2O_3 (Fluka, Germany) in 2.5 mL 10% NaOH and filled to 25 mL by deaerated DIW. As certain trace content of Bi (contamination) in all standard solutions of the aforementioned elements (possible interferences) was found, it was quantified by ICP(MS)/MS (Agilent 8900). The quantified Bi contamination in the corresponding interferent solutions of Pb, Sb, Se, Sn, As and Hg was used to correct the results of the interference study and so the change in the response (AFS) was only caused by the presence of the interferent.

Certified reference materials (CRMs) 1643f Trace Elements in Water (National Institute of Standards and Technology, USA), Seronorm 1406264 Trace Elements Whole Blood L-2 (Sero, Norway) and Human hair GBW07601a (CRM from China, supplied by Swan Leaf, Australia) were used for validation of the developed methodology. Furthermore, Bi content was determined in NASS-7 and CASS-6 (National Research Council, Canada), the certified reference materials of sea water.

2.3 Sample preparation

NIST 1643f CRM was diluted 80-fold with 1 mol L^{-1} HCl while NASS-7 and CASS-6 were only spiked with concentrated HCl to obtain 1 mol L^{-1} . These samples were subjected to determination by HG-AFS.

Approximately 0.95 mL of Seronorm 1406264 Whole Blood L-2 and 0.15 g of GBW07601a were digested in 2 mL of concentrated HNO_3 using UltraWAVE system (Milestone, Italy) and 15 mL quartz digestion vials. Each sample and blank were

prepared in triplicates. The digestion was performed employing a two-step programme: 20 min ramp heating up to $240 \text{ }^\circ\text{C}$, 20 min hold at $240 \text{ }^\circ\text{C}$, the initial pressure 40 bar. The digests were then diluted with HCl approximately 200-fold and 30-fold for hair and blood samples, respectively, before the analysis with HG-AFS.

2.4 Hydride generator

A similar flow injection hydride generator operated under the same conditions as described previously²⁰ was employed with only minor modifications (see Fig. 2). The chemifold was constructed exclusively using PTFE (1 mm i.d.) and Tygon tubing. The solutions of the reductant (1.2 mL min^{-1}) and the carrier (4 mL min^{-1}) were pumped continuously by a peristaltic pump (PP1 in Fig. 2). The sample (1 mL) was manually injected by means of an injection valve into the flow of the carrier and subsequently merged with the reductant. A glass gas-liquid separator (GLS, volume of 5 mL) with a forced waste removal by a second peristaltic pump (PP2) was employed for separation of the gas phase containing bismuthane. A 5 cm long PEEK capillary (0.25 mm i.d.) was used to introduce 80 mL min^{-1} argon ($\text{Ar}_{\text{carrier}}$) upstream the GLS in order to reduce fluctuations of argon flow caused by hydrogen forming in the reaction coil (11 cm). The flow rate of hydrogen ($\text{H}_2_{\text{generator}}$) evolving from the reaction was approximately 15 mL min^{-1} , which was measured under given conditions of HG. The gas phase leaving the GLS was supplied with an additional flow of argon (Ar_{flame}) and hydrogen ($\text{H}_2_{\text{flame}}$) to maintain a stable flame of the atomizers.

2.5 Atomizers

Fig. 3 shows the atomizers used. MDF was actually a vertical quartz support tube (6 mm i.d.) with a side inlet arm (2 mm i.d.) through which argon, hydrogen and bismuthane were introduced. The observation height (OH) was defined as the distance from the top of the support tube to the centre of the optical beam. Regarding FIGS, there was also a capillary (i.d. 0.53 mm) in the axis of the support tube protruding 3 mm above the rim of the support tube, serving to introduce oxygen at the flow rate

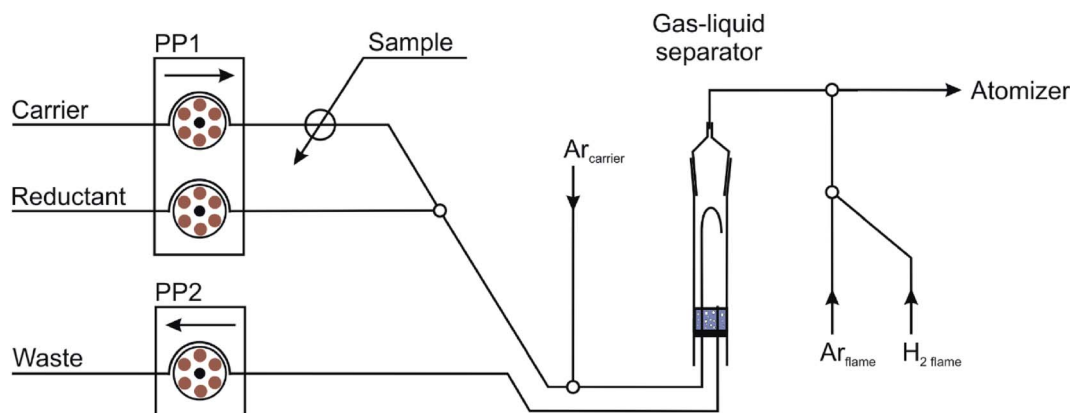


Fig. 2 Experimental setup of the hydride generator; PP1,2 – peristaltic pumps.

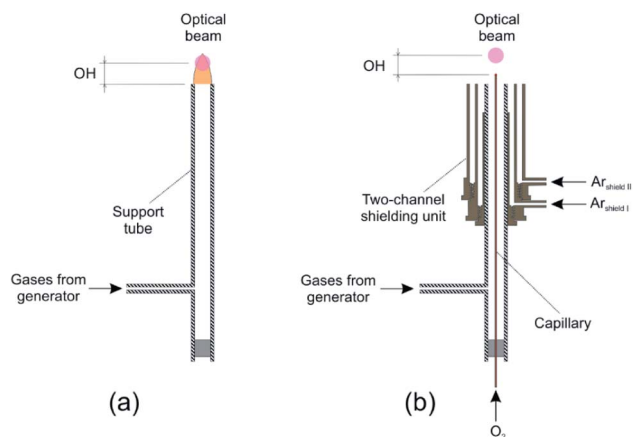


Fig. 3 MDF (a) and FIGS (b) atomizers; OH – observation height.

of 7 mL min^{-1} , unless otherwise stated. The microflame, resulting from the reaction of oxygen with an excess of hydrogen, was formed right above the capillary top. A two-channel brass shielding unit¹⁵ was fitted around the support tube and served to introduce the shielding (laminar) flows of argon (inner $\text{Ar}_{\text{shield I}}$ and outer $\text{Ar}_{\text{shield II}}$). In the case of FIGS, OH was defined as the distance from the top of the capillary to the centre of the optical beam.

For a simplified description of the different gas supplies to the atomizers, the following conventions were established. Total flow rate of hydrogen comprises of the hydrogen flow rate evolved from the generator ($\text{H}_2_{\text{generator}}$) and of hydrogen flow rate introduced downstream the GLS ($\text{H}_2_{\text{flame}}$). Total flow rate of argon comprises of a flow rate of argon introduced upstream the GLS ($\text{Ar}_{\text{carrier}}$) and of argon introduced downstream the GLS (Ar_{flame}). Ultimately, the total gas flow rate comprises of $\text{Ar}_{\text{carrier}}$, Ar_{flame} , $\text{H}_2_{\text{generator}}$ and $\text{H}_2_{\text{flame}}$. The hydrogen fraction is then the relation of the total flow rate of hydrogen to the total gas flow rate.

2.6 Measurement procedure and treatment of recorded signals

With HG in operation (both peristaltic pumps running), the sample was manually injected into the carrier 5 s after the recording of the signal had started. The recording time was always set to 60 s, which was sufficient for the flow injection signal to decline back to the baseline.

The recorded signals from the PMT were treated the same way as described previously.^{15,16} In principle, the analyte fluorescence, the flame emission, the scattered radiation, the parasitic radiation and the PMT dark current all contribute to the detector response. The value of the dark current is very low for the type of the PMT employed²¹ and is thus negligible compared to other contributing factors mentioned. Owing to the isolation of the AFS instrument from the laboratory environment, the contribution of the parasitic radiation was also negligible in all relevant experiments as proven by a measurement with the lamp off in absence of the flame. As the lamp feeding current was modulated (40 Hz), the detector response

could be registered in two channels – one (channel 0) registered the response when the lamp was on (the analyte fluorescence, the flame emission and scattered radiation were detected) and the other (channel 1) when the lamp was off (only the flame emission was detected). Essentially, the resulting signal was corrected to the flame emission. The detector response from channel 1 was subtracted from the response from channel 0, hence the resulting signal (given in μV) reflects only the analyte fluorescence and the scattered radiation. The baseline of the resulting signal then reflected, besides the fluorescence of an analyte contamination of used reagents, the scattered radiation. The useful analytical parameters were peak area (in $\mu\text{V s}$) and peak height (in μV). Both peak area and peak height were always evaluated and corrected to the baseline using a program written in MS Excel.

2.7 Data evaluation

The peak area and a signal to noise ratio (SNR) were the parameters used to evaluate the data. SNR was determined by dividing the peak height of $1 \mu\text{g L}^{-1}$ Bi standard by the uncertainty of the baseline. The baseline uncertainty was estimated as an average ($n = 3$) of the standard deviations (SDs) of the baseline which was calculated from 400 values recorded in 10 s.

All the given peak areas are presented as median ($n \geq 3$) \pm SD. In the figures, SDs are so little in most cases that they are indiscernible from the data points. Combined SDs are used when the results are related to a reference measurement. If sensitivity is mentioned, it refers to the peak area related to the analyte concentration. Limit of detection (LOD) was calculated as $3 \times \text{SD}$ of peak area of blank ($n = 10$) divided by the slope of the calibration function.

3 Results and discussion

3.1 AFS instrument

Commercially available AFS instruments typically employ boosted-discharge hollow cathode lamps as the radiation source. For in-house assembled instruments, the use of commercially available EDLs showed to be much more suitable owing to a higher radiation intensity and the resultant lower LODs.^{15,16} Bismuth emission lines present in the spectrum of the employed EDL (Fig. S1 in ESI†) correspond to the intensive Bi fluorescence lines reported²² – namely to 206.16, 222.82, 223.06, 302.46 and 306.77 nm.

Great emphasis was put on the selection of a suitable interference filter. The 193, 202, 223 and 307 nm interference filters (see Section 2.1) were employed to cover the intensive Bi fluorescence lines. See Fig. S1 (in ESI†) for a schematic representation of transmission bandwidth of 202, 223 and 307 nm filters. In general, the character of the transmittance profile of a filter controls both the sensitivity and the baseline noise. The sensitivity observed when using a filter depends on the overlap of the filter transmittance profile with the absorption profile of the electron transition corresponding to an excitation of a fluorescence line. In addition, the intensity of different Bi fluorescence lines varies and the response of the PMT is not constant

Table 1 Sensitivity ($\text{mV s L } \mu\text{g}^{-1}$) obtained with various interference filters and atomizers^a

	193 nm filter	202 nm filter	223 nm filter	307 nm filter	No filter
MDF	0.014	0.011	0.13	0.17	2.3
FIGS	0.038	0.033	0.29	0.42	4.8

^a Experiment carried out under optimum conditions for both atomizers (Table 2).

through the whole spectral interval of 165–320 nm. The peak wavelength appears approximately at 200 nm and the response of the PMT rapidly decreases at both higher and lower wavelengths.²¹ The sensitivities acquired with individual filters are summarized in Table 1.

For both atomizers, the highest sensitivity was observed in the absence of any filter. However, such arrangement was not further considered since the determination would be then most susceptible to spectral interferences (see below). The other disadvantage of working in the absence of any filter is the imperative of achieving an efficient isolation of the spectrometer from the parasitic radiation from the laboratory environment. Naturally, using various interference filters resulted in lower sensitivity. Filters 307 nm and 223 nm provided approximately one order of magnitude higher sensitivity compared to 193 nm and 202 nm filters.

The sensitivity is a relevant parameter, however, the SNR is the most important. It is controlled by the sensitivity as well as by the baseline noise. The baseline noise depends on the overlap of the filter transmittance profile with the emission spectrum of the atomizer flame and even though the flame emission is compensated in the resulting signal (see Section 2.6), its noise contributes to the noise of the baseline. The OH radicals are responsible for the flame emission namely in the region 305–320 nm.^{23,24} In general, MDF produces a lot of OH radicals and that results in approximately 1.9 better SNR provided by the 223 nm filter in comparison with the 307 nm filter. In the case of FIGS, which produces much less OH radicals, SNRs of these two filters do not differ considerably. The 193 and 202 nm filters provide approximately six times lower SNR compared to the other two filters. In contrast, D'Ulivo *et al.*²⁴ observed that FIGS required the use of the 306.8 nm fluorescence line since all other Bi fluorescence lines were either undetectable or too weak.

The optical path of the AF spectrometer was optimized so as to achieve the highest sensitivity and SNR. The mutual distances of the three main components slightly affect the sensitivity. The distance from the lens on the rim of the EDL and of the PMT to the centre of the atomizer support tube was set to 13 and 12 mm, respectively, which provided the highest sensitivity and SNR. This setup resulted in the radius of a vertical cross-section of the radiation beam (circular) above the vertical axis of the atomizer of approximately 5 mm. The feeding current of the EDL was optimized and the sensitivity rose with increasing feeding current up to 425 mA, which was the maximum current tested. However, the highest SNR was

obtained at 400 mA, which is also the recommended value by the manufacturer for the modulated mode and this particular type of the radiation source.

3.2 Optimization of atomization conditions

The influence of the relevant atomization conditions, *i.e.*, hydrogen fraction, the total gas flow rate and OH, on the sensitivity and SNR was investigated for both atomizers. Unless otherwise stated, to facilitate the experiments, the 223 nm filter was selected to be used in all the optimization studies as it delivered sufficiently high SNR and sensitivity for both atomizers (see Table 1).

In general, decreasing hydrogen fraction in both atomizers positively influenced both the sensitivity and SNR (Fig. 4). It is important to note that this experiment was examined at constant total gas flow rate of 600 mL min^{-1} , hence the change in sensitivity is driven only by hydrogen fraction. A possible explanation for the decrease of sensitivity is the Lorentz broadening of the absorption line with increased hydrogen fraction.²⁵ A broader absorption line causes a less efficient excitation of free analyte atoms leading to a lower fluorescence signal. Additionally, increased temperature at higher hydrogen fractions inevitably reduces fluorescence signal because of the thermal expansion even though this can be partially offset by a decrease of Lorentz broadening with higher temperature.²⁵ Another mechanism responsible for the sensitivity drop with the increasing hydrogen fraction can be the quenching of the Bi free atoms excited state either by hydrogen or by formed water vapor. The minimum feasible hydrogen fraction in MDF and FIGS, respectively, was 14% and 9% since flames became unstable at lower hydrogen fractions and often went out. The influence of the total gas flow rate and OH in MDF and FIGS at constant hydrogen fractions of 17% and 13%, respectively, was established as illustrated in Fig. 5 and 6. Flow rates lower than

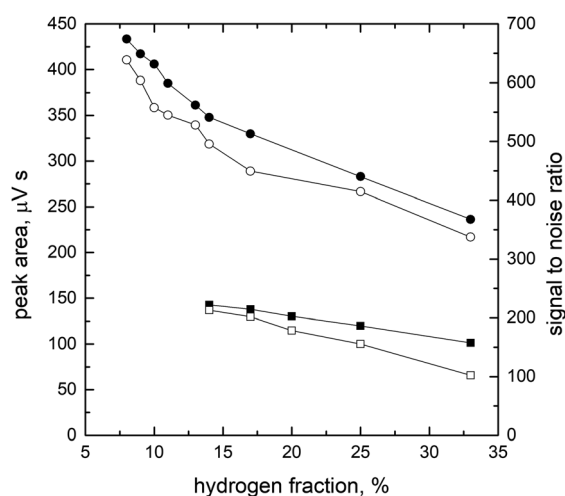


Fig. 4 Dependence of peak area (full) and SNR (empty) on hydrogen fraction in MDF (square) and FIGS (circle); both MDF and FIGS: $1 \mu\text{g L}^{-1}$ Bi, 600 mL min^{-1} total gas flow rate; MDF: OH = 7 mm; FIGS: OH = 6 mm, 7 mL min^{-1} oxygen flow rate, 1.5 ($A_{\text{rshield I}}$) and 2 L min^{-1} ($A_{\text{rshield II}}$) of shielding argon.

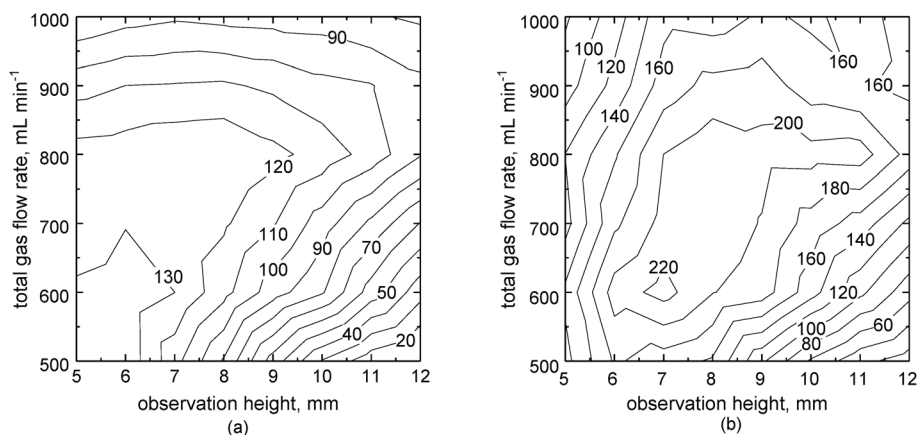


Fig. 5 Dependence of (a) peak area (in $\mu\text{V s}$) and (b) SNR on total gas flow rate and OH in MDF; $1 \mu\text{g L}^{-1}$ Bi, hydrogen fraction 17%. The OH points measured were in the range of 5–12 mm, by 1 mm steps. The total flow rate points measured were in the range of 500–1000 mL min^{-1} , by 100 mL min^{-1} .

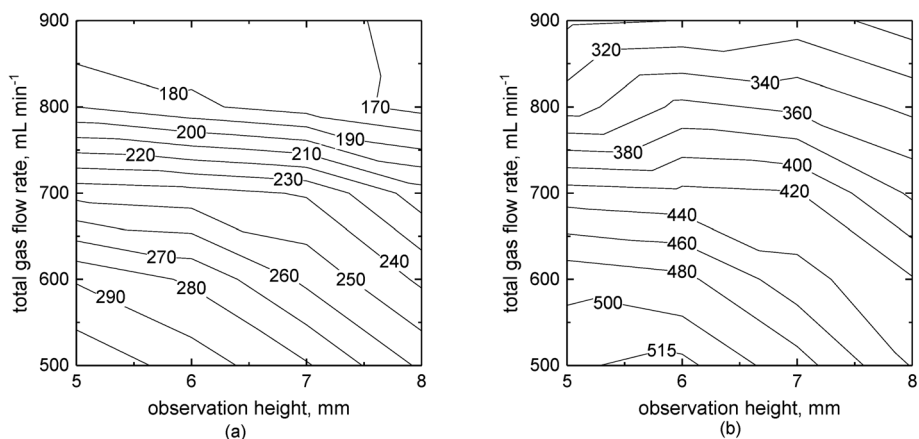


Fig. 6 Dependence of (a) peak area (in $\mu\text{V s}$) and (b) SNR on total gas flow rate and OH in FIGS; $1 \mu\text{g L}^{-1}$ Bi, hydrogen fraction 13%, 7 mL min^{-1} oxygen flow rate, $1.5 (\text{Ar}_{\text{shield I}})$ and $2 \text{ L min}^{-1} (\text{Ar}_{\text{shield II}})$ of shielding argon. The OH points measured were in the range of 5–8 mm, by 1 mm steps. The total flow rate points measured were in the range of 400–900 mL min^{-1} , by 100 mL min^{-1} .

500 mL min^{-1} could not be employed as flames were unstable under given conditions. The minimum OH of 5 mm could have been employed since at lower OHs the radiation from the EDL was prominently scattered on the top of the atomizer causing an unacceptable increase of the baseline.

In both MDF and FIGS, the sensitivity decreases with an increase of the total gas flow rate and OH from the feasible minimums (Fig. 5 and 6). The observed influence of the flow rate and OH can be interpreted in terms of the dilution of free atoms in the observation volume. The response of the SNR in both atomizers (Fig. 5 and 6) is similar except it is negatively influenced by an increase of the baseline of the resulting signal

and, correspondingly, an increase of the baseline uncertainty at OH below 7 mm and 6 mm, respectively, for MDF and FIGS. The chosen optimum values of the total gas flow rate and OH were 600 mL min^{-1} and 7 mm for MDF and 500 mL min^{-1} and 6 mm for FIGS (see Table 2).

Regarding FIGS, due to its more complex arrangement, also the oxygen flow rate and both shielding flows had to be optimized. The flow rate of 3 mL min^{-1} of oxygen is insufficient for an efficient atomization (Fig. 7). The maximum sensitivity and SNR are achieved for 5–7 mL min^{-1} of oxygen. The slight decline of sensitivity at higher oxygen flow rates may be associated with water vapor formation, which leads to fluorescence

Table 2 Optimum conditions of atomization in MDF and FIGS

	Total Ar (mL min^{-1})	Total H ₂ (mL min^{-1})	O ₂ (mL min^{-1})	Ar _{shield I} ; Ar _{shield II} (L min^{-1})	OH (mm)
MDF	500	100	—	—	7
FIGS	440	60	7	1.5; 1.5	6

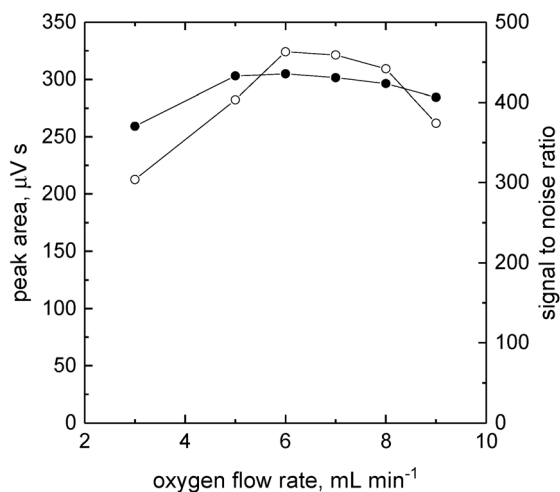


Fig. 7 Dependence of peak area (full circle) and SNR (empty circle) on oxygen flow rate in FIGS; $1 \mu\text{g L}^{-1}$ Bi, 500 mL min^{-1} total gas flow rate, hydrogen fraction 13%, $1.5 \text{ (Ar}_{\text{shield I}})$ and 2 L min^{-1} ($\text{Ar}_{\text{shield II}}$) of shielding argon, OH = 6 mm.

quenching. The same effect was previously described for the atomization of As in FIGS.¹⁶ Very similar influence of oxygen flow rate was also observed with the 307 nm filter, with maximum sensitivity and SNR achieved at 7 mL min^{-1} . This observation proves that OH bands emission in the range of applied oxygen flow rates ($4\text{--}10 \text{ mL min}^{-1}$) is not a serious problem. The value of 7 mL min^{-1} oxygen was selected for further experiments as optimum.

The last parameters to be optimized for FIGS were the two shielding argon flow rates (Fig. S2 in ESI†). The argon flow rate through the inner channel has a significantly larger impact on measured sensitivity than the outer flow rate. Using only the inner channel with argon flow rates $1, 1.5$ and 2 L min^{-1} high relative sensitivities (76%, 93% and 96%, respectively) can be reached in comparison with the optimum at 1.5 L min^{-1} through both inner ($\text{Ar}_{\text{shield I}}$) and outer ($\text{Ar}_{\text{shield II}}$) shielding argon. In contrast, when only the outer channel is utilized to introduce shielding argon the relative sensitivities are low (in the range 14–17%). In general, SNR depends on both shielding flow rates in a similar way as the sensitivity: the highest SNR was

achieved for 1.5 L min^{-1} of both inner ($\text{Ar}_{\text{shield I}}$) and outer ($\text{Ar}_{\text{shield II}}$) shielding argon flows, and therefore these were selected as the optimum values.

The chosen optimum conditions of atomization for both atomizers are summarized in Table 2.

3.3 Analytical characteristics

As discussed in Section 3.1, 223 nm and 307 nm filters are the most promising with regard to achieving low LODs. The analytical figures of merit of the proposed methodology with both these filters and for both atomizers were determined. The calibration functions constructed with 0, 0.04, 0.1, 0.25 and $1 \mu\text{g L}^{-1}$ Bi standards were linear ($R^2 > 0.9999$) for all four options. The values of achieved LODs ($3\sigma, n = 10$) do not exceed 2 ng L^{-1} for any configuration listed (Table 3). The lowest LOD of 0.9 ng L^{-1} as well as the highest sensitivity were obtained with the combination of FIGS atomizer and the 307 nm filter while LOD reached 1.4 ng L^{-1} using FIGS and 223 nm filter. LODs obtained with the MDF atomizer and both filters were the same: 1.8 ng L^{-1} . All the setups resulted in an outstanding repeatability $< 1\%$, expressed as the relative standard deviation ($n = 10$), at $1 \mu\text{g L}^{-1}$ Bi level.

The LODs in all examined setups (two filters and atomizers) were influenced substantially by the noise of the scattered radiation from the EDL source when the intensity of the scattered radiation was more than 9-fold higher than the flame emission. Hence, the LODs could be improved by a further reducing of the scattering.

3.4 Interference study

The effect of several hydride forming elements such as Sn, Pb, Sb, Se, As and Hg on accuracy of Bi determination was investigated employing FIGS operating under optimum conditions (Table 2). Concentrations of hydride forming elements varied from 1 to $100 \mu\text{g L}^{-1}$ while the concentration of Bi was $1 \mu\text{g L}^{-1}$ each time. Three interference filters (202, 223 and 307 nm) were chosen for the interference study to determine if the interference occurs at all detectable wavelengths of the fluorescence radiation, or more precisely at all Bi fluorescence lines, evenly. It appeared that there were no interferences whatsoever from Sn, Pb, Se and Hg in the tested concentration range for none of the

Table 3 The comparison of LODs using various methodologies

Method and atomizer	AFS instrumentation	LOD (ng L^{-1})	Reference
HG-AFS with MDF	Non-dispersive/self-designed	$1.8^a; 1.8^b$	This work
HG-AFS with FIGS	Non-dispersive/self-designed	$0.9^a; 1.4^b$	This work
HG-AFS with shielded MDF	Non-dispersive/self-designed/four channel	41	26
HG-AFS with MDF	Dispersive/self-designed	58	24
HG-AFS with FIGS	Dispersive/self-designed	10	24
HG-AFS with MDF	Non-dispersive/self-designed	$3\text{--}8^c$	27
HG-AFS with MDF	Non-dispersive/PSA 10.055 Millenium Excalibur	10	28 and 29
Nebulization ICP(MS)/MS	—	$0.2\text{--}0.5^d$	This work

^a 307 nm filter. ^b 223 nm filter. ^c Depending on the interference filter used. ^d Agilent 8900, depending on the gas mode in the reaction/collision cell (no gas or He).

three interference filters (see Table S1 in ESI† for details). In the case of As the sensitivity was depressed approximately by 30% at concentration of $100 \mu\text{g L}^{-1}$. Since this interference occurred at all three detection wavelengths, it is a non-spectral interference taking part during either HG or atomization.

Antimony had the most noticeable interfering effect which significantly varied with different interference filters. With the use of 202 and 223 nm filters the signal increased to 159% and 117%, respectively, even at $1 \mu\text{g L}^{-1}$ concentration of the interferent (1 : 1 analyte to interferent). At $100 \mu\text{g L}^{-1}$ of Sb (1 : 100 analyte to interferent) the signal reached up to 7400% and 2200%, respectively, related to the signal of $1 \mu\text{g L}^{-1}$ Bi without interferent. An explanation for that effect is that Bi EDL contains a certain amount of Sb and therefore Sb atoms can be excited with Bi EDL, as evidenced by the emission spectrum of the EDL in Fig. S1 (in ESI†). There are distinct Sb emission lines in the region of efficient transmittance of 202 and 223 nm filters. The strongest lines observed were namely at 206.83, 217.58, 228.90 and 231.15 nm. Since there is no intense Sb line present in the region 300–320 nm, no positive interference from Sb is evident with 307 nm filter at low concentration level. The signal slightly decreased with 307 nm filter at $100 \mu\text{g L}^{-1}$ Sb to 88%, which should be attributed to a non-spectral interference during HG or atomization analogously as described for As above. Although it bears no relation to Bi determination in our case, the Bi EDL seems to also contain mercury as Hg emission line was observed at 253.65 nm. It is important to note that the found impurities of Sb and Hg of similar amount were observed in three individual EDLs (System II).

3.5 Validation

To verify the accuracy and the practical feasibility, the proposed methodology was applied to Bi determination in several CRMs. The determination was performed under optimum conditions of atomization in FIGS atomizer (Table 2) and with the 307 nm filter. The Bi content was quantified using the external calibration curve and recovery values were calculated from the slopes obtained with the standard addition technique (two spiked concentrations of standard to one replicate of each sample) related to the slope of the external calibration. The results are shown in Table 4.

The water CRMs (NIST 1643f, CASS-6 and NASS-7) were subjected to a determination with HG-AFS. The result of Bi content in NIST 1643f after approximately 80-fold dilution with

1 mol L^{-1} HCl was in satisfactory agreement with the certified value. To demonstrate the necessity of using the 307 nm filter to obtain an accurate result, the same determination was performed with the 223 nm filter and both MDF and FIGS atomizers. The concentrations found were $14.0 \pm 0.2 \mu\text{g L}^{-1}$ and $13.8 \pm 0.2 \mu\text{g L}^{-1}$, respectively. These significantly higher values of Bi content most probably come from the noticeable positive interference from Sb ($55.45 \pm 0.40 \mu\text{g L}^{-1}$ certified), which has to be overcome by using the 307 nm filter as shown in Table S1 (in ESI†).

The practical feasibility of the developed ultrasensitive methodology was demonstrated on the analysis of sea water CRM NASS-7 and CASS-6. No certified or informative values are available as well as no data have been provided in the literature yet. The concentration of bismuth in sea water is generally very low and the values of approximately $10\text{--}20 \text{ ng L}^{-1}$ are typically considered,^{30–32} despite a huge dispersion of the published data.³³ Therefore, it is better not to dilute the sea water CRMs more than necessary. The determined concentration of 22 and 24 ng L^{-1} Bi are in accordance with the expected range.^{30–32} Furthermore, the spiked recovery in the range 89–100% for CASS-6 and NASS-7 proved that Bi determination at trace/ultratrace levels by HG-AFS could be accomplished even from a matrix as complex as sea water without the necessity of a significant dilution.

The HG-AFS method was also verified using Seronorm 1406264 Whole Blood L-2 and GBW07601a Human hair samples which required sample digestion with the use of nitric acid prior to determination. The effect of the remaining nitric acid on HG-AFS was investigated when it was mixed with a standard of $1 \mu\text{g L}^{-1}$ Bi in 1 mol L^{-1} HCl. No interference was found in the whole concentration range of $0.1\text{--}4 \text{ mol L}^{-1}$ nitric acid. The results of HG-AFS determination are in Table 4. There is an excellent agreement with the certified value for GBW07601a Human hair while the measured value for Seronorm 1406264 Whole Blood L-2 is on the upper edge of the recommended range.

3.6 Comparison of MDF and FIGS

The FIGS atomizer is more complex and the experimental work is undeniably more demanding. The considerable Ar consumption and the gas flow rate control requirements should be taken into account as well (see Table 2). However, the Ar consumption can be reduced by employing only the inner

Table 4 The determined content of Bi in certified reference materials presented as median value ($n = 3$) \pm SD and recoveries measured with HG-AFS, FIGS atomizer and 307 nm filter

CRM	Certified value ($\mu\text{g L}^{-1}$)	Value obtained ($\mu\text{g L}^{-1}$)	Recovery ^a (%)
NIST 1643f	12.62 ± 0.11	12.8 ± 0.1	102 ± 1
CASS-6	—	0.024 ± 0.003	89 ± 3
NASS-7	—	0.022 ± 0.001	100 ± 3
1406264 Seronorm Whole Blood L-2	5 ± 1.01	6.2 ± 0.2	105 ± 1
GBW07601a Human hair	21 ± 2	20.1 ± 0.6	99 ± 1

^a Spiked recovery = slope of standard additions (no addition and two spiked concentrations to a sample)/slope of external calibration.

shielding channel without a significant loss of sensitivity as shown above. A gradual increase of the sensitivity was observed for FIGS and it took approximately 90 minutes for the signal to stabilize. This obstacle can be overcome by igniting the flame with hydrogen and argon first and operating the atomizer in the MDF mode for 30 minutes. This lets the shielding unit of FIGS heat up and then oxygen and shielding argon can be introduced in order to switch to the FIGS mode.¹⁶ That applies to a measurement independent of the analyte. However, the amount of time necessary for the heating up of the atomizer is negligible compared to the warm-up time of the Bi EDL. In the case of bismuth, the EDL operated in the modulated mode needed at least 120 minutes so as to warm up properly.

The highest sensitivity is obtained with the FIGS atomizer and the 307 nm interference filter and is 3.7-fold higher than with MDF and the 223 nm filter. The lowest LOD, 0.9 ng L⁻¹, is achieved with the same atomizer/filter configuration, though LODs do not vary appreciably for other configurations (Table 3). All achieved LODs are significantly lower compared to those published in other works so far or to the declared values in commercial AFS instruments. The values are even better than LOD of 2.8 ng L⁻¹, reported for a complicated preconcentration system coupled with HG-AFS.³⁴ The LODs are also comparable to those typically obtained with the latest ICP(MS)/MS instrumentation (see Table 3).

4 Conclusion

A non-dispersive AFS, assembled from commercially available parts at low cost, was adapted for Bi determination using hydride generation as a sample introduction technique. The atomization in two hydride atomizers, MDF and FIGS, was investigated in detail and the atomizers were compared. The definite advantage of the FIGS atomizer is that it allows us to employ Bi fluorescence lines at >300 nm where serious OH emission can be an obstacle with the standard MDF atomizer.^{18,24} The exceptionally low LOD at ng L⁻¹ level achieved without any preconcentration step can be ascribed mainly to high intensity radiation source (EDL) in which, however, the impurities of Sb and Hg were identified. These impurities result in serious positive interference from Sb on Bi determination with 202 nm and 223 nm filters. However, this can be overcome by using the 307 nm filter as no Sb line is present in this region. FIGS as the atomizer and the 307 nm filter were finally chosen to be suitable for Bi determination in real samples which was demonstrated by the analysis of water, blood and hair CRMs. The proposed method seems to be also suitable for Bi determination in samples with matrix as complex as sea water. Such high concentration of dissolved salts is known to be an obstacle and requires significant sample dilution prior to determination by solution nebulization ICPMS which is commonly a trademark of unparalleled sensitivity.

Conflicts of interest

There are no conflicts of interest to declare.

Acknowledgements

The support of the Grant Agency of the Czech Republic (17-04329S), Czech Academy of Sciences (Institutional support RVO: 68081715) and Charles University (project SVV260560 and project GAUK 1048120) is gratefully acknowledged.

References

- 1 K. Norisuye and Y. Sohrin, *Anal. Chim. Acta*, 2012, **727**, 71–77.
- 2 F. A. M. Planchon, C. F. Boutron, C. Barbante, G. Cozzi, V. Gaspari, E. W. Wolff, C. P. Ferrari and P. Cescon, *Earth Planet. Sci. Lett.*, 2002, **200**(1), 207–222.
- 3 Y. Cai and G. Liu, *Encyclopedia of Analytical Chemistry: Applications, Theory and Instrumentation*, 2006, pp. 1–24.
- 4 W. T. Corns, P. B. Stockwell, L. Ebdon and S. J. Hill, *J. Anal. At. Spectrom.*, 1993, **8**(1), 71–77.
- 5 Y. W. Chen and A. D'Ulivo, *Anal. Lett.*, 1989, **22**(6), 1609–1622.
- 6 R. S. Hobbs, G. F. Kirkbright and T. S. West, *Talanta*, 1971, **18**(9), 859–864.
- 7 R. M. Dagnall, K. C. Thompson and T. S. West, *Talanta*, 1967, **14**(12), 1467–1475.
- 8 S. Kobayashi, T. Nakahara and S. Musha, *Talanta*, 1979, **26**(10), 951–957.
- 9 L. Ebdon, J. R. Wilkinson and K. W. Jackson, *Anal. Chim. Acta*, 1982, **136**, 191–199.
- 10 S. Brandt, A. Schütz, F. Klute, J. Kratzer and J. Franzke, *Spectrochim. Acta, Part B*, 2016, **123**, 6–32.
- 11 J. Dědina, *Spectrochim. Acta, Part B*, 2007, **62**(9), 846–872.
- 12 J. Dědina, A. D'Ulivo, L. Lampugnani, T. Matoušek and R. Zamboni, *Spectrochim. Acta, Part B*, 1998, **53**(13), 1777–1790.
- 13 J. Dědina and A. D'Ulivo, *Spectrochim. Acta, Part B*, 1997, **52**(12), 1737–1746.
- 14 A. D'Ulivo, J. Dědina, L. Lampugnani and T. Matoušek, *J. Anal. At. Spectrom.*, 2002, **17**(3), 253–257.
- 15 S. Musil, T. Matoušek, J. M. Currier, M. Stýblo and J. Dědina, *Anal. Chem.*, 2014, **86**(20), 10422–10428.
- 16 K. Marschner, S. Musil and J. Dědina, *Spectrochim. Acta, Part B*, 2015, **109**, 16–23.
- 17 K. Marschner, S. Musil and J. Dědina, *Anal. Chem.*, 2016, **88**(7), 4041–4047.
- 18 K. Marschner, Á. H. Pétursdóttir, P. Bucker, A. Raab, J. Feldmann, Z. Mester, T. Matoušek and S. Musil, *Anal. Chim. Acta*, 2019, **1049**, 20–28.
- 19 NIST atomic spectra database [electronic resource], accessed from <https://nla.gov.au/nla.cat-vn4265688>, accessed 20.03.2020.
- 20 S. Musil and J. Dědina, *J. Anal. At. Spectrom.*, 2013, **28**(4), 593–600.
- 21 https://www.perkinelmer.com/cmsresources/images/44-6570dts_photomultipliersmoleculardetectionanalyticalapplicationsmedicaldiagnostics.pdf, accessed 22.11.2019.
- 22 V. Sychra, V. Svoboda and I. Rubeška, *Atomic Fluorescence Spectroscopy*, Van Nostrand Reinhold Company, 1975.

- 23 A. D'Ulivo, P. Papoff and C. Festa, *Talanta*, 1983, **30**(12), 907–913.
- 24 A. D'Ulivo, I. Paolicchi, M. Onor, R. Zamboni and L. Lampugnani, *Spectrochim. Acta, Part B*, 2009, **64**(1), 48–55.
- 25 J. Dédina, *Spectrochim. Acta, Part B*, 1991, **46**(3), 379–391.
- 26 Z. Li, X. Yang, Y. Guo, H. Li and Y. Feng, *Talanta*, 2008, **74**(4), 915–921.
- 27 A. D'Ulivo, E. Bramanti, L. Lampugnani and R. Zamboni, *Spectrochim. Acta, Part B*, 2001, **56**(10), 1893–1907.
- 28 <https://www.psanalytical.com/products/millenniumexcalibur.html>, accessed 20.03.2020.
- 29 P. Cava-Montesinos, M. L. Cervera, A. Pastor and M. de la Guardia, *J. AOAC Int.*, 2003, **86**(4), 815–822.
- 30 Š. Komorsky-Lovrić, *Anal. Chim. Acta*, 1988, **204**, 161–167.
- 31 J. E. Portman and J. P. Riley, *Anal. Chim. Acta*, 1966, **34**, 201–210.
- 32 T. R. Gilbert and D. N. Hume, *Anal. Chim. Acta*, 1973, **65**(2), 451–459.
- 33 M. Filella, *J. Environ. Monit.*, 2010, **12**(1), 90–109.
- 34 H. Wu, B. Du and C. Fang, *Anal. Lett.*, 2007, **40**(14), 2772–2782.

Atomic fluorescence spectrometry for ultrasensitive determination of bismuth based on hydride generation – the role of excitation source, interference filter and flame atomizers

Barbora Štádlarová,^{a,b,*} Marta Kolrosová,^{a,b} Jiří Dědina,^a and Stanislav Musil^a

^a Institute of Analytical Chemistry of the Czech Academy of Sciences, Veveří 97, 602 00 Brno, Czech Republic

^b Charles University, Department of Analytical Chemistry, Hlavova 8, 128 43 Prague, Czech Republic

* corresponding author; E-mail: stadlerova@iach.cz (B. Štádlarová)

Abstract

This supplementary material describes in detail: the emission spectrum of Bi EDL (Fig. S1); dependence of peak area on the flow rate of inner Ar_{shield I} and outer Ar_{shield II} in FIGS (Fig. S2); and table with the results of the interference study (Table S1).

3 Results and discussion

3.1 AFS instrument

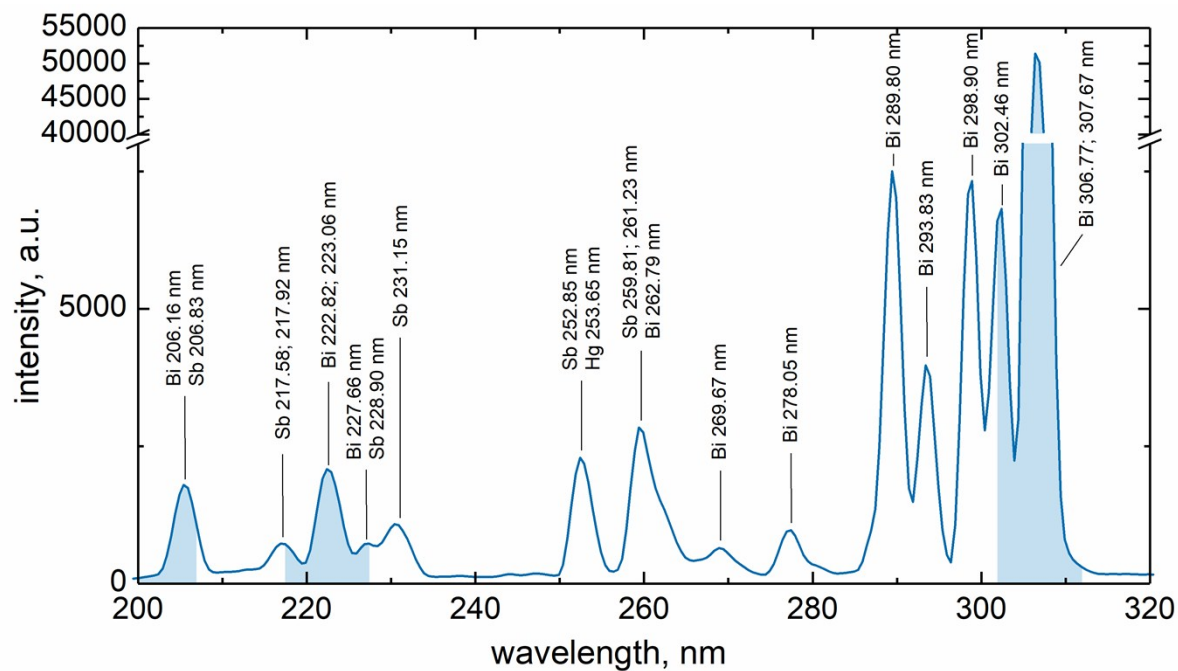


Fig. S1 Emission spectrum of Bi EDL (System II) obtained with a fiber optics UV-vis spectrometer. Transmission bandwidth (FWHM 10 nm) of 202, 223 and 307 nm filters shown in blue color for clarity.

3.2 Optimization of atomization conditions

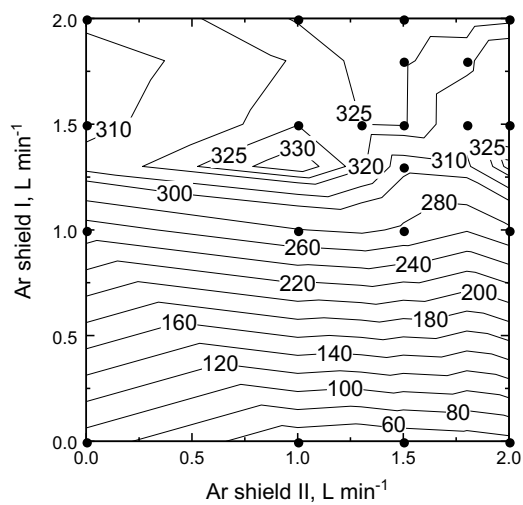


Fig. S2 Dependence of peak area on the flow rate of inner $Ar_{shield I}$ and outer $Ar_{shield II}$; $1 \mu\text{g L}^{-1}$ Bi, 500 mL min^{-1} total gas flow rate, hydrogen fraction 13%, 7 mL min^{-1} oxygen flow rate, $OH = 6 \text{ mm}$. Measured points are displayed for clarity.

3.4 Interference studyTable S1 The interference from hydride forming elements (Sn, Pb, Sb, Se, As and Hg) on Bi determination ($1 \mu\text{g L}^{-1}$) using FIGS and various interference filters

interferent	concentration of interferent ($\mu\text{g L}^{-1}$)	recovery ^a (%)		
		202 nm filter	223 nm filter	307 nm filter
Sn	1	99	100	100
	10	100	100	102
	100	100	99	100
Pb	1	102	100	100
	10	101	99	101
	100	101	100	100
Sb	1	159	117	99
	10	738	288	100
	100	7427	2209	88
Se	1	101	101	99
	10	101	100	99
	100	102	100	99
As	1	99	100	99
	10	99	97	97
	100	66	73	69
Hg	1	101	100	101
	10	100	99	100
	100	99	99	99

^arelative combined SD (combined SD/recovery) is < 3% for all recovery values



Efficient photochemical vapor generation of bismuth using a coiled Teflon reactor: Effect of metal sensitizers and analytical performance with flame-in-gas-shield atomizer and atomic fluorescence spectrometry

Jaromír Vyhnanovský^{a,b,*}, Dilek Yildiz^{a,c}, Barbora Štádlarová^{a,b}, Stanislav Musil^a

^a Czech Academy of Sciences, Institute of Analytical Chemistry, Veverří 97, 602 00 Brno, Czech Republic

^b Charles University, Faculty of Science, Department of Analytical Chemistry, Hlavova 8, Prague 2, 128 43, Czech Republic

^c Mugla University, Environmental Problems Research and Application Center, 48000 Mugla, Turkey

ARTICLE INFO

Keywords:

Bismuth
Photochemical vapor generation
Atomic absorption spectrometry
Atomic fluorescence spectrometry
Inductively coupled plasma mass spectrometry

ABSTRACT

Photochemical vapor generation (PVG) of bismuth was accomplished in a simple flow-injection system with a standard Hg low-pressure tube lamp and a coiled Teflon reactor. The influence of a reaction medium flow rate (irradiation time) and composition was investigated using a miniature diffusion flame atomizer and high-resolution continuum source atomic absorption spectrometry. Combination of 40% (v/v) acetic acid, 1.25% (v/v) formic acid and a metal sensitizer at a flow rate of 3 mL min⁻¹ (irradiation time of 90 s) was found optimal. The use of various metals as sensitizers was studied to initiate and enhance PVG substantially. The evident positive effect was found for four metal cations and the enhancement effect was in the following order: Cu²⁺ < Cd²⁺ < Fe²⁺ << Co²⁺. At 50 mg L⁻¹ Co²⁺ as the sensitizer, the overall PVG efficiency of 54 ± 2% was determined from relative comparison of sensitivities obtained with PVG and liquid nebulization coupled simultaneously to inductively coupled plasma mass spectrometry. In order to reach low limits of detection (LOD) at low operation cost, a coupling of PVG to atomic fluorescence spectrometry was tested and conditions of atomization in two flame atomizers were optimized. A blank-limited LOD of 12 ng L⁻¹ was obtained with an advanced flame-in-gas-shield atomizer, which competes with PVG coupled to inductively coupled plasma mass spectrometry (5 ng L⁻¹). Interferences from commonly used inorganic acids (HNO₃, HCl and H₂SO₄) and other elements (As³⁺, Pb²⁺, Sb³⁺, Se⁴⁺ and Te⁴⁺) were also investigated and the accuracy was verified by analysis of water Standard Reference Material NIST 1643f.

1. Introduction

Bismuth is an element that can be found in environmental samples at ultra-trace concentrations, often hardly detectable by standard analytical atomic spectrometric methods [1]. Therefore, the development of new ultrasensitive analytical methodologies is still of significant importance. In this respect, atomic fluorescence spectrometry (AFS) or inductively coupled plasma mass spectrometry (ICP-MS) in combination with vapor generation techniques seems to be highly promising.

Photochemical vapor generation (PVG) has been emerging as an alternative to hydride generation (HG), offering similar benefits such as the separation of the analyte from the matrix and higher introduction efficiency than that of pneumatic nebulization [2]. Compared to HG, it is applicable to a broader range of elements, including typical hydride-

forming elements (As, Sb, Bi, Se, Te, Pb, Sn and Tl) and Hg [3–9], Cd [10,11], transition metals (Fe, Co, Ni, Cu, Mo, Rh, Pd, Ag, W, Os, Ir, Pt and Au) [3,12–19] and nonmetals (F, Cl, Br and I) [20–23]. A volatile species is produced by UV irradiation of the liquid phase containing the analyte in the presence of a photochemical agent (in most cases low molar mass organic acids such as formic and acetic acid, but in some cases even alcohols, aldehydes or nitric acid) [2,24,25]. This produces reducing radical species (H•, R• and COO•⁻) and aquated electrons (e_(aq)⁻) that subsequently react with the analyte to produce volatile species - hydrides, carbonyls, alkylated species or oxides - depending on the analyte and the photochemical agent used [2,26]. Recently, the positive effect of photocatalysts (usually TiO₂) [27] and so-called sensitizers (various transition metal ions) on the PVG efficiency has been described for the PVG of several elements, namely the use of Fe³⁺ for As³⁺ [28];

* Corresponding author at: Czech Academy of Sciences, Institute of Analytical Chemistry, Veverří 97, 602 00 Brno, Czech Republic.

E-mail address: vyhnanovsky@iach.cz (J. Vyhnanovský).

<https://doi.org/10.1016/j.microc.2021.105997>

Received 9 October 2020; Received in revised form 1 December 2020; Accepted 24 January 2021

Available online 1 February 2021

0026-265X/© 2021 Elsevier B.V. All rights reserved.

Cd²⁺ for both As³⁺ and As⁵⁺ [29]; Cd²⁺ for Se⁶⁺ [30]; Co²⁺ and Ni²⁺ for Pb²⁺ [31]; Cu²⁺ for Cl⁻ [21]; Cu²⁺ for Ir³⁺ and Rh³⁺ [15]; Co²⁺ for Te⁴⁺ [32]; Fe²⁺ and Fe³⁺ for Te⁴⁺ and Te⁶⁺ in the presence of nano TiO₂ [33]; Fe³⁺ and a mixture of Co²⁺ and Cu²⁺ for Mo⁶⁺ [12,34]; Co²⁺ for Tl⁺ [8]; Cd²⁺, Fe²⁺ and Cu²⁺ for W⁶⁺ [13], and most recently Cu²⁺ for F⁻ [23] and Fe²⁺ for Cd²⁺ [11]. Details about the use of sensitizers for Bi³⁺ are given below.

The feasibility of PVG of Bi was firstly demonstrated by Guo et al. in 2004 [3] within a 20 element study using a batch style UV reactor. This was followed by a more in-depth study by Zheng et al. in 2010 [5] who employed a more conventional PVG reactor consisting of a quartz tube wrapped around a 125 W high-pressure Hg UV lamp. A significant step forward was made by Gao's group [35–37] who found Fe³⁺ ions to enhance the PVG efficiency substantially in a system based on a thin-film flow-through UV reactor with ready access to vacuum UV radiation (185 nm). The authors also identified the volatile Bi species as (CH₃)₃Bi. Very recently, the same group reported a further enhancement of the PVG efficiency using Co²⁺ ions as the sensitizer [38]. The same effect was presented independently by our group in a conference proceeding employing a Teflon coiled reactor [39].

The key characteristic to evaluate the state of optimization of PVG and its coupling to a detector is the overall PVG efficiency. It is defined as the fraction of the analyte converted to a volatile species, released from the liquid phase and then transported to the atomizer or plasma for the detection. The majority of works assigned little importance to its determination and relied only on an indirect approach based on the comparison of concentrations in the feeding solution and concentration determined in the waste after PVG. However, this approach neglects the sorption and deposition of the analyte (reduced presumably to elemental state) on the walls of the PVG apparatus, both in the liquid and gas phase, which can potentially result in unconvincing data and overestimated PVG efficiency [11,40]. The accurate way should lay in a direct determination of the analyte fraction in the gas entering the detector. This can be carried out e.g. by trapping of the volatile species on a suitable sorbent or filter and its subsequent determination [41], or by a comparison with a different sample introduction technique (most commonly the nebulization), of which the efficiency is either known or can be assessed with accuracy [11,13]. The use of a radioactive isotope (radiotracer) of the investigated analyte enables quantification of the overall PVG efficiency as well as of all fractions of the analyte trapped onto the apparatus parts or leaving the generator in the waste. Regarding PVG, such determination was carried out only for Se [41]. However, suitable radioactive isotopes (gamma emitters) are not available for all analytes and the preparation and handling of radiotracers requires a special professional competence. Comparison with liquid nebulization can be a suitable and fast approach enabling reliable quantification of the analyte fraction entering the detector after PVG. The crucial issue is the knowledge of an accurate value of the nebulization efficiency, which depends on several factors (flow rates of liquid and gas for nebulization and transport of aerosol, nebulizer type, etc.). Determination of the nebulization efficiency has gained a particular importance in the past decade, especially within the methodologies dealing with the measurement of number concentration and size of nanoparticles by single particle ICP-MS [42]. Very elegant, simple and easily applicable way of the determination of the nebulization efficiency was described by Cuello-Nuñez et al. [43], who revisited a waste collection method, originally described by Gustavsson [44], and demonstrated that it provided accurate values of the nebulization efficiency (note that the authors called it a transport efficiency). This approach has been already applied to the determination of the nebulization efficiency and the overall PVG efficiency of W [13] and Cd [11].

The majority of works on PVG of Bi have so far relied on inductively coupled plasma (ICP) with optical emission spectrometry (OES) and primarily with mass spectrometry (MS) as the detector. The only exception is the work by Zheng et al. [5] who used a miniature diffusion flame (MDF) atomizer and commercial AFS within a multi-element PVG

study. The achieved limit of detection (LOD) for Bi was not outstanding (0.1 µg L⁻¹) and in no way convincing about the excellent features of AFS for detection following PVG. However, it was demonstrated recently that AFS equipped with an intense electrode discharge lamp (EDL) in combination with HG can provide extremely high sensitivity in terms of LOD (less than 1 ng L⁻¹) but at substantially lower investment and operational costs [45] than ICP based approaches. Moreover, an advanced flame in-gas-shield (FIGS) atomizer enabled to employ intense Bi fluorescence lines at >300 nm where serious hydroxyl bands emission can be an obstacle with the standard MDF atomizer. No detailed investigation of atomization in the MDF and FIGS atomizers following PVG has been carried out yet to exploit the full potential of those atomizers in combination with AFS for sensitive detection of Bi.

In this work, we focused on several issues regarding PVG of Bi. Firstly, although the latest papers have described highly efficient PVG of Bi in special thin-film flow-through reactors [35–38] that permit more intense irradiation of a sample [46], we focused on PVG of Bi using a PTFE reactor coiled around a standard Hg low-pressure tube lamp to offer simple and easily manufacturable apparatus. The feasibility of several metal ion sensitizers to enhance PVG was investigated in detail. Secondly, we dealt with the determination of the overall PVG efficiency, an issue that is currently not treated in the literature with the required accuracy. Finally, we coupled the generator to an in-house designed atomic fluorescence spectrometer, studied the atomization of Bi volatile species in two flame atomizers, i.e., MDF and FIGS [45,47–49], and the optimal setup was utilized to determine analytical characteristics and verify accuracy.

2. Experimental

2.1. Reagents

All reagents were of analytical reagent grade or higher purity. Deionized water (DIW, <0.2 µS cm⁻¹, Ultrapur, Watrex, USA) was used for the preparation of all solutions. Formic acid (98%, p.a., Lach-Ner, Czech Republic) and acetic acid (99.8%, p.a., Lach-Ner, Czech Republic) were used for the preparation of the reaction medium. If explicitly stated, these acids and DIW were purified in a Teflon BSB-939-IR sub-boiling distillation apparatus (Berghof, Germany). A stock solution 1000 mg L⁻¹ Bi (Sigma-Aldrich, USA) was used for the preparation of all sample solutions. Sensitizer stock solutions of various concentrations were prepared from: cadmium(II) acetate dihydrate (p.a., Lach-Ner, Czech Republic), cobalt(II) acetate tetrahydrate (p.a., Lach-Ner, Czech Republic), copper(II) acetate monohydrate (p.a., Merck, Germany), nickel(II) acetate tetrahydrate (p.a., Sigma-Aldrich, USA) and iron(II) sulfate heptahydrate (p.a., Lachema, Czech Republic). Nitric acid (65%, semiconductor grade, Sigma-Aldrich, USA), hydrochloric acid (37%, p.a., Merck, Germany), sulfuric acid (98%, p.a., Lach-Ner, Czech Republic), arsenic(III) oxide (Lach-Ner, Czech Republic), lead(II) acetate trihydrate (p.a., Sigma-Aldrich, USA), sodium selenite(IV) pentahydrate (p.a., Merck, Germany), sodium tellurite(IV) (99%, Sigma-Aldrich, USA) and antimony standard solution (as SbCl₃ in 5 M HCl, Fluka, Switzerland), were used for an interference study. In order to verify the accuracy of the developed methodologies, Bi content was determined in the Standard Reference Material 1643f Trace Elements in Water (National Institute of Standards and Technology, USA).

2.2. Photochemical vapor generator

A schematic of the photochemical vapor generator is shown in Fig. 1. Almost all tubing was made of PTFE (typically 1 mm internal diameter (i.d.), Vici Jour Research, Switzerland), except for tubes used in peristaltic pumps. The photoreactor consisted of a 15 W low-pressure Hg germicidal lamp (Cole-Parmer, USA) which was wrapped around with 6 m of PTFE tubing (1 mm i.d., 1.59 mm o.d., Vici Jour Research, Switzerland; internal volume 4.7 mL). A steady flow of the reaction

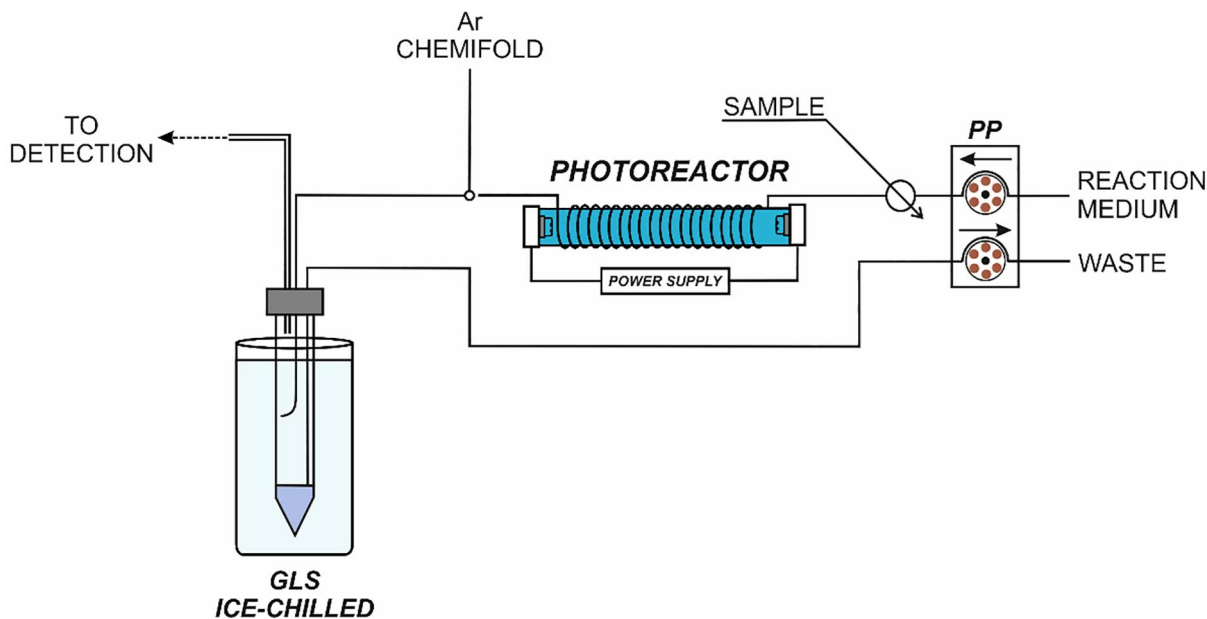


Fig. 1. A schematic of the photochemical vapor generation system; PP – peristaltic pump, GLS – gas-liquid separator.

medium was supplied by a peristaltic pump (Reglo ICC, Ismatec, Switzerland) equipped with Tygon tubing (1.02 mm i.d., Ismatec, Germany). Sample solutions were introduced into a stream of the reaction medium using an injection valve (V-451, IDEX Health and Science, USA; sample loop volume 0.56 mL). The effluent from the photoreactor was mixed with a flow of argon (Ar chemifold, 100 mL min^{-1}), and carried to a plastic gas-liquid separator (GLS, described in detail in ref. [13]), where the volatile species were separated from the liquid waste. The GLS with an internal volume of 15 mL was immersed in an ice bath to reduce the release of organic acid vapors into the atomizer/plasma. A separate channel was used to evacuate the waste from the GLS and a stable liquid level ($\approx 2 \text{ mL}$) was maintained inside the GLS by the peristaltic pump.

2.3. Atomizers

Two atomizers were employed – the miniature diffusion flame (MDF) and the flame-in-gas-shield (FIGS) atomizers (Fig. 2a, b). Both MDF and FIGS consist of a vertical quartz support tube (6 mm i.d.) with a side inlet arm (2 mm i.d.). In addition to Ar (chemifold) containing Bi volatile species released in the GLS, the MDF atomizer is also supplied with

carrier Ar and flame H_2 , premixed before entering the support tube (not shown in Fig. 2a, b). In the case of FIGS, there was also a capillary (i.d. 0.53 mm) in the axis of the support tube protruding 3 mm above its rim, serving to introduce a small amount of O_2 . A two channel brass shielding unit [48] was fitted around the support tube and served to introduce the shielding laminar flows of argon (1500 mL min^{-1} in both channels). The observation height (OH) was defined for MDF and FIGS as the distance from the center of the optical beam to the top of the support tube or the capillary, respectively.

2.4. PVG-HR-CS-AAS

The measurements were performed with a high-resolution continuum source atomic absorption spectrometer (HR-CS-AAS) ContrAA 300 (Analytik Jena AG, Germany) at 223.061 nm. Peak volume selected absorbance [50], which was the integrated absorbance (dimensionless) summed over three pixels (central (CP) and two adjacent pixels ($\text{CP} \pm 1$)) of the CCD array detector, corresponding to a spectral interval of $\approx 4.3 \text{ pm}$, was used for signal evaluation. A commercial flame sample introduction system and a burner were replaced with the MDF atomizer.

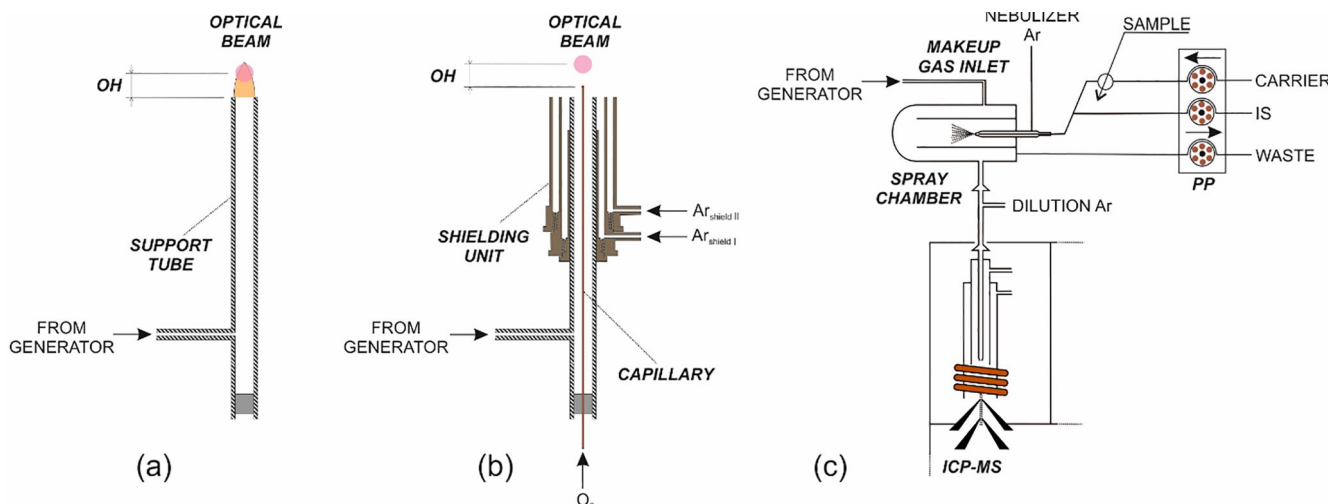


Fig. 2. MDF (a) and FIGS (b) atomizers used with PVG and coupling of PVG to ICP-MS (c).

The optical axis of the spectrometer, i.e., the axis of the radiation beam, intersected the vertical axis of the atomizer. The lower edge of the radiation beam was set just above the top of the atomizer. The flow rates of 100 mL min⁻¹ for both Ar (chemifold) and flame H₂ were chosen based on our previous experience with this type of atomizer for AAS measurements [51–53].

2.5. PVG-AFS

An in-house assembled non-dispersive atomic fluorescence spectrometer [48] was used as a detector. A Bi EDL (Perkin-Elmer, System 2) was used as a radiation source with the feeding current square-wave modulated at frequency of 40 Hz. The operating current for EDL was 400 mA. A solar-blind channel photomultiplier tube (PMT, 165–320 nm, MH 1922, Perkin-Elmer, Germany) supplied with negative voltage served as the detector and was placed perpendicularly to the EDL to collect the produced fluorescence radiation emitted from the atomizer. A 222.63 nm interference filter (full width at half maximum 10 nm and transmittance 18%, Melles Griot, USA) covering mainly Bi fluorescence lines at 222.8 and 223.1 nm was employed with MDF and a 307.1 nm filter (10 nm, 17%, Edmund Optics, USA) covering mainly the lines at 306.8 and 302.5 nm was employed with FIGS, unless otherwise stated. The optimal settings of the AFS instrument and mutual positions of the individual components for Bi determination were taken from ref. [45].

2.6. PVG-ICP-MS

An Agilent 7700x single quadrupole ICP-MS (Agilent Technologies, USA) was used for a comparison of the analytical performance of AFS and for the determination of the overall PVG efficiency.

The outlet from the GLS was connected to the inlet of a Scott-type spray chamber (Fig. 2c) that was originally intended to introduce makeup argon. To provide more robust wet plasma conditions and to monitor plasma stability, DIW as a carrier liquid was mixed with a 10 µg L⁻¹ Rh internal standard solution (IS) in 2% HNO₃ and was subsequently nebulized by a MicroMist nebulizer into the spray chamber during PVG. Signal intensities of ²⁰⁹Bi and ¹⁰³Rh isotopes were recorded in time resolved analysis mode. Optimal settings of ICP-MS are summarized in Table 1.

Overall PVG efficiency, defined as the fraction of the analyte that is generated, released and transported to the atomizer/detector, was calculated from an enhancement factor multiplied with the nebulization efficiency of ICP-MS setup. The enhancement factor was calculated as a ratio of absolute sensitivities obtained with PVG and with nebulization of Bi standard solutions to the ICP-MS under the same plasma conditions as described previously [11,13,54]. The comparison of sensitivities was carried out by introducing the sample either with the injection valve (0.56 mL) directing the sample to the PVG system or with the injection valve (0.26 mL) available in the chemifold for sample delivery to the nebulizer (see Fig. 2c). When a standard in 2% HNO₃ was injected and nebulized, PVG was simultaneously running so that the conditions in the plasma remained unchanged and vice versa. The liquid sample nebulization efficiency, traditionally representing the fraction of the analyte

Table 1
Typical ICP-MS parameters for coupling with PVG.

RF power	1600 W
RF matching	2.2 V
Sampling depth	7 mm
Nebulizer Ar	1.05 L min ⁻¹
Dilution Ar	0.0 L min ⁻¹
Ar (chemifold) for PVG	100 mL min ⁻¹
Sample flow rate	0.32 mL min ⁻¹ carrier liquid, 0.07 mL min ⁻¹ IS
Spray chamber temperature	2 °C
Reaction/Collision cell mode	no gas mode
Measurement mode	time resolved analysis
Measured isotopes (dwell time)	¹⁰³ Rh (0.05 s), ²⁰⁹ Bi (0.1 s)

that is transported to and enters the plasma, was determined using a modified waste collection method [11,13,54]. The plasma was being ignited and the instrument parameters set for optimal operation with the PVG system. Approximately 15 mL of the solution containing 2 µg L⁻¹ Bi and 10 µg L⁻¹ Rh in 2% HNO₃ was placed in a vial on an analytical balance and tubing for aspiration of both the carrier liquid and IS was immersed into this solution. After stabilization (30 min), the outlet for waste from the spray chamber was also introduced into this vial, hence the solution was recirculated. The weight of the solution was recorded every 5 min over a 60 min period. Recorded weights were plotted against time. The nebulization efficiency was calculated by dividing the slope of this weight loss plot by the total solution flow rate (0.39 mL min⁻¹ = carrier liquid + IS) entering the nebulizer.

2.7. Measurement procedure and conventions

Flow injection (FI) was utilized for sample introduction to the generator throughout. With PVG in continuous operation (both channels of the peristaltic pump running), the sample was manually injected into the carrier 5 s after the recording of the signal had been initiated. Peak volume selected absorbance evaluated from 3 pixels was employed as a measure of the analyte response in HR-CS-AAS. In the case of ICP-MS, peak areas were evaluated from transient signal of ²⁰⁹Bi and corrected for any sensitivity drift relative to changes in the steady-state ¹⁰³Rh IS signal intensity. In the case of PVG-AFS, peak area and more importantly signal to noise ratio (SNR) were the main parameters used for data evaluation. SNR was determined by dividing the peak area of 1 µg L⁻¹ Bi standard by the uncertainty of the baseline, which was estimated as an average (n = 3) of the standard deviations (SDs) of the baseline calculated from 1600 values recorded in 40 s. The data from the spectrometers were exported in .csv format and the signals were integrated in MS Excel.

Medians of at least 3 replicates are shown in all relevant figures. Uncertainties are presented as ± standard deviation (SD) or combined SD where results are relative. If sensitivity is mentioned, it refers to peak area related to the analyte mass taken for the measurement. LOD is expressed as 3 × SD(blank)/sensitivity.

2.8. Treatment of certified reference material

SRM NIST 1643f was evaporated to dryness in order to get rid of HNO₃ that causes interference during PVG. 3 mL of NIST 1643f were pipetted into a 40 mL quartz vial, evaporated using a thermoblock (temperature: ≈100 °C; 4 replicates) and subsequently diluted ca. 33 fold with the reaction medium containing Co²⁺ ions as the sensitizer. A sample preparation blank, 3 mL of DIW, was prepared as well.

3. Results and discussion

3.1. Optimization of PVG conditions

The PVG conditions (composition of the reaction medium, irradiation time and effect of the presence of metal sensitizers) were optimized using the MDF atomizer and HR-CS-AAS. Composition of the reaction medium is an important parameter that predestines generated radicals in the liquid phase under UV treatment and identity of generated volatile species (hydrides, carbonyls or alkyl-derivates) [2]. PVG of Bi has been so far conducted from acetic acid medium without the addition of metal sensitizers [5,7,55,56], or very recently from a mixture of acetic (20–30%) and formic acid (5–10%) with the use of Fe³⁺ or Co²⁺, to yield volatile (CH₃)₃Bi [35–38]. Following these papers [35–38], initial composition of the reaction medium PVG conditions was chosen as 40% (v/v) acetic acid, 10% (v/v) formic acid and with the addition of 50 mg L⁻¹ of Fe²⁺ into the sample as a sensitizer.

The first parameter to be optimized was the sample irradiation time (IT), which is inversely proportional to the flow rate of the reaction

medium. The highest sensitivity was obtained at 3 mL min^{-1} . This flow rate corresponds to IT of approximately 90 s, which was determined experimentally by following an air bubble that was introduced into the coiled reactor during irradiation of the reaction medium. Longer UV exposures (flow rates of 1 and 2 mL min^{-1}) did not lead to an enhancement of sensitivity but significantly increased the time necessary for flushing of the injected sample from the PVG generator and thus prolonged FI signals. Higher flow rates led to a gradual decrease in sensitivity (by $\approx 17\%$ at 4 mL min^{-1} and by $\approx 37\%$ at 5 mL min^{-1}), which is most probably caused by an insufficient irradiation of the sample.

The dependence of the sensitivity on the composition of the reaction medium at 3 mL min^{-1} using $50 \text{ mg L}^{-1} \text{ Fe}^{2+}$ as a sensitizer is depicted in Fig. 3. The highest sensitivity was observed using a reaction medium consisting of 40% (v/v) acetic acid and 1.25% (v/v) formic acid and the synergistic effect of both acids was found to be crucial for the efficient PVG of Bi. In other words, no PVG was achieved when only sole acid, either formic or acetic, was used. This corresponds to previously published works by Gao's group [35–38] who conducted PVG with the use of Fe^{3+} or Co^{2+} as sensitizers. On the contrary, Romanovskiy et al. [7] reported only 30% acetic acid without any sensitizer as the optimal conditions using a “thin-film” photoreactor of their own design.

The effect of added sensitizers was investigated with the mixture of 40% (v/v) acetic acid and 1.25% (v/v) formic acid and is illustrated in Fig. 4. All the sensitizers were added in the form of their acetates, with the exception of Fe^{2+} that was added as a sulfate, so as not to introduce any counterion (i.e., nitrates or chlorides) that could potentially interfere with the PVG (see below). In the absence of any sensitizer no signal response of bismuth could be detected. Four sensitizers with a positive effect on the PVG of Bi were identified and mutually compared, with their respective increasing enhancement effect being in the following order: $\text{Cu}^{2+} < \text{Cd}^{2+} < \text{Fe}^{2+} \ll \text{Co}^{2+}$. The maximum sensitivity was achieved using $500 \text{ mg L}^{-1} \text{ Co}^{2+}$ as a sensitizer but the sensitivity did not vary much in a broad range of Co^{2+} (50–1000 mg L^{-1}). Since Co^{2+} can be also partially co-generated as a volatile carbonyl [17,57,58], which can cause large deposits in the atomizers of the AAS and AFS or the torch, cones and lenses of the ICP-MS, $50 \text{ mg L}^{-1} \text{ Co}^{2+}$ was chosen for all further experiments as a compromise. The sensitivity at this concentration was only lower by 12% in comparison to 500 mg L^{-1} . In the case of Fe^{2+} , the optimal concentrations were in the range 250–1000 mg L^{-1} , but the sensitivity was about 3.9–4.5-fold lower than with $50 \text{ mg L}^{-1} \text{ Co}^{2+}$. Measurements with high concentrations of Fe^{2+} caused yellow–brown deposits in the coiled reactor and even in the atomizer because

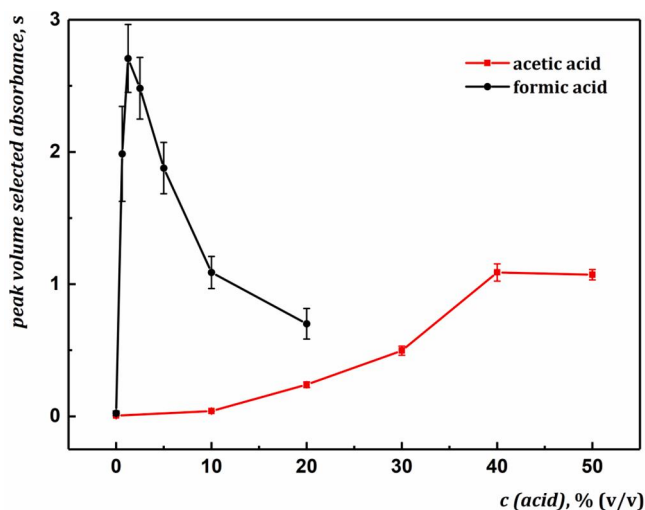


Fig. 3. Influence of composition of reaction medium on AAS response; experimental conditions: $2 \text{ mg L}^{-1} \text{ Bi}$, reaction medium flow rate 3 mL min^{-1} , $50 \text{ mg L}^{-1} \text{ Fe}^{2+}$ as a sensitizer in the sample, 10% (v/v) formic acid for the optimization of acetic acid, 40% (v/v) acetic acid for the optimization of formic acid.

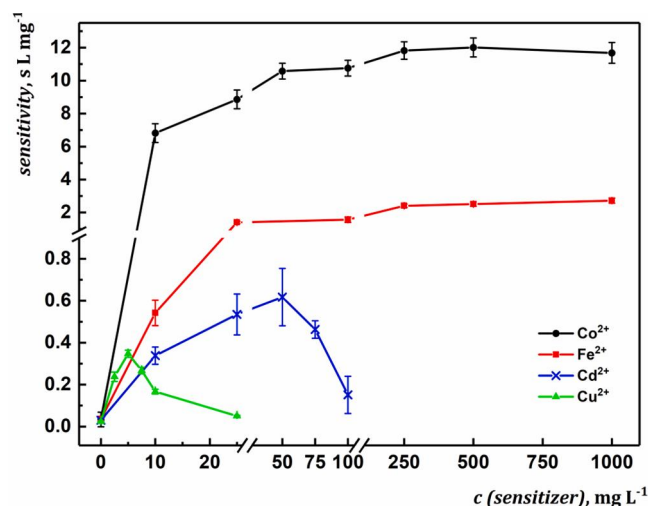


Fig. 4. Effect of added sensitizers on AAS sensitivity; experimental conditions: reaction medium flow rate 3 mL min^{-1} , reaction medium 40% (v/v) acetic acid and 1.25% (v/v) formic acid, sensitizer added to sample.

small fraction of Fe could be generated in the form of $\text{Fe}(\text{CO})_5$ and introduced to the MDF. The optimal concentration for Cd^{2+} was found to be 50 mg L^{-1} but the repeatability of the measurements was significantly worse (RSD up to 22%) and the sensitivity was about 17-fold lower than that of $50 \text{ mg L}^{-1} \text{ Co}^{2+}$. Lastly, Cu^{2+} exhibited some positive effect as well, with a very sharp maximum of sensitivity at 5 mg L^{-1} . Its enhancement effect was the lowest of all the tested sensitizers, being about 30-fold lower than with $50 \text{ mg L}^{-1} \text{ Co}^{2+}$. Lastly, the addition of Ni^{2+} ions was also examined but it did not exhibit any positive effect in the tested range 20–100 mg L^{-1} .

A synergistic effect of multiple sensitizers has been previously described for the PVG of Mo [34], hence the addition of various concentrations of Fe^{2+} (50, 200 and 500 mg L^{-1}), Cd^{2+} (10, 25 and 50 mg L^{-1}) or Cu^{2+} (2.5, 5 and 7.5 mg L^{-1}) to a sample already containing $50 \text{ mg L}^{-1} \text{ Co}^{2+}$ was investigated. No further improvement in the sensitivity and thus overall PVG efficiency was achieved, and the addition of Cu^{2+} caused a serious interference with the signal of Bi disappearing altogether for all tested concentrations.

The exact nature of the positive effect of Co^{2+} (and other sensitizers) ions is still rather hypothetical. Hu et al. [34] investigated the action of Co^{2+} and Cu^{2+} ions synergistically enhancing PVG of Mo with the electron paramagnetic resonance spin trapping technique recently. They found that the metal ions promoted higher production of highly reducing radicals $\text{COO}^{\bullet-}$ during UV irradiation of formic acid. The same results were subsequently confirmed for PVG of Te with Co^{2+} as the sensitizer [32] employing very similar composition of the reaction medium (20% (v/v) acetic acid and 5% (v/v) formic acid) as used in this work. Increased production of $\text{COO}^{\bullet-}$ radicals can facilitate sequential reduction of Bi^{3+} to Bi^0 , which is followed by rapid uptake of CH_3 derived from the photolysis of acetic acid to yield volatile $(\text{CH}_3)_3\text{Bi}$. Metal sensitizers can enhance the rate of oxidation of formic acid that was shown to photodissociate about 100-fold faster than acetic acid in the presence of Fe^{3+} [2,59]. Furthermore, formic acid exhibits higher absorption than acetic acid at 254 nm [25]. All of the above-mentioned facts may explain the role of metal sensitizers as well as the role of formic acid as the prevalent source of $\text{COO}^{\bullet-}$ although there is no clear indication as to why just Co^{2+} has such a significant enhancing effect on PVG of Bi and the other metals don't. The addition of both Co^{2+} and formic acid seems to be crucial to enhance PVG efficiency that most probably significantly exceeds the efficiencies achieved in studies in which only acetic acid was employed as the reaction medium without any sensitizer [5,7,55,56].

The following conditions were chosen as optimal and were used for

all further experiments: 40% (v/v) acetic acid and 1.25% (v/v) formic acid at a flow rate of 3 mL min⁻¹, with the addition of 50 mg L⁻¹ Co²⁺ to the sample/blank.

3.2. Overall PVG efficiency

In this work, the overall PVG efficiency under chosen optimal conditions of PVG was determined from a comparison of PVG sample introduction to a conventional liquid sample nebulization that were simultaneously coupled to the ICP-MS (see Fig. 2c). The important variables for this determination are the values of the nebulization efficiency and the enhancement factor.

The nebulization efficiency, representing the fraction of the analyte that is transported to and enters the plasma, was determined using the modified waste collection method as $8.2 \pm 0.1\%$. This efficiency is almost the same as determined in our previous studies on PVG of Cd ($8.3 \pm 0.1\%$) [11] and HG of Te ($8.2 \pm 0.4\%$) [54] under almost the same conditions of aerosol transport into the ICP-MS. The enhancement factor was quantified as a ratio of absolute sensitivities evaluated from peak area (counts ng⁻¹) obtained with PVG and with nebulization of Bi standard solutions to the ICP-MS, both measured under identical plasma conditions. The calibration curve for PVG-ICP-MS was constructed with 0, 0.05, 0.1 and 0.25 ng mL⁻¹ (0, 0.028, 0.055 and 0.14 ng absolute) Bi standards prepared in 40% acetic acid, 1.25% formic acid with the addition of 50 mg L⁻¹ Co²⁺ while nebulizing 2% HNO₃ and 10 ng mL⁻¹ Rh as IS. The calibration curve for nebulization was measured with 0, 1, 2 and 5 ng mL⁻¹ (0, 0.26, 0.53, 1.3 ng absolute) Bi standards in 2% HNO₃ while only the reaction medium (40% acetic acid and 1.25% formic acid) was continuously aspirated to and irradiated in the PVG system. The enhancement factor equaled 6.5 ± 0.2 . Taking into account this value and the value of the nebulization efficiency (8.2%), the overall PVG efficiency was quantified as $54 \pm 2\%$.

The obtained analytical sensitivity in the atomic detectors reflects overall PVG efficiency when relevant experimental conditions, such as gas flow rates, atomizer and spectrometer settings, etc., are maintained. If we take into account the sensitivities measured with various metal sensitizers (see Fig. 4) and relate them to the sensitivity measured at the optimal conditions with 50 mg L⁻¹ Co²⁺, we can estimate the overall PVG efficiencies for the other metal sensitizers as: $\approx 8\%$ and $\approx 14\%$ at 100 mg L⁻¹ and 1000 mg L⁻¹ Fe²⁺, respectively, $\approx 3.2\%$ at 50 mg L⁻¹ Cd²⁺ and $\approx 1.8\%$ at 5 mg L⁻¹ Cu²⁺. It is evident that only Co²⁺ and possibly also 1000 mg L⁻¹ Fe²⁺ are the sensitizers that offer the overall PVG efficiency of an essential importance. However, as noted above, high concentration of Fe²⁺ is not suitable for routine use due to a potential huge load of Fe (in the form Fe(CO)₅) into the atomizer/detector.

Only few authors attempted to estimate/determine the (overall) PVG efficiency of Bi. Zheng et al. [5] estimated the PVG efficiency of Bi generated from acetic acid based medium and in a reactor made of a quartz tube wrapped around a high-pressure UV lamp in the range 20–30%. They compared the analytical sensitivity obtained with PVG-AFS to that of HG-AFS assuming the efficiency of HG is 100%. Yu et al. [35,38] also reported the PVG efficiency achieved with a thin-film flow-through UV reactor and they found the value of 55% employing 20% (v/v) acetic acid, 5% (v/v) formic acid, 60 mg L⁻¹ Fe³⁺ as the sensitizer and 13 s irradiation time [35] and 88% employing 30% (v/v) acetic acid, 10% (v/v) formic acid, 80 mg L⁻¹ Co²⁺ as the sensitizer and 50 s irradiation time [38]. However, it has to be emphasized that this estimate was based on the indirect approach from the remaining Bi found in the waste solution after UV irradiation and it does not have to really reflect the fraction of an analyte introduced to the detector because it neglects any analyte deposition in the apparatus parts.

3.3. Interferences

Interferences from HNO₃, HCl and H₂SO₄ were examined with PVG-HR-CS-AAS (Fig. 5) considering the possible application of this

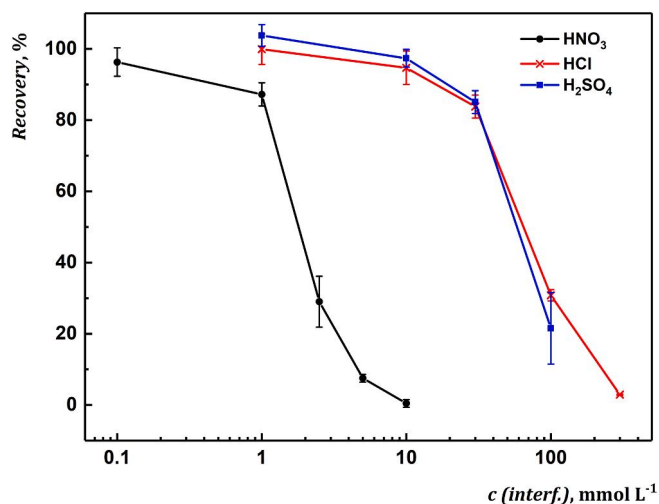


Fig. 5. Relative effects of added interferences on PVG response of 0.25 mg L⁻¹ Bi; experimental conditions: reaction medium flow rate 3 mL min⁻¹, reaction medium 40% (v/v) acetic acid and 1.25% (v/v) formic acid, 50 mg L⁻¹ Co²⁺ added to sample.

methodology for the analysis of Bi in real matrices. HNO₃ was found to be a severe interferent, even at concentration as low as 1 mmol L⁻¹ ($\approx 0.04\%$ v/v) it caused a drop in sensitivity by 13%. The PVG system was substantially more tolerant to the presence of HCl and H₂SO₄ wherein a similar drop (by 15% and 16%, respectively) was observed at concentrations of 30 mmol L⁻¹ ($\approx 0.9\%$ (v/v) HCl and $\approx 1.6\%$ (v/v) H₂SO₄). These results are very similar to those in other works [38], although a different PVG generator was employed. Considering the wide use of these acids (especially HNO₃) for mineralization, extraction, preservation of samples, etc. this poses a big challenge in the application of PVG methods to real samples (see also Section 3.5 dealing with a treatment of nitric acid interference).

Interferences from typical “hydride” forming elements, i.e., As³⁺, Pb²⁺, Sb³⁺, Se⁴⁺ and Te⁴⁺, were also studied (Table 2) because volatile species of these elements can be efficiently generated under very similar conditions (composition of the reaction medium with or without metal sensitizers) [5,28–32,60]. Solutions containing reaction medium and Co²⁺ as the sensitizer were spiked with each element and a special attention was paid to avoid adding any counterion, especially nitrate, that could interfere with PVG (see above). The aqueous stock solutions were prepared from solid selenite, tellurite, arsenic oxide or lead acetate with the exception of Sb³⁺ which was spiked with the solution prepared from commercial analytical standard stabilized in 5 M HCl. Nevertheless, even at the highest tested level for Sb³⁺ (2.5 mg L⁻¹) the concentration of HCl in the reaction medium was around 12.5 mM, which should still be within the range where PVG is not affected by the presence of HCl (see Fig. 5). As shown in Table 2, all the investigated ions had no serious or only limited impact on Bi determination up to 0.25 mg

Table 2

Influence of various co-existing ions on Bi determination (0.25 mg L⁻¹) examined by PVG-HR-CS-AAS.

Interferent concentration (mg L ⁻¹)	Recoveries (%) ^a in the presence of the interferent				
	As ³⁺	Pb ²⁺	Sb ³⁺	Se ⁴⁺	Te ⁴⁺
0.025	98 ± 6	92 ± 6	94 ± 6	104 ± 6	95 ± 3
0.25	90 ± 5	107 ± 7	92 ± 7	87 ± 5	99 ± 3
2.5	55 ± 5	55 ± 4	62 ± 6	7 ± 1	85 ± 2
25	– ^b	– ^b	– ^b	– ^b	3 ± 0

^a Uncertainty expressed as combined SD.

^b Not determined.

L^{-1} but all of them tend to interfere at higher concentrations. The order of severity of interference could be summarized as follows: $Se^{4+} > As^{3+}$, Pb^{2+} , $Sb^{3+} > Te^{4+}$.

3.4. PVG-AFS

PVG of Bi was coupled to non-dispersive AFS and two atomizers, MDF and FIGS, were tested and the conditions of atomization optimized. MDF is generally considered a robust atomizer. However, higher sensitivity, SNR and lower LOD are usually achieved with FIGS [45,47,48]. FIGS produces significantly less hydroxyl radicals than MDF [61]. This is especially advantageous with respect to Bi determination because it allows us to employ Bi fluorescence line at 306.8 nm where a serious hydroxyl bands emission can be an obstacle with the standard MDF [45]. On the contrary, the disadvantage of FIGS lies in higher susceptibility towards atomization interferences [62].

The SNR was employed as a relevant parameter for evaluation (see Section 2.7) rather than sensitivity because the maximum sensitivity achieved with some atomizer settings does not have to result in the best SNR. SNR is controlled by the sensitivity as well as by the baseline noise and thus reflects the resultant LOD. In AFS, the baseline noise strongly depends (besides the contribution of an analyte contamination to the fluorescence radiation) on the scattered radiation from the light source and on the overlap of the interference filter transmittance profile with the emission spectrum of the atomizer flame, i.e., on the flame emission. The flame emission differs significantly with the atomization conditions employed (gas flow rates, OH, etc.) and atomizer used [45]. The scattering of the radiation from the EDL was found dominant especially at low OH (<5 mm) [45]. Therefore, higher flow rates ($\geq 500 \text{ mL min}^{-1}$) have to be used to form much "bigger" flames above the atomizer support tube than the flow rates satisfactorily used in AAS (also used in this work).

The default conditions for the atomization in MDF and FIGS were taken from our previous work [45] in which AFS was coupled to HG. It was assumed that the optimal atomization conditions for MDF (total gas flow rate, H_2 fraction, OH) and FIGS (the same parameters plus O_2 flow rate) might differ for PVG approach, especially due to high concentrations of organic acids (40% acetic and 1.25% formic acid) necessary for efficient PVG of Bi. Although the reaction medium is only slightly warmed up during the transfer through the coiled reactor (to 28°C), vapors of acids are continuously stripped from the GLS by Ar (chemiflod) stream. Karadjova et al. [63,64] pointed out a serious interference from organic solvents during atomization of AsH_3 in MDF. Even a presence as little as 6% of methanol, ethanol or propanol in HCl solution used for HG caused a serious suppression of sensitivity on the account of decrease of the atomization efficiency. This was explained by the formation of carbon radicals and carbon particles that caused a decay of the analyte free atoms and/or reduced the population of H radicals that are responsible for atomization.

In this work, it was found out that the optimum atomization conditions using PVG with MDF and 223.1 nm interference filter do not substantially differ from optimum conditions for HG [45]. Optimum total gas flow rate (=argon + hydrogen) to the atomizer was 600 mL min^{-1} with H_2 fraction of 17% and OH 6 mm (Table 3). Taking into consideration different sample volumes (0.56 mL for PVG and 1 mL for HG [45]) as well as different generation efficiencies of PVG ($\approx 54\%$) and

HG ($\geq 90\%$), the comparison of sensitivities (in $\mu\text{V s ng}^{-1}$) for PVG and HG showed relatively low suppression of the atomization efficiency (by $\approx 15\%$) given by the presence of organic vapors. On the other hand, the same comparison for FIGS revealed lower sensitivity for PVG by 25% in comparison to HG. In an atomizer type similar to our FIGS, flame-in-flame atomizer, Karadjova et al. [64] reported that higher flow rate of added O_2 suppressed the extent of "carbon" interference. Hence, the effect of the flow rate of O_2 through the capillary was examined, in addition to OH, total gas flow rate and H_2 fraction. It was clearly demonstrated that the optimum conditions of FIGS employing PVG-AFS were different from those employing HG-AFS (see Table 3). The major discrepancy lay in O_2 flow rate which corresponded to 20 mL min^{-1} as opposed to 7 mL min^{-1} for HG [45] and in OH which had to be elevated from 6 mm to 9 mm. Higher optimum flow rate of O_2 corresponds to the results published by Karadjova et al. [63,64] and provides better resistance towards the "carbon" interference. The total gas flow rate had to be adjusted only slightly – from 500 mL min^{-1} to 600 mL min^{-1} while the H_2 fraction remained the same (12%).

The aforementioned results can be summarized as follows. Both MDF and FIGS are negligibly or only partly impaired by the presence of higher amount of organic acids vapor released from the generator and the atomization efficiency still remains high. Moreover, it can be predicted that it does not matter which volatile species is introduced (BiH_3 in the case of HG, $(CH_3)_3Bi$ in the case of PVG). The resultant SNR was some 1.8-fold better with FIGS atomizer than with MDF. Hence, FIGS was employed further to evaluate the analytical performance and for the analytical application.

3.5. Analytical characteristics and accuracy

Analytical characteristics of FI-PVG-AFS were determined using the optimal conditions of PVG and atomization for FIGS (Table 3). The calibration function constructed with 0, 0.1, 0.25, 0.5, 1 and $2 \mu\text{g L}^{-1}$ Bi standard solutions was linear ($R^2 = 0.9998$). The repeatability, expressed as the relative standard deviation ($n = 10$), was 4% at $1 \mu\text{g L}^{-1}$. The LODs were found to be impaired by Bi contamination in the reaction medium and/or in the sensitizer. There was always a peak shaped blank over the measured baseline because $Bi(CH_3)_3$ vapors can be generated only in a zone of the injected sample/blank where Co^{2+} is present as the sensitizer while PVG cannot be accomplished from the reaction medium without the sensitizer. Using FI-PVG-ICP-MS, Bi concentration corresponding to this peak was estimated to be approximately 20 ng L^{-1} when the reaction medium was prepared from non-distilled acids and DIW while it was lowered to less than 10 ng L^{-1} when the acids as well as DIW were purified by sub-boiling distillation. Hence, a significant portion of the blank may originate from the added Co(II) acetate. The use of Co(II) acetate from a different supplier did not further reduce Bi contamination. The lowest relative and absolute LOD (3σ , $n = 10$) achieved with FI-PVG-AFS using purified acids and DIW corresponded to 12 ng L^{-1} and 6.7 pg, respectively. For comparison, the same analytical characteristics were also determined with FI-PVG-ICP-MS and can be summarized as follows: repeatability of 4% ($n = 6$) at $0.05 \mu\text{g L}^{-1}$ and the relative and absolute LOD (3σ , $n = 12$) of 5 ng L^{-1} and 2.8 pg, respectively. A comparison of the achieved relative LODs to the already published methods based on PVG with different atomic spectrometric detectors is in Table 4.

Table 3
Atomization conditions for MDF and FIGS atomizer used in AFS.

Atomizer	Generator	Total Ar (mL min^{-1})	Total H_2 (mL min^{-1})	O_2 (mL min^{-1})	OH (mm)	Ar shield (L min^{-1})
MDF	PVG	500	100	–	6	–
	HG ^a	500	100	–	7	–
FIGS	PVG	528	72	20	9	1.5; 1.5
	HG ^a	440	60	7	6	1.5; 1.5

^a Taken from Reference [45].

Table 4
Comparison of LODs for bismuth determination based on PVG (listed chronologically).

	Reaction medium/Sensitizer	Photoreactor	LOD (ng L ⁻¹)	Reference (Year)
PVG-ICP-OES	50% (v/v) AA/no sensitizer	Thin-film	270	[55] (2010)
PVG-AFS	5–10% AA/no sensitizer	Coiled quartz	100	[5] (2010)
PVG-MIP-OES	40% (v/v) AA/no sensitizer	Ultrasonic nebulization with UV pen lamp	22,000	[56] (2013)
PVG-ICP-MS	30% AA/no sensitizer	Thin-film cylindrical	13 ^a ; 60 ^b	[7] (2018)
PVG-ICP-MS	20% AA and 5% FA/60 mg L ⁻¹ Fe ³⁺	Thin-film flow-through	0.3	[35] (2018)
PVG-ICP-MS	30% AA and 10% FA/80 mg L ⁻¹ Co ²⁺	Thin-film flow-through	0.3	[38] (2020)
PVG-ICP-MS	40% AA and 1.25% FA/50 mg L ⁻¹ Co ²⁺	Coiled PTFE	5	This work
PVG-AFS	40% AA and 1.25% FA/50 mg L ⁻¹ Co ²⁺	Coiled PTFE	12	This work

^a single element mode ICP-MS; ^b multi-element mode ICP-MS.

The LOD with PVG-AFS can be also easily compared to that achieved with HG [45] using the same AFS instrumentation and settings. The absolute LOD obtained with PVG was around 8 times higher which can be attributed to several aspects – all are associated with the disturbance in sensitivity or SD (blank). Firstly, the generation efficiency for PVG approach was around 54% while $\geq 90\%$ is expected for HG. Secondly, a full width at half maximum of the measured peaks was ca. 2-fold greater which necessitated longer integration time for evaluation. And finally, the SD (blank) was affected by a contamination, resulting in the peak shaped blank signals as treated above.

In order to validate the PVG-AFS methodology, Bi content was determined in SRM NIST 1643f. This material is stabilized in 0.32 mol L⁻¹ nitric acid, which represents a huge obstacle as a severe interference from nitric acid was observed even at mM level (see Fig. 5). There is no effective and universal solution to negate these interferences and a sample dilution or evaporation of sample to dryness and its redissolving with the reaction medium is usually employed [65]. Very recently Mollo et al. [66] described a way to negate interferences of HNO₃ (up to 21% w/w) for the PVG of Se by treating the sample with formaldehyde and evaporating it to near dryness. Other potential procedures were investigated by Lopes et al. [65] and only a reduction of NO₃⁻ by hydrazine sulfate during UV irradiation at basic pH and subsequent elimination of residual NO₂⁻ with sulfamic acid was found the most suitable for nitrate removal. These sample preparation scenarios are rather laborious and may be a potential source of contamination. Moreover, the treatment with formaldehyde [66] was not found to be as effective in our work and provided unreliable results. Hence, a simple evaporation to dryness, dissolving with the reaction medium containing Co²⁺ as the sensitizer had been applied before the sample was subjected to analysis by PVG-AFS. The Bi content was determined using a standard additions technique (comprising of two spiked concentrations) and the recovery was evaluated as a ratio of slope of standard additions to a slope of external calibration. The determined content of 12.1 ± 0.9 µg L⁻¹ is in good agreement with the certified value of 12.62 ± 0.11 µg L⁻¹ and the recovery of 97 ± 5% suggests efficient removal of nitric acid enabling fit-for-purpose quantification even using external calibration. Very similar concentration of 12.0 ± 1.1 µg L⁻¹ was also quantified by PVG-ICP-MS using the same analytical treatment.

4. Conclusion

PVG of Bi was conducted in the PTFE reactor wrapped around the standard germicidal Hg low-pressure tube lamp for the first time. In addition to earlier reported sensitizing effect of Fe³⁺ [35] and Co²⁺ [38,39], the positive effect of Cu²⁺ and Cd²⁺ was also demonstrated. Nevertheless, only Co²⁺ ions are recommended as the sensitizer in terms of the sufficient overall PVG efficiency and long-term stability of the analytical performance. A great effort was made to determine the overall PVG efficiency. Fairly high efficiency of 54% suggests that irradiation with 254 nm line is sufficient for PVG of Bi because our arrangement does not permit efficient irradiation with 185 nm in comparison to the thin-film flow-through photoreactors used by other authors previously

[35–38]. Unlike these special photoreactors, our photoreactor can be easily fabricated in a laboratory.

This work also represents the first study of conditions of atomization in the flame atomizers for AFS following the PVG. While the analytical performance of MDF seems to be independent of the generation technique (PVG vs. HG), the conditions of atomization in FIGS need to be adapted (increase of the oxygen supply) due to the presence of organic acid vapors released from the generator. Although the achieved LOD is still limited with the analyte contamination, it is by one order of magnitude lower than that achieved in the only study published on Bi determination by PVG-AFS [5].

CRedit authorship contribution statement

Jaromír Vyhnanovský: Investigation, Formal analysis, Visualization, Writing - original draft, Writing - review & editing. **Dilek Yildiz:** Investigation, Formal analysis. **Barbora Štádlarová:** Investigation, Formal analysis, Funding acquisition, Writing - review & editing. **Stanislav Musil:** Conceptualization, Visualization, Data curation, Funding acquisition, Project administration, Supervision, Writing - review & editing.

Declaration of Competing Interest

The authors declare that they have no known competing financial interests or personal relationships that could have appeared to influence the work reported in this paper.

Acknowledgements

The support of the Czech Science Foundation (Project No. 19-17604Y), Czech Academy of Sciences (Institutional support RVO: 68081715) and Charles University (project SVV260560 and GAUK 1048120) is gratefully acknowledged. The authors are much obliged to Prof. Jiří Dědina for his valuable comments to the manuscript.

References

- [1] M. Filella, How reliable are environmental data on 'orphan' elements? the case of bismuth concentrations in surface waters, *J. Environ. Monit.* 12 (2010) 90–109.
- [2] R.E. Sturgeon, Photochemical vapor generation: a radical approach to analyte introduction for atomic spectrometry, *J. Anal. At. Spectrom.* 32 (2017) 2319–2340.
- [3] X. Guo, R.E. Sturgeon, Z. Mester, G.J. Gardner, Vapor generation by UV irradiation for sample introduction with atomic spectrometry, *Anal. Chem.* 76 (2004) 2401–2405.
- [4] C.B. Zheng, Y. Li, Y.H. He, Q. Ma, X.D. Hou, Photo-induced chemical vapor generation with formic acid for ultrasensitive atomic fluorescence spectrometric determination of mercury: potential application to mercury speciation in water, *J. Anal. At. Spectrom.* 20 (2005) 746–750.
- [5] C.B. Zheng, Q. Ma, L. Wu, X.D. Hou, R.E. Sturgeon, UV photochemical vapor generation-atomic fluorescence spectrometric determination of conventional hydride generation elements, *Microchem. J.* 95 (2010) 32–37.
- [6] H.L. Duan, Z.B. Gong, S.F. Yang, Online photochemical vapour generation of inorganic tin for inductively coupled plasma mass spectrometric detection, *J. Anal. At. Spectrom.* 30 (2015) 410–416.

- [7] K.A. Romanovskiy, M.A. Bolshov, A.V. Münz, Z.A. Temerdashev, M.Y. Burylin, K. A. Sirota, A novel photochemical vapor generator for ICP-MS determination of As, Bi, Hg, Sb, Se and Te, *Talanta* 187 (2018) 370–378.
- [8] T. Xu, J. Hu, H.J. Chen, Transition metal ion Co(II)-assisted photochemical vapor generation of thallium for its sensitive determination by inductively coupled plasma mass spectrometry, *Microchem. J.* 149 (2019), 103972.
- [9] X. Guo, R.E. Sturgeon, Z. Mester, G.J. Gardner, UV vapor generation for determination of selenium by heated quartz tube atomic absorption spectrometry, *Anal. Chem.* 75 (2003) 2092–2099.
- [10] J.A. Nóbrega, R.E. Sturgeon, P. Grinberg, G.J. Gardner, C.S. Brophy, E.E. Garcia, UV photochemical generation of volatile cadmium species, *J. Anal. At. Spectrom.* 26 (2011) 2519–2523.
- [11] E. Nováková, K. Horová, V. Červený, J. Hranáček, S. Musil, UV photochemical vapor generation of Cd from a formic acid based medium: optimization, efficiency and interferences, *J. Anal. At. Spectrom.* 35 (7) (2020) 1380–1388.
- [12] J. Soukal, R.E. Sturgeon, S. Musil, Efficient photochemical vapor generation of molybdenum for ICPMS detection, *Anal. Chem.* 90 (2018) 11688–11695.
- [13] J. Vyhnanovský, R.E. Sturgeon, S. Musil, Cadmium assisted photochemical vapor generation of tungsten for detection by inductively coupled plasma mass spectrometry, *Anal. Chem.* 91 (2019) 13306–13312.
- [14] Z.L. Zhu, D. He, C.Y. Huang, H.T. Zheng, S.C. Zhang, S.H. Hu, High-efficiency photooxidation vapor generation of osmium for determination by inductively coupled plasma-optical emission spectrometry, *J. Anal. At. Spectrom.* 29 (2014) 506–511.
- [15] R. Macedo de Oliveira, D.L.G. Borges, UV photochemical vapor generation of noble metals (Au, Ir, Pd, Pt and Rh): a feasibility study using inductively coupled plasma mass spectrometry and seawater as a test matrix, *J. Anal. At. Spectrom.* 33 (2018) 1700–1706.
- [16] X.M. Guo, R.E. Sturgeon, Z. Mester, G. Gardner, UV photosynthesis of nickel carbonyl, *Appl. Organomet. Chem.* 18 (2004) 205–211.
- [17] H. Deng, C.B. Zheng, L.W. Liu, L. Wu, X.D. Hou, Y. Lv, Photochemical vapor generation of carbonyl for ultrasensitive atomic fluorescence spectrometric determination of cobalt, *Microchem. J.* 96 (2010) 277–282.
- [18] C. Zheng, L. Yang, R.E. Sturgeon, X. Hou, UV Photochemical vapor generation sample introduction for determination of Ni, Fe, and Se in biological tissue by isotope dilution ICPMS, *Anal. Chem.* 82 (2010) 3899–3904.
- [19] Y. Gao, R.E. Sturgeon, Z. Mester, E. Pagliano, R. Galea, P. Saull, X.D. Hou, L. Yang, On-line UV photochemical generation of volatile copper species and its analytical application, *Microchem. J.* 124 (2016) 344–349.
- [20] P. Grinberg, R.E. Sturgeon, Photochemical vapor generation of iodine for detection by ICP-MS, *J. Anal. At. Spectrom.* 24 (2009) 508–514.
- [21] J. Hu, R.E. Sturgeon, K. Nadeau, X. Hou, C. Zheng, L. Yang, Copper ion assisted photochemical vapor generation of chlorine for its sensitive determination by sector field inductively coupled plasma mass spectrometry, *Anal. Chem.* 90 (2018) 4112–4118.
- [22] R.E. Sturgeon, Detection of bromine by ICP-oe-ToF-MS following photochemical vapor generation, *Anal. Chem.* 87 (2015) 3072–3079.
- [23] R.E. Sturgeon, E. Pagliano, Evidence for photochemical synthesis of fluoromethane, *J. Anal. At. Spectrom.* 35 (2020) 1720–1726.
- [24] Y. He, X. Hou, C. Zheng, R.E. Sturgeon, Critical evaluation of the application of photochemical vapor generation in analytical atomic spectrometry, *Anal. Bioanal. Chem.* 388 (2007) 769–774.
- [25] R.E. Sturgeon, P. Grinberg, Some speculations on the mechanisms of photochemical vapor generation, *J. Anal. At. Spectrom.* 27 (2012) 222–231.
- [26] D. Leonori, R.E. Sturgeon, A unified approach to mechanistic aspects of photochemical vapor generation, *J. Anal. At. Spectrom.* 34 (2019) 636–654.
- [27] Z.R. Zou, J. Hu, F.J. Xu, X.D. Hou, X.M. Jiang, Nanomaterials for photochemical vapor generation-analytical atomic spectrometry, *TrAC, Trends Anal. Chem.* 114 (2019) 242–250.
- [28] Y. Wang, L. Lin, J. Liu, X. Mao, J. Wang, D. Qin, Ferric ion induced enhancement of ultraviolet vapour generation coupled with atomic fluorescence spectrometry for the determination of ultratrace inorganic arsenic in surface water, *Analyst* 141 (2016) 1530–1536.
- [29] J. Zhou, D. Deng, Y.Y. Su, Y. Lv, Determination of total inorganic arsenic in water samples by cadmium ion assisted photochemical vapor generation-atomic fluorescence spectrometry, *Microchem. J.* 146 (2019) 359–365.
- [30] F. Xu, Z. Zou, J. He, M. Li, K. Xu, X. Hou, In situ formation of nano-CdSe as a photocatalyst: cadmium ion-enhanced photochemical vapour generation directly from Se(VI), *Chem. Commun. (Cambridge, U. K.)* 54 (2018) 4874–4877.
- [31] Y. Gao, M. Xu, R.E. Sturgeon, Z. Mester, Z. Shi, R. Galea, P. Saull, L. Yang, Metal ion-assisted photochemical vapor generation for the determination of lead in environmental samples by multicollector-ICPMS, *Anal. Chem.* 87 (2015) 4495–4502.
- [32] W. Zeng, J. Hu, H.J. Chen, Z.R. Zou, X.D. Hou, X.M. Jiang, Cobalt ion-enhanced photochemical vapor generation in a mixed acid medium for sensitive detection of tellurium(IV) by atomic fluorescence spectrometry, *J. Anal. At. Spectrom.* 35 (2020) 1405–1411.
- [33] H. He, X. Peng, Y. Yu, Z. Shi, M. Xu, S. Ni, Y. Gao, Photochemical vapor generation of tellurium: synergistic effect from ferric ion and nano-TiO₂, *Anal. Chem.* 90 (2018) 5737–5743.
- [34] J. Hu, H. Chen, X. Hou, X. Jiang, Cobalt and Copper Ions Synergistically Enhanced Photochemical Vapor Generation Of Molybdenum: Mechanism Study And Analysis Of Water Samples, *Anal. Chem.* 91 (2019) 5938–5944.
- [35] Y. Yu, Y. Jia, Z. Shi, Y. Chen, S. Ni, R. Wang, Y. Tang, Y. Gao, Enhanced photochemical vapor generation for the determination of bismuth by inductively coupled plasma mass spectrometry, *Anal. Chem.* 90 (2018) 13557–13563.
- [36] Y. Jia, Q. Mou, Y. Yu, Z. Shi, Y. Huang, S. Ni, R. Wang, Y. Gao, Reduction of Interferences Using Fe-Containing Metal-Organic Frameworks for Matrix Separation and Enhanced Photochemical Vapor Generation of Trace Bismuth, *Anal. Chem.* 91 (2019) 5217–5224.
- [37] Y. Zhen, Y. Yu, A. Zhang, Y. Gao, Matrix-assisted photochemical vapor generation for determination of trace bismuth in FeNi based alloy samples by inductively coupled plasma mass spectrometry, *Microchem. J.* 151 (2019), 104242.
- [38] Y. Yu, Q. Zhao, H.L. Bao, Q. Mou, Z.M. Shi, Y.L. Chen, Y. Gao, Determination of trace bismuth in environmental waters by ICP-MS with cobalt ion-assisted photochemical vapour generation, *Geostand. Geoanal. Res.* 44 (2020) 617–627.
- [39] J. Vyhnanovský, D. Yıldız, S. Musil, Effect of metal sensitizers on photochemical vapor generation of bismuth for analytical atomic spectrometry, in: K. Nesměrál (Ed.) 15th International Students Conference Modern Analytical Chemistry, Prague, 2019, pp. 257–262.
- [40] T. Matoušek, The efficiency of chemical vapour generation of transition and noble metals, *Anal. Bioanal. Chem.* 388 (2007) 763–767.
- [41] M. Rybinová, S. Musil, V. Červený, M. Vobecký, P. Rychlovský, UV-photochemical vapor generation of selenium for atomic absorption spectrometry: optimization and Se-75 radiotracer efficiency study, *Spectrochim. Acta, Part B* 123 (2016) 134–142.
- [42] H.E. Pace, N.J. Rogers, C. Jarolimek, V.A. Coleman, C.P. Higgins, J.F. Ranville, Determining transport efficiency for the purpose of counting and sizing nanoparticles via single particle inductively coupled plasma mass spectrometry, *Anal. Chem.* 83 (2011) 9361–9369.
- [43] S. Cuello-Núñez, I. Abad-Álvarez, D. Bartczak, M.E. del Castillo Busto, D.A. Ramsay, F. Pellegrino, H. Goenaga-Infante, The accurate determination of number concentration of inorganic nanoparticles using spICP-MS with the dynamic mass flow approach, *J. Anal. At. Spectrom.* 35 (2020) 1832–1839.
- [44] A. Gustavsson, The determination of some nebulizer characteristics, *Spectrochim. Acta, Part B* 39 (1984) 743–746.
- [45] B. Štádlířová, M. Kolrosová, J. Dědina, S. Musil, Atomic fluorescence spectrometry for ultrasensitive determination of bismuth based on hydride generation – the role of excitation source, interference filter and flame atomizers, *J. Anal. At. Spectrom.* 35 (2020) 993–1002.
- [46] D. Qin, F. Gao, Z. Zhang, L. Zhao, J. Liu, J. Ye, J. Li, F. Zheng, Ultraviolet vapor generation atomic fluorescence spectrometric determination of mercury in natural water with enrichment by on-line solid phase extraction, *Spectrochim. Acta, Part B* 88 (2013) 10–14.
- [47] K. Marschner, S. Musil, J. Dědina, Flame-in-gas-shield and miniature diffusion flame hydride atomizers for atomic fluorescence spectrometry: optimization and comparison, *Spectrochim. Acta, Part B* 109 (2015) 16–23.
- [48] S. Musil, T. Matoušek, J.M. Currier, M. Stýblo, J. Dědina, Speciation analysis of arsenic by selective hydride generation-cryotrapping-atomic fluorescence spectrometry with flame-in-gas-shield atomizer: achieving extremely low detection limits with inexpensive instrumentation, *Anal. Chem.* 86 (2014) 10422–10428.
- [49] K. Marschner, S. Musil, J. Dědina, Achieving 100% efficient postcolumn hydride generation for as speciation analysis by atomic fluorescence spectrometry, *Anal. Chem.* 88 (2016) 4041–4047.
- [50] U. Heitmann, B. Welz, D.L.G. Borges, F.G. Lepri, Feasibility of peak volume, side pixel and multiple peak registration in high-resolution continuum source atomic absorption spectrometry, *Spectrochim. Acta, Part B* 62 (2007) 1222–1230.
- [51] Y. Arslan, S. Musil, T. Matoušek, J. Kratzer, J. Dědina, Gold volatile species atomization and preconcentration in quartz devices for atomic absorption spectrometry, *Spectrochim. Acta, Part B* 103 (2015) 155–163.
- [52] J. Soukal, O. Benada, T. Matoušek, J. Dědina, S. Musil, Chemical generation of volatile species of copper—optimization, efficiency and investigation of volatile species nature, *Anal. Chim. Acta* 977 (2017) 10–19.
- [53] J. Vyhnanovský, J. Kratzer, O. Benada, T. Matoušek, Z. Mester, R.E. Sturgeon, J. Dědina, S. Musil, Diethylthiocarbamate enhanced chemical generation of volatile palladium species, their characterization by AAS, ICP-MS, TEM and DART-MS and proposed mechanism of action, *Anal. Chim. Acta* 1005 (2018) 16–26.
- [54] K. Buřková, S. Musil, J. Kratzer, P. Dvořák, M. Mrkvíčková, J. Voráč, J. Dědina, Generation of tellurium hydride and its atomization in a dielectric barrier discharge for atomic absorption spectrometry, *Spectrochim. Acta, Part B* 171 (2020), 105947.
- [55] C. Zheng, R.E. Sturgeon, C. Brophy, X. Hou, Versatile thin-film reactor for photochemical vapor generation, *Anal. Chem.* 82 (2010) 3086–3093.
- [56] H. Matusiewicz, M. Slachcinski, Ultrasonic Nebulization/UV Photolysis Vapor Generation Sample Introduction System for the Determination of Conventional Hydride (As, Bi, Sb, Se, Sn) and Cold Vapor (Hg, Cd) Generation Elements in Reference Materials in the Presence of Acetic Acid by Microwave-Induced Plasma Spectrometry, *Spectrosc. Lett.* 46 (2013) 315–326.
- [57] P. Grinberg, Z. Mester, R.E. Sturgeon, A. Ferretti, Generation of volatile cobalt species by UV photoreduction and their tentative identification, *J. Anal. At. Spectrom.* 23 (2008) 583–587.

- [58] H.C. de Jesus, P. Grinberg, R.E. Sturgeon, System optimization for determination of cobalt in biological samples by ICP-OES using photochemical vapor generation, *J. Anal. At. Spectrom.* 31 (2016) 1590–1604.
- [59] M. Bideau, B. Claudel, L. Faure, M. Rachimoallah, Homogeneous and heterogeneous photoreactions of decomposition and oxidation of carboxylic acids, *J. Photochem.* 39 (1987) 107–128.
- [60] Y. Gao, R.E. Sturgeon, Z. Mester, X. Hou, C. Zheng, L. Yang, Direct determination of trace antimony in natural waters by photochemical vapor generation ICPMS: method optimization and comparison of quantitation strategies, *Anal. Chem.* 87 (2015) 7996–8004.
- [61] A. D'Ulivo, I. Paolicchi, M. Onor, R. Zamboni, L. Lampugnani, Flame-in-gas-shield miniature flame hydride atomizers for ultra trace element determination by chemical vapor generation atomic fluorescence spectrometry, *Spectrochim. Acta, Part B* 64 (2009) 48–55.
- [62] J. Dédina, Atomization of volatile compounds for atomic absorption and atomic fluorescence spectrometry: on the way towards the ideal atomizer, *Spectrochim. Acta, Part B* 62 (9) (2007) 846–872.
- [63] I.B. Karadjova, L. Lampugnani, M. Onor, A. D'Ulivo, D.L. Tsalev, Continuous flow hydride generation-atomic fluorescence spectrometric determination and speciation of arsenic in wine, *Spectrochim. Acta, Part B* 60 (2005) 816–823.
- [64] I.B. Karadjova, L. Lampugnani, J. Dédina, A. D'Ulivo, M. Onor, D.L. Tsalev, Organic solvents as interferents in arsenic determination by hydride generation atomic absorption spectrometry with flame atomization, *Spectrochim. Acta, Part B* 61 (2006) 525–531.
- [65] G.S. Lopes, R.E. Sturgeon, P. Grinberg, E. Pagliano, Evaluation of approaches to the abatement of nitrate interference with photochemical vapor generation, *J. Anal. At. Spectrom.* 32 (2017) 2378–2390.
- [66] A. Mollo, M. Knochen, Towards the abatement of nitrate interference on selenium determination by photochemical vapor generation, *Spectrochim. Acta, Part B* 169 (2020), 105875.



Comparison of bismuth atomic lamps for a non-dispersive atomic fluorescence spectrometry

Barbora Štádlarová^{a,b,*}, Jiří Dědina^a, Stanislav Musil^a

^a Institute of Analytical Chemistry of the Czech Academy of Sciences, Veveří 97, Brno 602 00, Czech Republic

^b Charles University, Faculty of Science, Department of Analytical Chemistry, Albertov 6, Prague 128 43, Czech Republic

ARTICLE INFO

Keywords:

Atomic fluorescence spectrometry
Bismuth
Hydride generation
Radiation source

ABSTRACT

The performance of two types of radiation sources – an electrodeless discharge lamp (EDL) and a boosted discharge hollow cathode lamp (Superlamp) – for atomic fluorescence spectrometry (AFS) was studied and compared using bismuth as a model analyte at 222.8 and 223.1 nm fluorescence lines. Hydride generation was used for analyte introduction to a miniature diffusion flame where the generated bismuthane was atomized. An in-house assembled non-dispersive atomic fluorescence spectrometer was adjusted so that either of the sources could be employed. The optimization of the radiation sources at chosen 40 Hz modulation rate included a duty cycle and applied currents (primary and boost), in addition to proper focusing on the flame atomizer. With optimum operation parameters the sensitivity achieved with the EDL was around an order of magnitude higher than that with the Superlamp, in agreement with the higher radiation intensity measured by an optical power meter and resulting limits of detection of 1.5 pg and 11 pg, for the EDL and the Superlamp, respectively.

1. Introduction

Atomic fluorescence spectrometry (AFS) coupled to hydride generation (HG) has the potential to reach very low limits of detection (LODs) and because of its low purchase and operating costs, it provides an attractive alternative even to mass spectrometric techniques. Its advantages over AAS in terms of LOD and linear range were demonstrated a long time ago [1,2], however, the potential of HG-AFS to reach such LODs can generally be fully achieved only when using very mild atomization conditions which are typically compatible with the atomization of volatile hydrides. This is the reason why AFS is currently associated prevalently with HG [3].

The simple and sensitive non-dispersive AFS apparatus [4] employs an interference filter for the selection of the detection wavelength interval placed in front of a detector, typically a photomultiplier [1,5–11]. The other two essential components of a non-dispersive atomic fluorescence spectrometer include a radiation source and an atomizer. Even though the simple apparatus can be easily assembled from available components [5,7,12], HG-AFS became a widely used analytical tool for the determination of elements forming volatile hydrides after the availability of the first commercial AFS instrument [8] and since that time it has been considered as a well-established technique for the

determination of mercury and hydride forming elements (As, Sb, Se, Bi, etc.) [13].

Since the introduction of AFS as an analytical method in 1964 [14,15], mainly two types of line radiation sources have been used - the hollow cathode lamp [16], as well as its high intensity version, i.e., boosted discharge hollow cathode lamp [17], and the electrodeless discharge lamps (EDL) [14,18–20]. Their construction has developed and the lamps have begun to be produced commercially, but their status among the most used sources in AFS remained unchanged up until today. Nowadays, the EDLs contain a small amount of the element to be determined or its volatile salt sealed in a quartz bulb filled with an inert gas that is placed inside a radiofrequency generator. The principle of the emission of a characteristic line spectrum from the lamp lies in the ionization of the inert gas by a radiofrequency field and subsequent vaporization, atomization and excitation of the element [21]. The boosted discharge hollow cathode lamp (Superlamp, as called by the manufacturer) consists of an anode, a cylindrical cathode made of the element of interest and a second “hot” cathode. The normal sputtering discharge operates between the anode and the cylindrical cathode. The secondary discharge, provided by the secondary cathode, improves the excitation efficiency of the sputtered atoms significantly [22]. Among the advantages of the Superlamp is most importantly the market

* Corresponding author at: Institute of Analytical Chemistry of the Czech Academy of Sciences, Veveří 97, Brno 602 00, Czech Republic.
E-mail address: stadlerova@iach.cz (B. Štádlarová).

availability for various analytes and relatively fast stabilization time of its emission intensity. Conversely, the EDLs are believed to provide higher intensity, but need substantially longer stabilization. In addition, their use is limited to volatile hydride forming elements, Hg, Cd, Cs, Rb and P [21].

To the best of our knowledge, any direct comparison of these two currently available radiation sources in terms of emission intensity and sensitivity in AFS has not been provided yet. This may be to some extent due to the fact that commercially available spectrometers [8,23] exclusively employ the Superlamp as the radiation source while EDLs are predominantly used as the radiation sources in laboratory-made research-grade spectrometers [7,12]. In their study, D'Ulivo et al. [11] examined the LODs achieved for As, Bi, Sb and Se using a laboratory-assembled non-dispersive AFS instrument that employed EDL as the excitation source. They compared these LODs with those achieved using a commercial spectrometer equipped with the Superlamp [24]. It was found that the EDL provided 2.5–10-fold lower LODs for all the aforementioned analytes [11]. However, it cannot be ruled out that other factors may have contributed to the lower LODs, in addition to the type of the radiation source, such as the atomization/detection step.

The aim of this work was to study and optimize the conditions of operation of the EDL and Superlamp and to compare the sources according to the analytical characteristics obtained for the methodology of bismuth determination by HG-AFS using a laboratory-made non-dispersive atomic fluorescence spectrometer with a miniature diffusion flame (MDF) atomizer. In this vein, the absolute intensity of emitted radiation of a relevant spectral line emitted from both radiation sources was assessed.

2. Experimental

2.1. Reagents and chemicals

Deionized water was used for preparation of all solutions. A 0.5% (m/v) NaBH_4 in 0.4% (m/v) KOH was used as a reductant. A stock solution of 1 mol L^{-1} HCl (Merck, Germany) was used as a carrier and blank. Working Bi solutions were prepared fresh daily by serial dilution of a 1000 mg L^{-1} Bi standard (Sigma-Aldrich, Germany) in 1 mol L^{-1}

HCl. Compressed gases Ar (99.996% purity) and H_2 (99.95% purity) were sourced from SIAD Czech, Ltd.

2.2. Hydride generator

The employed flow injection hydride generator was identical to that described previously [25]. The continuous flows of the reductant (1.2 mL min^{-1}) and the carrier (4 mL min^{-1}) were employed. The Bi standard solution (1 mL) was manually injected by means of an injection valve into the flow of the carrier and subsequently merged with the reductant. A glass gas-liquid separator (GLS) with a forced waste removal served to separate the gas phase containing bismuthane from the liquid phase which continued to the waste. 80 mL min^{-1} argon was introduced upstream the GLS after merging of the carrier and reductant. The flow rate of hydrogen evolving from the reaction in the GLS was approximately 15 mL min^{-1} .

2.3. Atomic fluorescence spectrometer

A laboratory-made non-dispersive atomic fluorescence spectrometer is described in detail in Ref. [25]. It consists of three main components – radiation source, atomizer and detector with an interference filter (Fig. 1).

2.3.1. Atomizer

The MDF atomizer was a vertical quartz tube (6 mm i.d.) with a side inlet arm (see Ref. [25] for a description and details on the optimization of the atomization conditions for Bi). It was supplied with the gas phase leaving the GLS (80 mL min^{-1} argon and 15 mL min^{-1} hydrogen from decomposition of NaBH_4) that was further mixed with additional flows of argon (420 mL min^{-1}) and hydrogen (85 mL min^{-1}) in order to maintain a stable flame. Consequently, the total gas flow rate to the atomizer was 600 mL min^{-1} comprising 500 mL min^{-1} argon and 100 mL min^{-1} hydrogen. All the introduced gas flow rates were controlled by mass flow controllers. The observation height defined as the distance from the top of the support tube to the center of the optical beam was 7 mm during measurements.

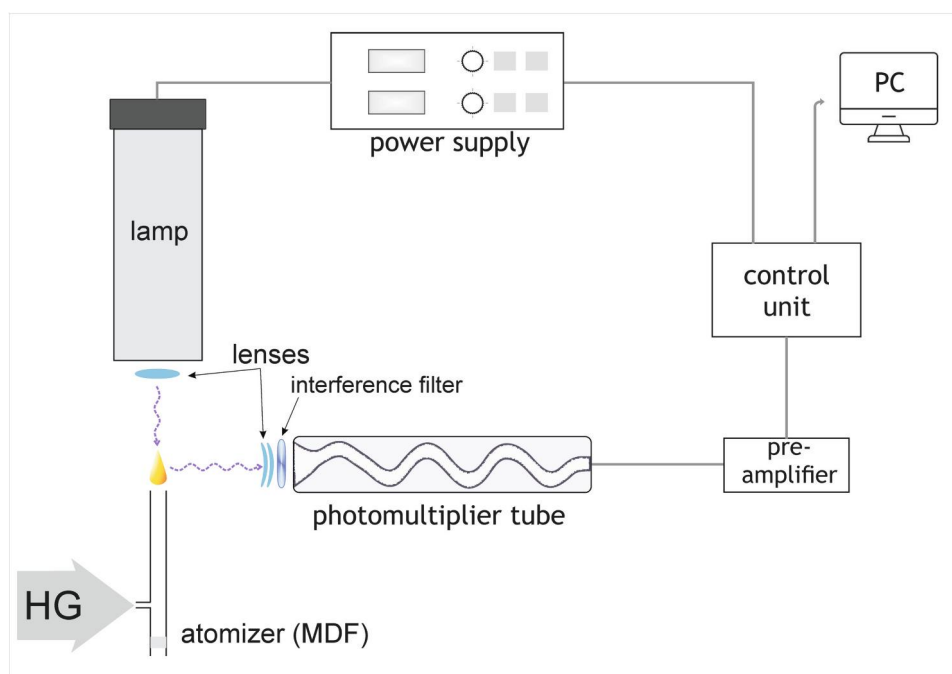


Fig. 1. Experimental setup of the atomic fluorescence spectrometer.

2.3.2. Radiation sources

A Bi EDL (System 2, PerkinElmer, USA) and a Bi Superlamp (P806SF, Photron, Australia) were employed as the radiation sources. A dual-channel power supply incorporating a radiofrequency lamp driver was used for operating the EDL. A power supply for the operation and modulation of the primary current for the Superlamp was constructed by a DIRAM company (Prague, Czech Republic). A commercial Superlamp power supply (P200, 3 V, Photron, Australia) was used to add an arbitrary boost current on the Superlamp. This device allows only to transmit a boost current at the same modulation rate as used for the primary current. The feeding current for both the EDL and Superlamp was square-wave modulated with a duty cycle of either 52% or 28% at frequency of 40 Hz.

The radiation from the EDL was focused onto the volume of the flame using a combination of two UV fused silica lenses: a planoconvex lens ($d = 25$ mm, focal length 40 mm) and a biconvex lens ($d = 22$ mm, focal length 45 mm). The Superlamp was placed in a plastic tube of the same dimensions as the EDL and a UV fused silica planoconvex lens ($d = 25$ mm, focal length 40 mm), in a circular holder, was attached to the rim of this tube.

2.3.3. Fluorescence detector

The detector was oriented perpendicularly to the lamp to collect the fluorescence radiation emitted by the analyte from the atomizer, as can be seen in Fig. 1. A combination of two positive meniscus UV fused silica lenses ($d = 17$ and 22 mm; 21 mm focal length) was used to focus the produced radiation on the entrance window of the solar-blind channel photomultiplier (PMT, MH 1922, 165–320 nm, PerkinElmer Optoelectronics, USA). The interference filter (222.63 nm, full width at half maximum 10 nm, Melles Griot, USA), covering the Bi fluorescence lines at 222.8 and 223.1 nm was used for the detection wavelength selection.

The preamplifier, control unit synchronizing modulation of the lamps and fluorescence emission reading, and a dedicated software were designed by DIRAM company (Prague, Czech Republic).

2.4. Other detectors

A miniature fiber optics UV–vis spectrometer BLACK-Comet C (StellarNet Inc., USA) was employed to acquire the emission spectra of both radiation sources, see Ref. [25] for details. The intensity of the emitted radiation from both radiation sources was measured with the 1918-C Optical Meter (Newport, USA) equipped with a high performance photodiode sensor (UV Silicon detector, 200–1100 nm, OD3 attenuator, DB15z, Newport, USA). The radiation from the lamps was focused using the same lenses as described in Section “Radiation sources” for atomic fluorescence measurements and the distance from the lens to the sensor window was 22 mm. This arrangement made it possible to focus the maximum fraction of the radiation emitted from both lamps on the sensor window. The radiation passed through an interference filter with a central wavelength at 307.1 nm (full width at half maximum 10 nm, peak transmittance 17%, Edmund Optics, USA) to cover the most intensive Bi emission lines at 306.8 and 307.7 nm. The output from the detector thus yielded the radiation intensity of the aforementioned Bi lines (in W) integrated over the lamp image, averaged over the modulation period. It should be highlighted that the registered intensity was attenuated due to the absorption in the interference filter.

2.5. Measurement procedure and data evaluation

The Bi standard was injected into the hydride generator 5 s after the signal recording had started. Total time for the signal recording was 60 s. The detector output provided signals in μV . Peak area (in $\mu\text{V s}$) and peak height (in μV) were corrected to the baseline.

All the given peak areas are presented as median ($n \geq 3$) \pm standard deviation (SD). Signal to noise ratio (SNR) was determined by dividing

the peak height corresponding to Bi standard by an average standard deviation of three baseline measurements (each measured for 20 s, representing thus 800 values). For the baseline measurements, the carrier was used as the sample. LOD was calculated as $3 \times \text{SD}$ of peak area of blank ($n = 10$) divided by the slope of the calibration function.

3. Results and discussion

The optimization of Bi determination by HG-AFS with the use of the EDL is covered in our previous work [25]. The conditions of HG and atomization were adopted for the present study which is focused on optimization of Superlamp parameters and on the comparison of the performance of the EDL and the Superlamp. It should be highlighted that the EDL and the Superlamp differ in their emission spectra (Fig. 2). The presented intensities of emitted radiation of both lamps are not in the same scale as they were not recorded with the same geometry. There are more lines present in the EDL emission spectrum. It has been shown that the EDL contains especially Sb impurities responsible for emission lines at 206.8, 217.6, 217.9, 228.9, 231.2, 252.9, 259.8 and 261.2 nm but also Hg responsible for emission line at 253.7 [25].

3.1. Introductory considerations

The temporal value of the AFS signal, resulting from analyte introduction in the flow injection mode, is given by a product of two basically independent variables: (1) a supply function, which is the analyte mass delivered to the spectrometer per time unit in the form of volatile species (dimension: mass/time) and (2) the proportionality factor (S , dimension: detector output \times time/mass), which in fact represents the sensitivity of the particular spectrometer employed [3,25]. The spectrometer sensitivity (S) is controlled by spectroscopic character of the given analyte (atomic absorption coefficient and oscillator strength), by atomizer parameters (such as atomizer geometry and temperature, gas flow rate and atomization efficiency) and by geometry and character of the radiation and detection train. Especially, it is directly proportional to radiation intensity focused to the atomizer [3,26–28]. S is actually the peak area sensitivity, i.e., slope of the calibration peak area versus analyte mass and it is very useful and simple to estimate parameter characterizing sensitivity of the employed spectrometer. However, the relevant metric for practical analysis is the LOD. When the analytical parameter is the peak area, LOD (dimension: mass) depends on the SD of repeated blank measurements (SD_{blank}). LOD is a fundamental quantity but its rigorous determination is rather time consuming. Therefore, an auxiliary parameter - SNR, is employed for optimizations of the spectrometer:

$$\text{SNR} = H / \text{SD}_{\text{baseline}} \quad (1)$$

where H and $\text{SD}_{\text{baseline}}$, respectively, stand for the peak height and SD of repeated baseline measurements. Obviously, LOD is inversely proportional to SNR. Even though the proportionality constant cannot be analytically expressed, SNR, which can be estimated much faster than LOD, is a very convenient measure of the potential of the given spectrometer setup in terms of LOD.

For all the optimizations and comparisons treated below, the spectrometer sensitivity S , SNR, LOD and the intensity of the radiation source were the relevant parameters. The first three parameters were evaluated for the spectrometer setup described in Experimental section employing the interference filter with a central wavelength at 222.63 nm since it appeared optimal for Bi determination with the MDF atomizer [25]. However, the intensity of the radiation source was characterized by measuring the emission of the lamps after passing through an interference filter with a central wavelength at 307.1 nm. The reason for that was a low sensitivity of the photodiode sensor at the wavelength around 223 nm. This wavelength was chosen because it covers the most intensive Bi emission lines (see Fig. 2) and it is also reliably detected by the

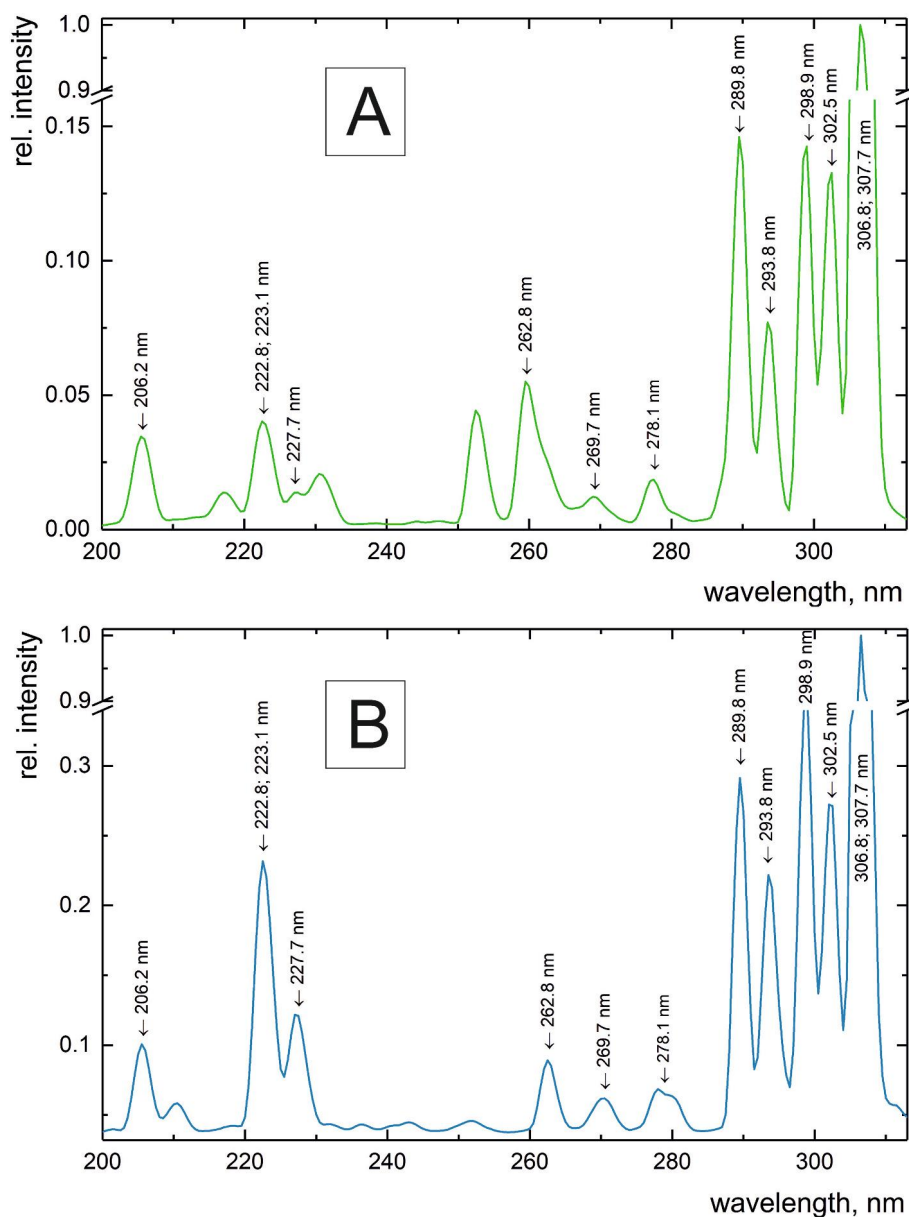


Fig. 2. Emission spectra of (A) EDL and (B) Superlamp of Bi. Intensities shown are related to that of the most intensive line at 307 nm, the arrows indicate the most intense Bi lines.

photodiode sensor.

Typically, *SNR* was used for optimizations whereas *LOD*, *S* and the intensity of the radiation source were evaluated for final comparisons.

3.2. Optimization of the optical path

The essential point to be addressed when optimizing the setup of a laboratory-made spectrometer is the optical path, i.e., the arrangement of radiation source, atomizer and detector.

The distance between the atomizer and the PMT, including all the optical elements attached (meniscus lenses, diaphragms and interference filter, see Fig. 1), should be as short as possible. The minimum feasible distance between the axis of the atomizer support tube and the meniscus lenses was 12 mm. The lenses were not significantly affected by the burning flame at such a distance (increase only by ca. 3 °C compared to the ambient temperature).

Due to a difference in the dimension of the EDL and Superlamp (o.d. 51 and 37 mm, respectively) and the resulting cross-section of the

emitted radiation at the exit of the lamp (ca. 50 and 25 mm, respectively), the focusing of the emitted radiation onto the volume of the flame needed to be addressed individually. In the case of the EDL, a combination of two lenses appeared to be optimal: a planoconvex lens was inserted into the exit orifice of the cavity (see Fig. 3) containing the bulb and a biconvex lens, in a circular lens holder, was attached to the rim of the lamp. This setup resulted in the 13 mm distance between the

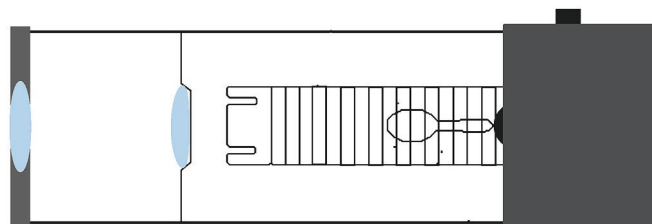


Fig. 3. Location of the planoconvex and biconvex lenses in the EDL.

lens plane and the axis of the atomizer support tube and in approximately 5 mm radius of a vertical cross-section of the radiation beam (circular) above the vertical axis of the atomizer [25]. The radiation beam from the Superlamp was focused using a planoconvex lens ($d = 25$ mm) with 40 mm focal length attached to the rim of the lamp, which resulted in the highest sensitivity. The optimum distance between the lens plane and the axis of the atomizer support tube corresponded to 20 mm and the vertical cross-section of the radiation beam (circular) above the vertical axis of the atomizer corresponded to approximately 2 mm.

3.3. Optimization of the radiation sources

The other important point to be addressed is the optimization of the operational parameters of radiation sources. For the EDL, the previously optimized parameters included operating current of 400 mA and 52% duty cycle at the frequency of 40 Hz (13 ms lamp on, 12 ms lamp off) [25].

This work is focused on the optimization of operational parameters of the Superlamp that include the duty cycle, the primary current and the boost current. Firstly, it was found that for zero boost current, which means that the lamp operated as a standard hollow cathode lamp, the optimum conditions were 18 mA of primary current and 28% duty cycle (during a 25 ms period the lamp is powered only for the first 7 ms). These conditions at 28% duty cycle were taken as default for the boost current optimization, illustrated in Fig. 4.

Primary current of 18 mA and boost current of 12 mA were selected as optimal yielding 4-fold SNR than for zero boost current. In addition, it was observed that the optimum boost current was higher at lower primary currents. For instance, if primary current of 10 mA was employed, the highest sensitivity and SNR were achieved with boost current of 18 mA, however, such parameters did not yield better results.

The parameters for operating the EDL were partly optimized in our previous study leading to optimal performance at 52% duty cycle and 400 mA power supply [25]. Opposed to the Superlamp, 28% duty cycle did not prove fruitful for the EDL because at 52% duty cycle (the lamp powered for 13 ms and off for 12 ms) higher sensitivity was always reached and the intensity of the emitted radiation was also more stable. The measured baseline that reflected the intensity of the emitted radiation due to light scattering kept drifting at 28% duty cycle and the time necessary to stabilize the radiation intensity was substantially longer.

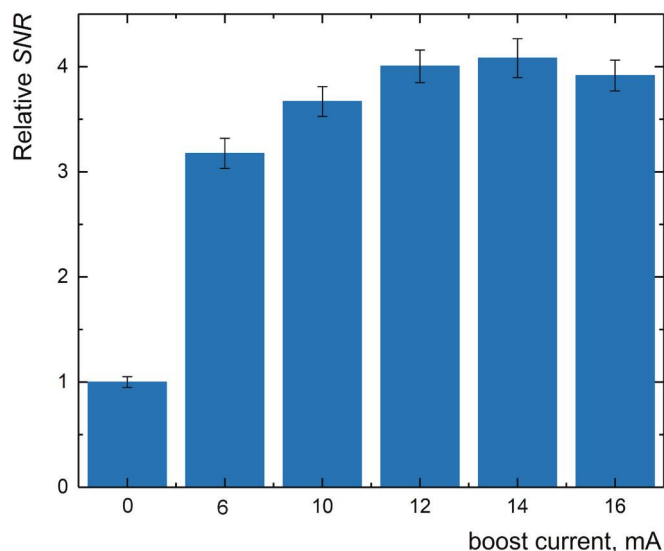


Fig. 4. Relative effect of the boost current at primary current of 18 mA and 28% duty cycle on SNR achieved with the Superlamp. SNR relative to that obtained during operation of the lamp as the hollow cathode lamp (0 mA of boost current), 10 ng L⁻¹ Bi taken for HG.

Note: the typical stabilization time required for the EDL at 52% duty cycle and 400 mA was around 90 min.

It should be highlighted that it is not just the highest SNR that needs to be considered for the choice of the optimum conditions but it is also important to observe the behavior of the lamps in time. Therefore, the final optimum conditions are a compromise of their performance during each experiment and also of their overall endurance. The optimum conditions of operation are summarized in Table 1 together with the optimum conditions of the EDL.

3.4. Assessment of analytical figures of merit

The intensity of the radiation emitted from the lamps was assessed using an optical power meter with a photodiode sensor (see Experimental). A comparison of the radiation intensities emitted from both lamps under their optimum operating conditions is given in Table 2. The line “Intensity” shows the time averaged radiation intensity whereas the line “Effective intensity” stands for the effective radiation intensity, i.e., the intensity during the time interval of the modulation period when the lamp is on. This table contains also the other relevant parameters of both lamps determined at their optimum operating conditions: S , H , SD_{blank} and $SD_{baseline}$. LOD and SNR values, respectively, are estimated from the ratio of S to SD_{blank} and H to $SD_{baseline}$. To make the comparison more complete, the relevant parameters were determined also for Superlamp operated with the duty cycle of 52%, i.e., the same as was found optimum for EDL. The primary and boost currents were optimized for this duty cycle by the same procedure as described above for the 28% duty cycle, see Table 2 for the results.

The substantial feature of data shown in Table 2 is that SD_{blank} is close to the same in all columns suggesting that blanks are not controlled either by contamination or by individual sensitivities. Further, the reasonably good correlation between SD_{blank} and $SD_{baseline}$ indicates that the above discussed approach to optimization based on SNR is well grounded. On the other hand, the proportionality between the effective lamp radiation intensity and measured sensitivity is not absolutely direct. The possible reasons for this discrepancy would be a subject of further investigations.

4. Conclusion

The most important outcome of this work is undoubtedly the direct comparison of two radiation sources - the EDL and the Superlamp – for determination of Bi by HG-AFS using the same laboratory-made non-dispersive atomic fluorescence spectrometer. Such a comparison has not been made yet, since the currently available spectrometers usually allow the use of only one of them. The radiation intensity of the EDL was proven to be higher, as expected, and is reflected in the higher sensitivity and lower LOD, which corresponded to 1.5 ng L⁻¹ (1.5 pg absolute).

The modified setup of our research-grade spectrometer can be now applied to the sensitive determination of an extended number of elements for which the EDLs are not market-available, including transitional metals (Co, Ni, etc.), especially in combination with alternative vapor generation techniques such as photochemical vapor generation [29,30].

Table 1
Optimum operating conditions of the radiation sources.

	EDL	Superlamp
frequency (Hz)	40	40
duty cycle (%)	52	28
current supply (mA)	400	18
boost current (mA)	–	12

Table 2

Analytical parameters of Bi determination by HG-AFS with EDL and Superlamp and their radiation intensities.

	EDL	Superlamp	Superlamp
duty cycle (%)	52	28	52
power supply (mA)	400	18 ^a ; 12 ^b	12 ^a ; 10 ^b
intensity ^c (μW)	5.9 ± 1.1	1.1 ± 0.2	0.88 ± 0.18
effective intensity (μW)	11.3 ± 2.1	3.9 ± 0.7	1.7 ± 0.3
S (μV s ng ⁻¹)	160 ± 23	15 ± 4	9.9 ± 0.2
H (μV ng ⁻¹)	9.7 ± 0.8	0.8 ± 0.2	0.5 ± 0.1
SD _{blank} (μV s)	0.079 ± 0.005	0.05 ± 0.01	0.06 ± 0.01
SD _{baseline} (μV)	0.055 ± 0.008	0.049 ± 0.005	0.04 ± 0.01
SNR ^d	175 ± 30	17 ± 4	13 ± 4
LOD (pg)	1.5	11	18

^a primary current,^b boost current,^c measured with 307.1 nm interference filter,^d related to 1 ng of Bi.

Declaration of Competing Interest

The authors declare that they have no known competing financial interests or personal relationships that could have appeared to influence the work reported in this paper.

Data availability

Data will be made available on request.

Acknowledgements

The support of the Czech Science Foundation (19-17604Y), Czech Academy of Sciences (Institutional support RVO: 68081715) and Charles University (Project SVV260690 and Project GAUK 1048120) is gratefully acknowledged.

References

- [1] K. Tsujii, K. Kuga, Determination of arsenic by non-dispersive atomic fluorescence spectrometry with a gas sampling technique, *Anal. Chim. Acta* 72 (1974) 85–90.
- [2] K.C. Thompson, Atomic-fluorescence determination of antimony, arsenic, selenium and tellurium by using hydride generation technique, *Analyst* 100 (1975) 307–310.
- [3] J. Dédina, Chapter 11, Nonplasma devices for atomization and detection of volatile metal species by atomic absorption and fluorescence, in: A. D'Ulivo, R. Sturgeon (Eds.), *Vapor Generation Techniques for Trace Element Analysis: Fundamental Aspects*, Elsevier, 2022.
- [4] T. Vickers, R. Vaught, Nondispersive atomic fluorescence analysis, *Anal. Chem.* 41 (1969) 1476–1478.
- [5] A. D'Ulivo, AF detectors, in: R.M. Harrison, S. Rapsomanikis (Eds.), *Environmental Analysis Using Chromatography Interfaced with Atomic Spectroscopy*, Ellis Horwood, Chichester, 1989, pp. 127–164.
- [6] P.L. Larkins, R.M. Lowe, J.V. Sullivan, A. Walsh, The use of solar-blind photomultipliers in flame spectroscopy, *Spectrochim. Acta B At. Spectrosc.* 24 (1969) 187–190.
- [7] A. D'Ulivo, P. Papoff, C. Festa, A simultaneous multielement non-dispersive atomic-fluorescence spectrometer using modulated sources and frequency discrimination of fluorescence signals, *Talanta* 30 (1983) 907–913.
- [8] W.T. Corns, P.B. Stockwell, L. Ebdon, S.J. Hill, Development of an atomic fluorescence spectrometer for the hydride-forming elements, *J. Anal. At. Spectrom.* 8 (1993) 71–77.
- [9] P.D. Warr, Use of a filter in atomic-fluorescence spectroscopy, *Talanta* 17 (1970) 543–548.
- [10] A. D'Ulivo, L. Lampugnani, G. Pellegrini, L. Romboli, R. Zamboni, Determination of Hydride Forming Elements at pg/ml Level by AFS Using Continuous Flow Hydride Generation: Application to Sediments, in: *Mediterraneanchem*, Taranto, 1995, pp. 67–68.
- [11] A. D'Ulivo, E. Bramanti, L. Lampugnani, R. Zamboni, Improving the analytical performance of hydride generation non-dispersive atomic fluorescence spectrometry. Combined effect of additives and optical filters, *Spectrochim. Acta Part B: At. Spectrosc.* 56 (2001) 1893–1907.
- [12] S. Musil, T. Matoušek, J.M. Currier, M. Stýblo, J., Dédina, Speciation analysis of arsenic by selective hydride generation-cryotrapping-atomic fluorescence spectrometry with flame-in-gas-shield atomizer: achieving extremely low detection limits with inexpensive instrumentation, *Anal. Chem.* 86 (2014) 10422–10428.
- [13] J. Dédina, Generation of volatile compounds for analytical atomic spectroscopy, in: R.A. Meyers (Ed.), *Encyclopedia of Analytical Chemistry*, Supplementary Volumes S1-S3, John Wiley & Sons, Ltd, Chichester, UK, 2011, pp. 897–936.
- [14] J.D. Winefordner, R.A. Staab, Determination of zinc, cadmium, and mercury by atomic fluorescence flame spectrometry, *Anal. Chem.* 36 (1964) 165–168.
- [15] J.D. Winefordner, T.J. Vickers, Atomic fluorescence spectroscopy as a means of chemical analysis, *Anal. Chem.* 36 (1964) 161–165.
- [16] J.O. Weide, M.L. Parsons, The use of pulsed hollow cathode lamps in atomic fluorescence flame spectrometry, *Anal. Lett.* 5 (1972) 363–369.
- [17] J.V. Sullivan, A. Walsh, High intensity hollow-cathode lamps, *Spectrochim. Acta* 21 (1965) 721–726.
- [18] J. Mansfield, J. Winefordner, C. Veillon, High sensitivity determination of zinc, cadmium, mercury, thallium, gallium, and indium by atomic fluorescence flame spectrometry, *Anal. Chem.* 37 (1965) 1049–1051.
- [19] R.M. Dagnall, K.C. Thompson, T.S. West, Studies in atomic-fluorescence spectroscopy—Part VI: The fluorescence characteristics and analytical determination of bismuth with an iodine electrodeless discharge tube as source, *Talanta* 14 (1967) 1467–1475.
- [20] R.M. Dagnall, K.C. Thompson, T.S. West, An investigation of some experimental parameters in atomic fluorescence spectrophotometry, *Anal. Chim. Acta* 36 (1966) 269.
- [21] Electrodeless Discharge Lamps, PerkinElmer. <http://www.perkinelmer.com/category/electrodeless-discharge-lamps> (accessed 20.2.2023).
- [22] Super Lamps, PHOTRON, <http://www.photronlamp.com/collections/super-lamps> (accessed 20.2.2023).
- [23] X. Wang, S. Zhang, Z. Xu, J. Lin, B. Huang, W. Hang, Atomic spectrometry in China: past and present, *J. Anal. At. Spectrom.* 30 (2015) 852–866.
- [24] L. Rahman, W. Corns, D. Bryce, P. Stockwell, Determination of mercury, selenium, bismuth, arsenic and antimony in human hair by microwave digestion atomic fluorescence spectrometry, *Talanta* 52 (2000) 833–843.
- [25] B. Štádlarová, M. Kolrosová, J. Dédina, S. Musil, Atomic fluorescence spectrometry for ultrasensitive determination of bismuth based on hydride generation – the role of excitation source, interference filter and flame atomizers, *J. Anal. At. Spectrom.* 35 (2020) 993–1002.
- [26] D. Sánchez-Rodas, W. Corns, B. Chen, P. Stockwell, Atomic fluorescence spectrometry: a suitable detection technique in speciation studies for arsenic, selenium, antimony and mercury, *J. Anal. At. Spectrom.* 25 (2010) 933–946.
- [27] J. Dédina, Atomization of volatile compounds for atomic absorption and atomic fluorescence spectrometry: On the way towards the ideal atomizer, *Spectrochim. Acta B At. Spectrosc.* 62 (2007) 846–872.
- [28] R.F. Browner, Atomic-fluorescence spectrometry as an analytical technique. A critical review, *Analyst* 99 (1974) 617–644.
- [29] J. Vyhnanovský, D. Yildiz, B. Štádlarová, S. Musil, Efficient photochemical vapor generation of bismuth using a coiled Teflon reactor: effect of metal sensitizers and analytical performance with flame-in-gas-shield atomizer and atomic fluorescence spectrometry, *Microchem. J.* 164 (2021), 105997.
- [30] J. Soukal, S. Musil, Detailed evaluation of conditions of photochemical vapor generation for sensitive determination of nickel in water samples by ICP-MS detection, *Microchem. J.* 172 (2022), 106963.



Cite this: *J. Anal. At. Spectrom.*, 2023, **38**, 1213

Chemical vapour generation assisted by Cr³⁺/KCN coupled to atomic fluorescence spectrometry for ultrasensitive determination of cadmium in water and rice samples

Barbora Štádlarová, *^{ab} Linda Sagapova^{ab} and Stanislav Musil ^a

A methodology for cadmium determination at ultratrace levels based on chemical vapour generation (CVG) coupled to atomic fluorescence spectrometry (AFS) was developed. Cd volatile species were generated in a four-channel flow injection CVG system by the reaction of the analyte with NaBH₄ in a HCl medium in the presence of Cr³⁺/KCN used as modifiers enhancing the CVG efficiency. An in-house assembled non-dispersive AFS was used as a detector of the volatile species in two types of flame atomizers – the miniature diffusion flame (MDF) and the flame-in-gas-shield (FIGS) atomizers. The atomization conditions were optimized for both atomizers and the tolerance towards interferences from hydride forming elements and mercury was examined. The sensitivity obtained with the FIGS atomizer was approximately twofold higher compared to that with the MDF atomizer; therefore, the FIGS atomizer was selected for further analytical applications, providing an excellent limit of detection of 0.42 ng L⁻¹ Cd (63 fg absolute). The accuracy of the proposed methodology was verified by analyses of certified reference materials of water with various matrix complexities (fresh water SRM 1643f, wastewater ERM-CA713 and seawater CASS-4 and NASS-5) and rice flour SRM 1568b after microwave digestion in a diluted acid medium with very good agreement with certified values. In addition, the practical application was successfully demonstrated by determination of Cd content in three samples of rice and rice flour with excellent agreement with the values obtained by solution nebulization inductively coupled plasma mass spectrometry.

Received 13th March 2023
 Accepted 19th April 2023

DOI: 10.1039/d3ja00083d

rsc.li/jaas

1 Introduction

Cadmium is a heavy metal that is considered to be one of the most serious hazardous toxic pollutants. Even though Cd emissions seem to be decreasing over the course of the last few decades thanks to improved technologies for the production and disposal of Cd-containing products, cadmium cannot be degraded any further and its concentrations in the environment are still steadily increasing due to anthropogenic activities.¹ The majority of Cd present in the environment comes from the production of batteries; the rest is usually used in alloys, coatings or fertilizers. A non-negligible amount of Cd is also consumed by smokers *via* tobacco products.^{2,3} Cadmium is considered a carcinogen;⁴ it negatively affects the cardiovascular system and the bone structure and is nephrotoxic. As the exposure of humans to Cd has obvious negative effects,^{1,2,5} it is important to continue developing analytical methodologies for

ultrasensitive Cd determination in a variety of biological, environmental or food samples.^{6–9}

Vapour generation (VG) as a sample introduction technique for methods of analytical atomic spectrometry is still attractive as it carries many inherent advantages.¹⁰ The analyte in the liquid phase is converted by a chemical, electrochemical or photochemical reaction to a volatile species, which is subsequently separated from the liquid matrix and transported to an ionization or atomization unit (atomizer) for detection. VG can be virtually coupled to atomic absorption spectrometry (AAS), atomic fluorescence spectrometry (AFS) and inductively coupled plasma with either optical emission (ICP-OES) or mass spectrometry (ICP-MS) detection. Among the detection techniques, AAS and AFS in combination with VG have gained particular attention especially thanks to the detection power comparable to that typically obtained with conventional solution nebulization ICP-MS but at significantly lower investment and running costs. Chemical vapour generation (CVG) based on the reaction of the analyte with a reducing agent (BH₄⁻) is a mature technique commonly used for the determination of so-called hydride forming elements (As, Bi, Ge, Pb, Sb, Se, Sn and Te) as well as Hg, which is generated in the form of cold vapour.^{11–13}

^aInstitute of Analytical Chemistry of the Czech Academy of Sciences, Veveří 97, 602 00 Brno, Czech Republic. E-mail: stadlerova@iach.cz

^bCharles University, Faculty of Science, Department of Analytical Chemistry, Hlavova 8, 128 43 Prague, Czech Republic

CVG efficiency reaches up to 100%, which implies that the analyte is completely converted to its volatile species, released from the liquid phase and transported to the detection unit. Lower but still fair CVG efficiency can be achieved for Cd, while CVG of other transition metals may be characterized by insufficient efficiency reflected in significantly worse repeatability and reproducibility.¹⁴

CVG of Cd has been thoroughly studied throughout recent years employing different approaches.^{15–35} A mixture of atomic and molecular volatile species is supposedly formed during CVG.^{15–18} It seems that their fraction, as well as CVG efficiency, depends profoundly on the experimental conditions, especially the $\text{BH}_4^-/\text{acid}$ ratio (pH), but also the oxygen dissolved in the reagents has shown to play a significant role. The presence of modifiers has been, however, identified as crucial in order to enhance CVG efficiency substantially. In our recent work,³⁶ the performance of CVG of Cd employing various modifiers (Co^{2+} ions/ascorbic acid/thiourea, Ti^{3+} or $\text{Ti}^{4+}/\text{KCN}$, and $\text{Cr}^{3+}/\text{KCN}$) was compared. The best results in terms of CVG efficiency (55–66%), inter-day repeatability and robustness were obtained with a four-channel system employing $\text{Cr}^{3+}/\text{KCN}$ as modifiers, reaching a limit of detection (LOD) of 60 ng L^{-1} using AAS and a quartz tube atomizer.³⁶ The mechanism of action of this combination of modifiers on CVG of Cd hasn't been fully elucidated but Yilmaz *et al.* proposed in their pioneering work that a $[\text{Cr}(\text{CN})_6]^{3-}$ complex is synthesized on-line in a slightly acidic medium from $\text{Cr}(\text{OH})_3$ and an excess of KCN, prior to mixing with BH_4^- . This complex subsequently interacts with BH_4^- to form reactive borane complex intermediates that can effectively react with Cd^{2+} and convert it to volatile species with high efficiency.²²

Excellent detection power can be obtained when CVG of Cd is coupled to AFS because Cd is an element particularly suited for AFS, primarily thanks to the availability of intense radiation sources, simplicity of Cd fluorescence spectra, favourable position of its main resonance line at 228.8 nm with high oscillator strength, very few spectral interferences and highly efficient atomization in various types of flames.^{37,38} Since the analyte is introduced in the form of volatile species, some type of “cool” hydrogen flame is usually used as the atomizer in CVG-AFS.³⁹ The simplest atomizer is a miniature diffusion flame (MDF) atomizer, which is also employed in commercial spectrometers.⁴⁰ It burns at the end of a support tube through which the volatile species and H_2 , as products of the CVG reaction, are introduced. The analyte is fully atomized in the volume of the flame by the action of hydrogen radicals formed in the outer parts of the flame and penetrating inwards.^{39,41} An advanced version of the MDF atomizer is the flame-in-gas-shield (FIGS) atomizer.^{42–45} A high laminar flow of Ar is employed for the protection of the observation volume from the ambient atmosphere and an additional low flow of O_2 is introduced through a capillary placed in the vertical axis of the support tube. A microflame burns at the top of this capillary as a result of the reaction of O_2 with the excess of H_2 , which forms hydrogen radicals inside the observation volume.^{43,45} The general benefits of a FIGS atomizer lie in its several-fold better sensitivity, lower emission of the microflame and lower background noise.³⁹

In this work, we aimed to fully exploit the potential of ultrasensitive detection of Cd by AFS. We adopted the CVG system that yielded the best results in terms of repeatability, reproducibility and CVG efficiency from our previous study,³⁶ which corresponded to using $\text{Cr}^{3+}/\text{KCN}$ modifiers, and coupled this system to a non-dispersive AFS constructed at our laboratory and equipped with an intense electrodeless discharge lamp (EDL) as a radiation source.^{43,44,46} Atomization in the two flame atomizers, *i.e.*, MDF and FIGS, was optimized, their performances were compared and the best of them in terms of sensitivity and tolerance towards interferences was selected for analytical applications. The developed methodology was validated for the determination of Cd content in various water samples as well as rice samples after microwave digestion in a diluted acid medium.

2 Materials and methods

2.1 Reagents

Ultrapure water Analpure (Analytika, Czech Republic) was used for the preparation of all the solutions unless otherwise stated. 5% (m/v) NaBH_4 ($\geq 99\%$, Honeywell, USA) in 0.4% (m/v) KOH (semiconductor grade, Sigma-Aldrich, Germany) was used as a reductant. A solution of 0.2 mol L^{-1} HCl (Analpure, Analytika) was used as a carrier and blank. Working Cd solutions in 0.2 mol L^{-1} HCl were prepared fresh daily by serial dilution of a 1000 mg L^{-1} Cd stock standard solution (Analytika). The modifiers were prepared in ultrapure water from the following compounds: 0.6 mmol L^{-1} working Cr^{3+} solution and 24 mmol L^{-1} solution used for semi-permanent modification of the CVG system from solid $\text{Cr}(\text{NO}_3)_3 \cdot 9\text{H}_2\text{O}$ ($\geq 99.99\%$ trace metal basis, Sigma-Aldrich) and 0.01 mol L^{-1} working KCN solution from solid KCN ($\geq 97\%$, Acros Organics, USA).

The 1000 mg L^{-1} stock solutions of elements employed for the interference study were sourced as follows: Se^{4+} and Sn^{4+} from Sigma-Aldrich, Sb^{3+} from Fluka (Germany), Pb^{2+} and Hg^{2+} from Analytika. As^{3+} solution was prepared by dissolving solid As_2O_3 (Fluka) in 10% NaOH and deionized water.

Concentrated semiconductor grade HNO_3 (Honeywell) and 30% H_2O_2 (p.a., Analytika) were used for preparation of the medium for the microwave digestion (see below).

2.2 Instrumentation

The scheme of the four-channel flow injection (FI)-CVG is shown in Fig. 1. The operating conditions were taken from our previous work³⁶ and were only slightly modified. The reductant (NaBH_4) and the carrier (HCl), both at 1 mL min^{-1} , and the solutions of modifiers 1 and 2 (Cr^{3+} and KCN), both at 0.5 mL min^{-1} , were pumped using a peristaltic pump Reglo Digital (Ismatec, Switzerland). The optimum CVG conditions are summarized in Table 1. The manifold was constructed from PTFE tubing with the exception of Tygon pump tubing. The standard/sample prepared in 0.2 mol L^{-1} HCl was injected through a 0.15 mL sample loop into the flow of the carrier (0.2 mol L^{-1} HCl) and subsequently merged with the modifiers and the reducing agent in particular reaction coils (RCs). RC 1

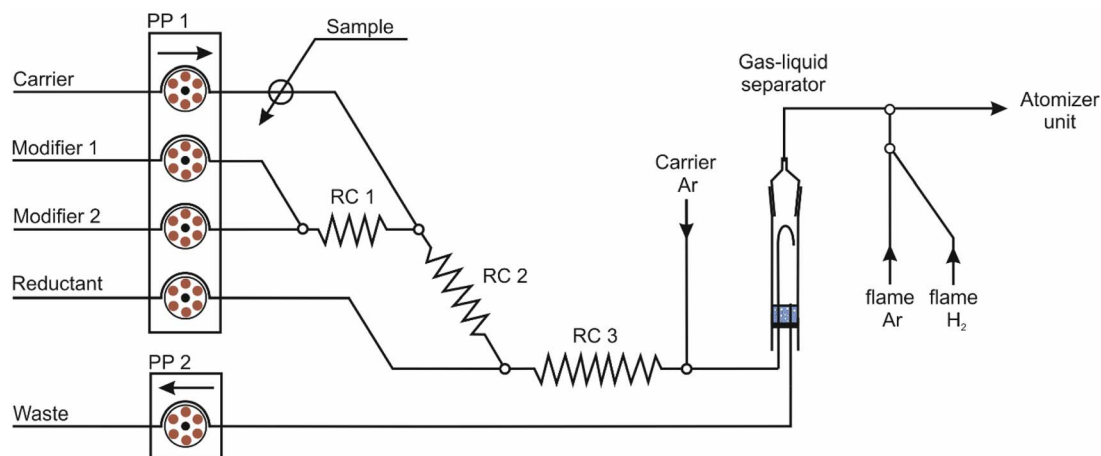


Fig. 1 Four-channel chemical vapour generation system with FI introduction of the sample (0.15 mL loop); PP 1–2 – peristaltic pumps and RC 1–3 – reaction coils.

Table 1 Optimum conditions of chemical vapour generation of Cd

Reagent	Composition	Flow rate (mL min ⁻¹)
Carrier	0.2 mol L ⁻¹ HCl	1
Modifier 1 ^a	0.6 mmol L ⁻¹ Cr ³⁺	0.5
Modifier 2	0.01 mol L ⁻¹ KCN	0.5
Reductant	5% (m/v) NaBH ₄ in 0.4% (m/v) KOH	1

^a 24 mmol L⁻¹ was used for modification of the CVG system prior to measurement.

and RC 2 (see Fig. 1) were made from PTFE tubing with a 1 mm i.d. and each volume corresponded to 63 μ L. RC 3 was from PTFE tubing with a 1.58 mm i.d. and the volume was 932 μ L.³⁶ A glass gas-liquid separator (5 mL) with a forced waste removal was employed for the separation of the gas phase containing volatile Cd species by introducing carrier Ar (80 mL min⁻¹). The amount of H₂ evolving from the CVG reaction was ca. 20 mL min⁻¹. The gas phase exiting the gas-liquid separator was supplied with an additional flow of Ar and H₂ (termed flame Ar and flame H₂) to maintain a stable flame of the atomizer (see below).

An in-house assembled non-dispersive atomic fluorescence spectrometer⁴³ was employed throughout. This spectrometer consists of three main components – an atomizer unit, an excitation source and a photomultiplier tube (PMT). Fig. 2 shows the employed atomizer unit that can be operated either as a MDF or FIGS atomizer. If operated as a FIGS atomizer, a vertical quartz support tube (6 mm i.d.) with a side inlet arm is supplied with Ar, H₂ and the volatile species of the analyte. A quartz capillary (0.53 mm i.d.) is added in the axis of the support tube protruding 3 mm above its rim and serves to introduce O₂. In addition, a two-channel brass shielding unit⁴³ fitted around the support tube is supplied with two flows of Ar (1.5 L min⁻¹ each) to shield the observation volume of the atomizer from ambient air (O₂). The observation height (OH) is defined as the distance from the top of the capillary to the centre of the optical beam.

Regarding the MDF operation mode, only a vertical quartz support tube with a side inlet arm is supplied with Ar, H₂ and the volatile species of the analyte. No flows of shielding Ar into

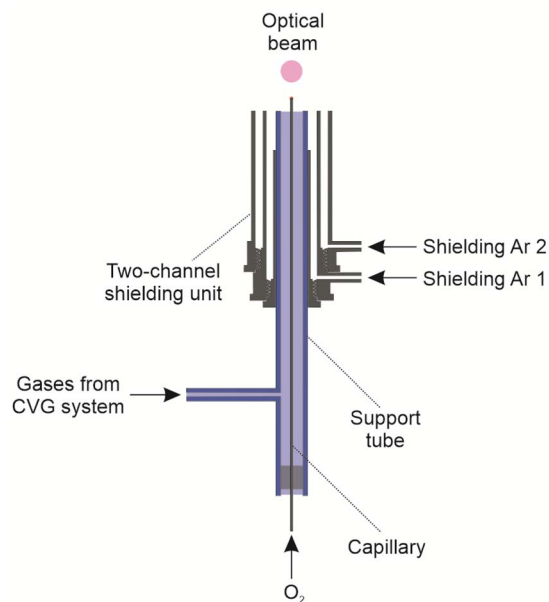


Fig. 2 Atomizer unit employed for operation as a miniature diffusion flame atomizer (MDF; shown in blue) and flame-in-gas-shield atomizer (FIGS; the whole atomizer).

the shielding unit and O₂ through the capillary are introduced and the capillary is removed from the support tube. OH is defined in this case as the distance from the very top of the support tube to the centre of the optical beam.

A Cd EDL (System 2, PerkinElmer, USA) was used as a radiation source with a feeding current square wave modulated at a frequency of 40 Hz and with a 52% duty cycle (13 ms on and 12 ms off). The operating current was 240 mA unless otherwise stated. The radiation beam from the source was focused above the atomizer unit using two UV fused silica lenses. A plano-convex lens ($d = 25$ mm, 40 mm focal length) was inserted into the exit orifice of the cavity containing the EDL bulb and a double convex lens ($d = 22$ mm, 45 mm focal length) was attached in a lens holder to the rim of the EDL.

A solar-blind channel PMT (165–320 nm, MH 1922, PerkinElmer Optoelectronics, Germany) was placed perpendicularly to the EDL to collect the produced fluorescence radiation. The PMT was supplied with negative voltage, typically in the range of 1200–1400 V. Two positive meniscus UV fused silica lenses ($d = 17$ and 22 mm; 21 mm focal length) were used to focus the radiation onto an interference filter (Melles Griot, USA) with central wavelength at 228 nm, full width at half maximum 10 nm and peak transmission 15%. The AFS instrument was placed inside a fume hood. The door was covered with a black curtain during all the measurements to avoid the contribution of any potential parasitic radiation from the laboratory environment to the measured signal.

ICP-MS with conventional solution nebulization as sample introduction was a reference methodology for the determination of Cd content in rice sample digests. An employed Agilent 7700x (USA) single quadrupole ICP-MS instrument was equipped with an ASX-500 autosampler, a MicroMist concentric nebulizer, a Scott double-pass spray chamber and high matrix introduction technology. The ICP-MS setting was as follows: RF power 1600 W, sampling depth 7 mm, nebulizer Ar 0.6 L min⁻¹, dilution Ar 0.55 L min⁻¹ and spray chamber temperature 2 °C. The measurement was carried out using a spectrum mode with no gas in a collision cell. The monitored isotopes were ¹¹¹Cd and ¹¹⁴Cd (both at a dwell time of 1 s) and ¹⁰³Rh (0.1 s), which was used as an internal standard.

An UltraWAVE system (Milestone, Italy) was used for microwave acid digestion of rice samples. The digestion programme is described in Section 2.4.

2.3 Procedure, data evaluation and conventions

Prior to the analysis, the EDL was turned on and left to stabilize for at least 1 hour. Then, the flame Ar and flame H₂ flows were introduced to the atomizer unit through the vertical support tube (see Fig. 2) and the flame was ignited (operated as MDF) to let the body of the atomizer heat up for *ca.* 30 minutes. In the case of the FIGS mode, the O₂ supply through the capillary was initiated after the heating-up period, followed by the introduction of two flows of shielding Ar. Meanwhile, it was crucial to modify the CVG system to quickly achieve the desired CVG efficiency and thus sensitivity. The CVG was conducted in a standard way but using 24 mmol L⁻¹ Cr³⁺ solution as modifier

1 for 10–15 minutes until the inner surface of RC 3 was covered by visible blue deposits.³⁶ Subsequently, the concentration of Cr³⁺ in modifier 1 was decreased to 0.6 mmol L⁻¹ and employed throughout all the measurements. This modification was repeated daily and whenever the sensitivity significantly dropped below the standard level.

The sample/standard was injected 10 s after the signal recording started. The total time for each signal recording was 90 s, which was sufficient to return the transition signal to the baseline. The recorded signals from the PMT (in μ V) were treated the same way as described in detail previously.⁴⁶ Peak area (in μ V s) corrected to the baseline or peak area sensitivity (in μ V s L ng⁻¹), and a signal to noise ratio (SNR) were the parameters used to evaluate the data. The SNR (in s) was estimated by dividing the peak area from a corresponding Cd standard by an uncertainty of the background level that was determined as an average ($n = 2$) of the standard deviations of background intensity 15 s before and after the peak, *i.e.*, calculated from 600 values.

For a simplified description of the different gases supplied to the support tube of the atomizer unit, the following conventions were established. The total flow rate of H₂ comprises the H₂ flow rate formed during CVG from the decomposition of NaBH₄ (generator H₂ \approx 20 mL min⁻¹) and H₂ flow rate introduced downstream the gas-liquid separator (flame H₂). The total flow rate of Ar comprises the flow rates of Ar introduced upstream the gas-liquid separator (carrier Ar) and Ar introduced downstream the gas-liquid separator (flame Ar). Ultimately, the total gas flow rate equals the sum of the carrier Ar, flame Ar, generator H₂ and flame H₂ flow rates. The hydrogen fraction is then the ratio of the total flow rate of H₂ to the total gas flow rate.

2.4 Real samples

The following certified reference materials (CRMs) were used during the validation of the developed methodology: fresh water SRM 1643f (National Institute of Standards and Technology, USA), wastewater ERM-CA713 (European Commission, Joint Research Centre, Institute for Reference Materials and Measurements, Belgium), nearshore seawater CASS-4 and seawater NASS-5 (National Research Council, Canada). These samples were diluted accordingly with HCl so that the resulting concentration corresponded to 0.2 mol L⁻¹.

Furthermore, the methodology was applied to Cd determination in rice samples after microwave digestion in a diluted acid medium. Rice flour SRM 1568b (National Institute of Standards and Technology, USA) was used as a reference. Three real samples were purchased at a local store: long grain rice (distributed by Vitana, Czech Republic), white rice flour (distributed by Cockbrand, Thailand) and rice flour (distributed by Paleta, European Union). Samples were milled to fine powder (if needed) and dried in an oven (2 hours, 95 °C; as recommended for the sample preparation for SRM 1568b⁴⁷). Each sample of approximately 0.25 g (three replicates) was weighed into 15 mL quartz digestion vials. 2.5 mL of 2 mol L⁻¹ HNO₃ were added to each sample replicate and left at room temperature overnight. A 1 mL of 30% H₂O₂ was added just prior to the

microwave digestion. The microwave digestion programme was as follows: 20 min ramp to 240 °C followed by 20 min holding at the same temperature, and the initial N₂ pressure was 40 bar. After cooling down, the digests were quantitatively transferred to 50 mL polypropylene centrifuge tubes, diluted with ultrapure water and prepared for parallel analysis by FI-CVG-AFS and conventional solution nebulization ICP-MS. While the samples for ICP-MS analysis were only spiked with concentrated HNO₃ to contain 2% (m/v) and directly analysed, the samples for FI-CVG-AFS analysis were diluted (1 : 1) with 0.4 mol L⁻¹ HCl to contain 0.2 mol L⁻¹ HCl.

3 Results and discussion

3.1 Initial assessment

The employed AFS instrument, constructed at our laboratory, excels in sensitivity thanks to the use of the intense EDL source, which may be documented by excellent LODs of developed methodologies for total As and Bi determination (around 1 pg)^{44,46} or speciation analysis of As.^{43,48–50} Compared to those analytes, Cd determination by AFS may become even more sensitive (lower LOD) due to the particular suitability of Cd for AFS detection^{37,38} provided the CVG efficiency remains high and the background intensity is low. The CVG efficiency is not a very limiting factor because the efficiency in the range of 55–66% was quantified in the current CVG system in our previous work.³⁶ The background level (and resulting background noise) particularly depends on the contribution of the analyte contamination to the fluorescence radiation, on the scattered radiation from the EDL source and on the overlap of the interference filter transmittance profile with the emission spectrum of the flame emission from the atomizer. Compared to the former two contributions, the flame emission in the employed 228 ± 10 nm range, defined by the interference filter, was proven negligible in both MDF and FIGS atomizers, based on the comparison of background signals measured with and without flames ignited and when the CVG was not in operation. In fact, the preliminary experiments with FI-CVG-AFS revealed that the highest contribution to the measured background signal arose from analyte contamination from the reagents, especially deionized water, solutions of KCN and Cr³⁺ used as modifiers. Hence, it was proven to be crucial to employ reagents of the highest purity. Subsequently, the concentrations of the modifiers used for the CVG were re-optimized and it was found that decreasing the concentration of KCN in modifier 2 from 0.1 mol L⁻¹ to 0.01 mol L⁻¹ resulted in a background signal more than 4 times lower while maintaining the same CVG efficiency. Considering the high toxicity of this modifier, this result represents a great improvement over the previous papers in which 10–16-fold higher concentrations of KCN in combination with Ti³⁺/Ti⁴⁺, V³⁺ or Cr³⁺ ions were necessary.^{22,23,35,36} The concentration of other reagents remained unchanged from that in ref. 36.

The optical path of the spectrometer (mutual distances of the three main components including the lenses used to focus the radiation) was optimized so as to achieve the highest peak area sensitivity and SNR. The optimal setting resulted in the radius

of a vertical cross-section of the radiation beam (circular) above the vertical axis of the atomizer unit being approximately 5 mm, thus almost fully covering the observation volume above the support tube (6 mm i.d.) of the atomizer unit. The power supply of the EDL source was optimized in the range of 220–260 mA. The response gradually increased with higher current, which means the higher the intensity of the radiation source the higher the fluorescence intensity detected. However, the optimum was selected to be at 240 mA, which is the value recommended by the manufacturer, not to compromise the lifetime of the EDL at higher feeding currents.

3.2 Optimization of the atomization conditions

The atomization conditions in the standard MDF atomizer and advanced FIGS atomizer were optimized using a 250 ng L⁻¹ Cd standard solution (if not stated otherwise). The optimized parameters were as follows: the total gas flow rate, hydrogen fraction and OH for both flame atomizers. In addition, the O₂ flow rate through the capillary was the inherent parameter for the FIGS atomizer.

The hydrogen fraction in the gas phase introduced to the atomizer unit was optimized at a constant total gas flow rate of 400 and 500 mL min⁻¹ for MDF and FIGS modes, respectively. The tested hydrogen fractions ranged from 17% to 50% for MDF and from 11% to 25% for FIGS, see Fig. 3. The lower the hydrogen fraction, the higher the sensitivity and also SNR in both flames. The hydrogen fractions of 17% and 13% were selected to be optimal for MDF and FIGS, respectively. These were the lowest applicable hydrogen fractions at which the flames still remained sufficiently stable and were not extinguished by small fluctuations.

The same optimization was carried out using the flows of Ar and H₂ through the support tube, thus operating similarly to MDF, but without the ignition of the flame. Since there was no flame maintained in this case, the gas phase containing only generator H₂ (20 mL min⁻¹, *i.e.*, the 5% hydrogen fraction) could be examined. A 500 ng L⁻¹ Cd standard was employed in this case. At a 17% hydrogen fraction the sensitivity corresponded to ≈ 65% of the sensitivity obtained with the ignited MDF (see Fig. 3a) and it even reached ≈ 97% when only Ar and generator H₂ were delivered into the atomizer (no flame H₂ used). This result clearly indicates that a significant fraction of Cd volatile species introduced into the atomizer unit is in the form of free Cd atoms while the rest is molecular (most probably as CdH₂), which is in agreement with our previous results³⁶ using the same CVG system but coupled to an unheated quartz tube atomizer for AAS. The exact value of the fraction of Cd free atoms is however not 65% because of a pronounced dilution of free atoms in the observation volume due to thermal expansion in the burning flame. The temperature inside the MDF atomizer is not uniformly distributed and may significantly vary (*e.g.*, 150–700 °C (ref. 39 and 51)). The situation becomes even more complicated because the introduced free atoms are not sufficiently shielded when the flame is not ignited and may be quickly oxidized by reactions with atmospheric O₂. From a practical point of view, the operation of the atomizer unit

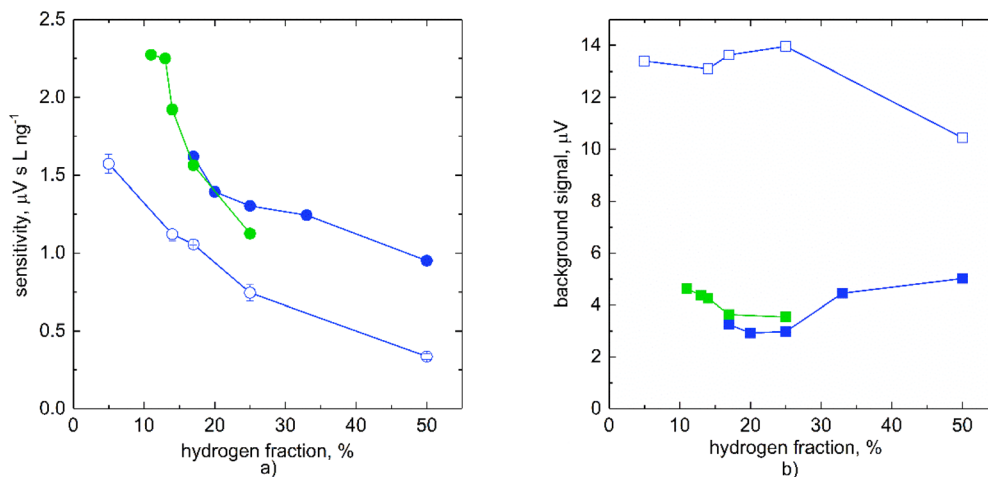


Fig. 3 The effect of the hydrogen fraction on sensitivity (a) and background signal (b) measured with MDF (blue), with flame ignition (full) and without flame ignition (empty), and in FIGS (green). The total gas flow rate corresponded to 400 and 500 mL min^{-1} for MDF and FIGS, respectively. SDs shown as error bars are indiscernible from the points in some cases.

without a real flame brings no benefits and the fluctuation of the signal at the peak and overall repeatability of peak areas are much worse. Another negative feature of such a setup lies in the approximately 4 times higher background signal (Fig. 3b), which certainly results in a poorer LOD. This may be explained by the occurrence of a scattering of the excitation radiation on small ballast aerosol droplets co-generated in the CVG system. The aerosol droplets of the reaction mixture are transported by the gas stream to the atomizer unit and are not evaporated at the lower OH as in the case of the ignited flame.

The next step was to optimize the total gas flow rate and OH at constant optimum hydrogen fractions, *i.e.*, at 17% and 13% for MDF and FIGS, respectively (Fig. 4 and 5). The lowest applicable total gas flow rate at which the flame in both MDF and FIGS modes remained stable was 400 mL min^{-1} . The peak area response and SNR were measured at various OHs for each total gas flow rate (400, 500, 600 and 700 mL min^{-1}). Generally,

the response decreases with higher total gas flow rates, which can be attributed to larger dilution of free atoms in the observation volume of both flames. While in the FIGS (Fig. 5a) there was no significant effect of OH in the range of 4–8 mm in the whole tested range of the total gas flow rate, the optimum OH in the MDF (Fig. 4a) shifted to higher values with increasing total gas flow rates, namely at total gas flow rates of 400, 500, 600 and 700 mL min^{-1} the maximum sensitivity was achieved at an OH of 5, 7, 8 and 9 mm, respectively. A minimum OH of 4 mm could be employed because at a lower OH the radiation from the EDL was prominently scattered on the shielding unit and support tube using the MDF and on the capillary using the FIGS, which caused an unacceptable increase in the background signal and thus a decrease in the SNR (Fig. 4b and 5b). The sufficient OH where the radiation from the EDL is not significantly scattered on top of the atomizer unit anymore corresponds to ≥ 7 mm for MDF and ≥ 5 mm for FIGS. The flow rate of 400 mL min^{-1} was

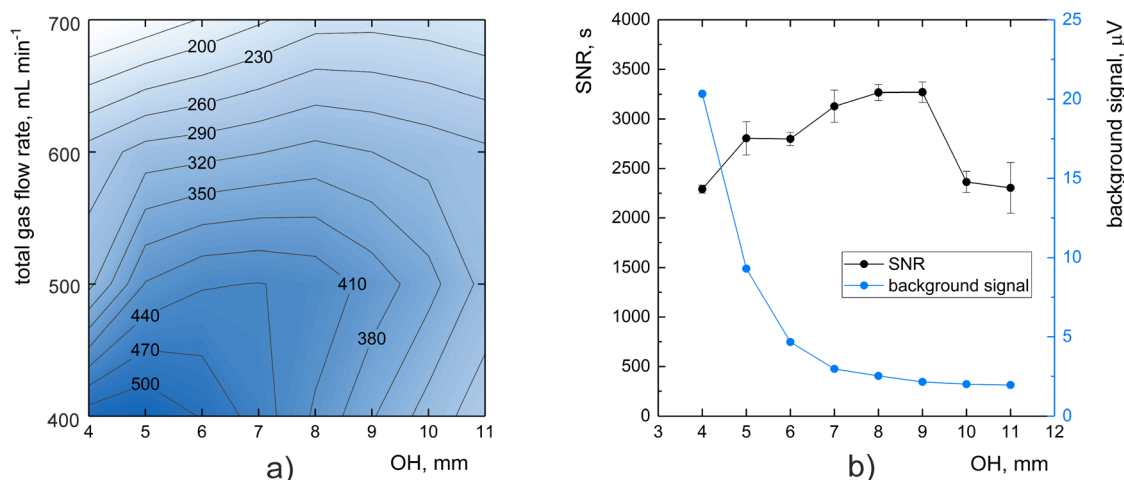


Fig. 4 The dependence of peak area in $\mu\text{V s}$ on the total gas flow rate and OH (a) and the effect of OH on the SNR (black) and background signal (blue) at an optimum total gas flow rate of 400 mL min^{-1} (b) for MDF, both measured at a 17% hydrogen fraction using 250 ng L^{-1} Cd.

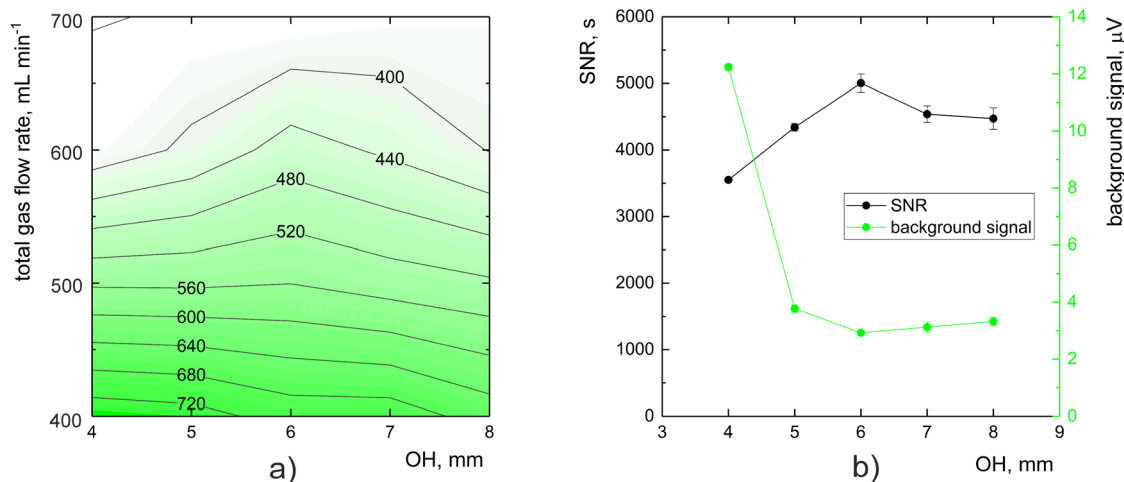


Fig. 5 The dependence of peak area in $\mu\text{V s}$ on the total gas flow rate and OH (a) and the effect of OH on the SNR (black) and background signal (green) at an optimum total gas flow rate 400 mL min^{-1} (b) for FIGS, both measured at a 13% hydrogen fraction using $250 \text{ ng L}^{-1} \text{ Cd}$.

Table 2 Optimum atomization conditions for both flame atomizers

	Total Ar (mL min^{-1})	Total H ₂ (mL min^{-1})	O ₂ (mL min^{-1})	Shielding Ar 1 and 2 (L min^{-1})	Observation height (mm)
MDF	335	65	—	—	7
FIGS	345	55	12	1.5, 1.5	6

chosen as optimal for both atomizers with OH of 7 and 6 mm for MDF and FIGS atomizers, respectively, as a compromise between the peak area sensitivity, SNR and the contribution of the scattered radiation from the EDL on the atomizer unit to the background signal.

The operation of the FIGS atomizer requires an optimization of additional parameters, most importantly the flow rate of O₂ through the capillary placed in the vertical axis of the support tube that is responsible for the formation of hydrogen radicals. The O₂ flow rate was optimized in the range of 5–15 mL min^{-1} . A clear plateau of maximum sensitivity was identified between 7 and 12 mL min^{-1} , with an indistinct maximum at 12 mL min^{-1} but also a significantly lower background signal and thus higher SNR in comparison to O₂ flow rates lower than 10 mL min^{-1} . Therefore, 12 mL min^{-1} was selected as the optimum. Lower flow rates are probably not sufficient for an efficient formation of hydrogen radicals and thus atomization of molecular volatile species of Cd. The shielding Ar flow rates supplied through the two-channel shielding unit were not optimized in this work as their effect on atomization of As and Bi was similar; hence the values were adopted from our previous studies.^{44,46} All the optimum atomization conditions for MDF and FIGS atomizers are summarized in Table 2.

3.3 Interference study

In general, both spectral and non-spectral interferences may occur in CVG-AFS. Spectral interferences are typically not a problem because the analyte passes into the atomizer in the form of volatile species while the majority of concomitants

remain in the liquid phase. The high selectivity is also ensured by the use of a single element lamp as the radiation source and an interference filter. The non-spectral interferences are thus more serious and may arise from the additional chemical reactions in the liquid phase (during CVG) and/or in the gas phase (especially during atomization).

Interferences from hydride forming elements and transition metals on CVG of Cd were previously investigated by Yilmaz *et al.*²² in a very similar CVG system and employing very similar CVG conditions (Cr³⁺/KCN modifiers) but using ICP-MS for detection.²² More serious interferences (response decreased by $\geq 10\%$) exhibited for several hydride forming elements, *e.g.*, at $100 \mu\text{g L}^{-1}$ for Sn²⁺ and $200 \mu\text{g L}^{-1}$ for Pb²⁺ and Sb³⁺,²² while no serious effects of Co²⁺, Cu²⁺, Fe³⁺, Mn²⁺, Ni²⁺ and Zn²⁺ were identified at the concentration of $1000 \mu\text{g L}^{-1}$, which might be ascribed to a good masking ability of the excess of CN⁻ ions. In addition to their effect in the liquid phase, hydride forming elements can potentially affect the atomization process in the flame atomizer because they can produce volatile species under the employed CVG conditions. Conversely, gas phase (atomization) interference is not expected from transition metals in our CVG system, even though some CVG action has been demonstrated for *ca.* 18 transition metals so far,¹⁴ and among them, especially Ag, Au, Cu, Pd and Zn yielded relatively high CVG efficiencies ($>10\%$).^{14,52–56} However, modified CVG configurations that allowed for rapid mixing with a reductant (without a reaction coil) were required along with the use of reaction modifiers that were entirely distinct from those used in this study.¹⁴ In this work, supporting evidence was provided for Zn

Table 3 Influence of various co-existing ions on Cd response (250 ng L^{-1}) examined by FI-CVG-AFS employing two flame atomizers

Interferent	Concentration ($\mu\text{g L}^{-1}$)	Recovery \pm combined uncertainty (%)	
		MDF	FIGS
As^{3+}	1	94 ± 2	98 ± 2
	10	94 ± 2	99 ± 2
	100	100 ± 2	101 ± 2
Hg^{2+}	1	98 ± 1	94 ± 1
	10	100 ± 1	102 ± 1
	100	100 ± 1	91 ± 2
Pb^{2+}	1	100 ± 3	101 ± 2
	10	89 ± 3	90 ± 1
	100	54 ± 2	62 ± 3
Sb^{3+}	1	102 ± 3	102 ± 1
	10	101 ± 3	99 ± 1
	100	105 ± 3	94 ± 2
Se^{4+}	1	99 ± 2	100 ± 1
	10	102 ± 1	102 ± 3
	100	105 ± 2	100 ± 2
Sn^{4+}	1	100 ± 3	101 ± 1
	10	101 ± 3	94 ± 1
	100	102 ± 3	91 ± 3

when no detectable signal was obtained even with $50 \mu\text{g L}^{-1}$ Zn^{2+} if the CVG setup was coupled to ICP-MS and operated under optimal conditions found for Cd (Table 1).

Hence, the interference study was focused only on hydride forming elements (As^{3+} , Pb^{2+} , Sb^{3+} , Se^{4+} and Sn^{4+}) and Hg^{2+} potentially affecting atomization in both flame atomizers. The interfering effects were examined by the addition of individual elements to the Cd standard solution of 250 ng L^{-1} in the concentration range of $1\text{--}100 \mu\text{g L}^{-1}$. It is apparent from Table 3 that there were no significant negative interferences (by $\geq 10\%$) observed from As^{3+} , Hg^{2+} , Sb^{3+} , Se^{4+} and Sn^{4+} ions up to $100 \mu\text{g L}^{-1}$. Only Pb^{2+} ions were identified to have a negative effect, wherein the response at $10 \mu\text{g L}^{-1}$ Pb^{2+} was suppressed by 11% and 10% for MDF and FIGS atomizers, respectively, and by 46% and 38% at $100 \mu\text{g L}^{-1}$, respectively. Since MDF is considered more tolerant towards atomization interferences than FIGS³⁹ and with respect to the very similar effect of Pb^{2+} observed with both atomizers, it is likely that this negative interference occurs in the liquid phase and not during atomization. However, this interference is something worth considering when employing this methodology for Cd determination in real samples with high Pb content. However, no such problems were encountered in this work (see below).

3.4 Analytical figures of merit

Analytical characteristics of the FI-CVG-AFS methodology for Cd determination were evaluated and compared under the optimum conditions of MDF and FIGS atomizers (Table 2). The sensitivities and LODs were evaluated from the calibration curves (measured with 0, 50, 75, 150 and 350 ng L^{-1} for the MDF atomizer and 0, 20, 40, 100 and 250 ng L^{-1} for the FIGS atomizer) and blanks ($n = 12$). The calibration curves were linear (R^2

Table 4 Comparison of LODs achieved with various VG techniques coupled to AFS or ICP-MS

Methodology	LOD (ng L^{-1})
CVG-AFS	8 (ref. 33), 10 (ref. 34), 12 (ref. 21), 10 (ref. 24)
CVG-AFS with a UV-atomizer	6 (ref. 18)
PVG ^a -AFS	1800 (ref. 57)
EcVG ^b -AFS	50 (ref. 58)
CVG-ICP-MS	5.2 (ref. 22), 4.5 (ref. 23), 3.2 (ref. 35)
PAVG ^c -AFS	8 (ref. 59)
Che-CVG ^d -AFS	190 (ref. 60)
CVG-AFS (this work)	1.4^e , 0.42^f

^a Photochemical vapour generation. ^b Electrochemical vapour generation. ^c Plasma assisted vapour generation. ^d Chelate chemical vapour generation. ^e MDF. ^f FIGS.

> 0.9995) in the measured concentration ranges for both atomizers. The sensitivity achieved with the FIGS atomizer was approximately 1.8-fold higher than that measured with the MDF atomizer. The LODs corresponded to 1.40 ng L^{-1} (0.21 pg) and 0.42 ng L^{-1} (0.063 pg) for the MDF and FIGS atomizers, respectively, which arose mainly from the difference in sensitivity. To the best of our knowledge, the presented LODs are the lowest reported ever for Cd using any VG based approach without resorting to preconcentration (see comparison with various VG techniques coupled to AFS or ICP-MS in Table 4). The reason for the superior LODs most likely lies in high CVG efficiency enhanced by $\text{Cr}^{3+}/\text{KCN}$ modifiers³⁶ as well as high intensity of the EDL used to excite the fluorescence.

The intra-day repeatability, expressed as a RSD of consecutively measured peak areas ($n = 11$) of the 250 ng L^{-1} Cd standard, amounted to 1.3% and 2.1% for the MDF and FIGS atomizers, respectively. The inter-day repeatability ($n = 7$) of average peak areas of the 250 ng L^{-1} Cd standard calculated over a period of several months was also satisfactory and reached 5.8% and 4.8% for the MDF and FIGS atomizers, respectively. The method is also characterized by a high sampling frequency of ≈ 40 samples per hour.

An instrumental LOD was assessed in order to illustrate the ultimate potential or the limitations of the developed methodology. For this, the flames were ignited and operated under optimum atomization conditions but only water was pumped through all channels of the CVG system. The resultant LODs corresponded to 0.3 ng L^{-1} (0.045 pg) for the MDF atomizer and 0.1 ng L^{-1} (0.015 pg) for the FIGS atomizer. The 4.2–4.7-fold difference between the real and instrumental LODs could be explained by the remaining Cd contamination of the reagents used for the reaction despite the use of high purity reagents. Another plausible reason is the occurrence of a light scattering from the EDL on the particles in the observation volume. The solid particles may be formed from the ballast aerosol droplets of the reaction mixture transported along with volatile species by vaporization in the flames. This is in line with the observation that a significantly higher background signal was detected

when the flame was not ignited (see Fig. 3b), likely due to the presence of larger particles or insufficiently dried droplets. The drying of the gas phase could bring a substantial improvement in the detection capabilities but no suitable dryer (without any significant loss of volatile species) was found.

3.5 Validation and application to real samples

Owing to its overall better analytical characteristics, the FIGS atomizer was applied further to validate the FI-CVG-AFS methodology and to determine Cd in real samples.

The accuracy was first verified by determination of Cd content in several water reference materials with different matrix complexities: fresh water (SRM 1643f), wastewater (ERM-CA713), nearshore seawater (CASS-4) and seawater (NASS-5). The content was quantified using an external calibration (0, 10, 50 and 250 ng L⁻¹ Cd standards). The SRM 1643f and ERM-CA713 materials were diluted 25-fold and 30-fold, respectively, with 0.2 mol L⁻¹ HCl to fit inside the calibration range. The certified Cd content in the two samples of seawater is around 25 ng L⁻¹ which leaves little to no room for any dilution with respect to the LOD. Hence, these two materials were only spiked with concentrated HCl to obtain 0.2 mol L⁻¹ in the final solution. The results obtained by FI-CVG-AFS are summarized in Table 5. It is evident that the determined values are in very good agreement with the certified values, including both seawater CRMs that were analysed with virtually no dilution. Furthermore, the recovery for the NASS-5 material was examined by comparison of the slope of the standard addition technique (comprising 50 and 150 ng L⁻¹ spiked concentrations) to the slope of external calibration and an excellent value of 101 ± 4% proved no matrix effects on the determination of Cd in seawater by FI-CVG-AFS. This is a remarkable benefit of this method because these high salinity matrices normally require significant dilution prior to the analysis by conventional methodologies such as ICP-MS with solution nebulization.

The practical application of the developed methodology was further examined by the determination of Cd in rice, which required a more complex sample preparation scenario. Rice is known to absorb a high amount of toxicologically relevant metals, such as As and Cd, along with nutrients during cultivation. The wet environment that is essential for the growth plays a big part in the metal uptake, meaning the water quality is then reflected in the quality or rather food safety of the produced rice.^{5,61} The European Commission (EC) set the

tolerable weekly intake for Cd at 2.5 µg kg⁻¹ body weight and also established the maximum level of Cd in rice as 150 µg kg⁻¹ wet weight.⁶²

Three store-bought rice or rice flour products and SRM 1568b (rice flour) were used for the validation. The typical medium for microwave acid digestion of such matrices consists of HNO₃ with the addition of H₂O₂. However, HNO₃ concentrations higher than 0.3 mol L⁻¹ in the sample (along with 0.2 mol L⁻¹ HCl) were found not to be fully compatible with CVG of Cd. To be more specific, a peak shaped blank appeared in the presence of 0.3 mol L⁻¹ HNO₃ in the standard, corresponding to 50 ng L⁻¹ Cd, while the blank corrected sensitivity increased only slightly, by ≈ 13%. In addition, the long-term performance of the CVG system was impaired and the modification with 24 mmol L⁻¹ Cr³⁺ solution had to be often repeated to restore the CVG efficiency. This effect was most probably caused by a decrease in pH of the reaction (from neutral to acidic), which led to a gradual washout of the semi-permanent modifier (blue coating from the Cr³⁺ modifier) from RC 3 after several injections of the standard. To reliably operate the CVG system, with no such interference and a minimal blank response, it was found that the samples had to be diluted to contain less than 0.1 mol L⁻¹ HNO₃. To avoid significant sample dilution, it was thus opted for 2 mol L⁻¹ HNO₃ to be used for the microwave digestion rather than concentrated HNO₃, which is usually used for similar sample preparations. Such a low concentration of HNO₃ in the medium was previously demonstrated to be efficient for microwave digestion of several plant materials.⁶³

The Cd content in the digests was determined by FI-CVG-AFS using an external calibration for the evaluation while the standard addition technique was applied for SRM 1568b only to evaluate the recovery. Concurrently, the Cd content was quantified by conventional solution nebulization ICP-MS employing an external calibration. There was a satisfactory agreement between the values obtained with both methods (Table 6). The results for SRM 1568b (rice flour) were also in satisfactory agreement with the certified value of 22.4 ± 1.3 µg kg⁻¹. The recovery for the digest of SRM 1568b, calculated as the ratio of the slope of the standard addition to the slope of the external calibration, was 101 ± 2%, proving that there were no matrix effects from the digest matrix and therefore Cd content could be safely evaluated using the external calibration. An important outcome is that the use of diluted HNO₃ for the microwave digestion proved to be sufficient, overcoming the potential

Table 5 Cd concentrations in water certified reference materials determined by FI-CVG-AFS using the FIGS atomizer; presented as median values ± SD (*n* = 3)

Samples	Cd concentration (µg L ⁻¹)	
	Determined	Certified
Fresh water SRM 1643f	5.98 ± 0.44	5.89 ± 0.13
Wastewater ERM-CA713	4.95 ± 0.07	5.09 ± 0.2
Nearshore seawater CASS-4	0.025 ± 0.001	0.026 ± 0.003
Seawater NASS-5	0.020 ± 0.001	0.023 ± 0.003

Table 6 Cd concentration in rice samples determined by FI-CVG-AFS using the FIGS atomizer and by conventional solution nebulization ICP-MS; presented as median values ± SD (*n* = 3)

Samples	Cd concentration (µg kg ⁻¹)	
	FI-CVG-AFS	Nebulization ICP-MS
Long grain rice (Vitana)	33.5 ± 0.5	32.2 ± 1.6
Rice flour (Paleta)	14.9 ± 0.9	14.1 ± 0.2
White rice flour (Cock brand)	9.0 ± 0.7	9.8 ± 0.2
SRM 1568b (rice flour)	19.9 ± 1.5	20.3 ± 1.1

interfering effect during CVG caused by higher concentrations of HNO₃ when the digestion is conducted with concentrated HNO₃ media.

4 Conclusion

This study focused on the development of a methodology for Cd determination at ultratrace levels based on CVG in the presence of Cr³⁺/KCN modifiers coupled to non-dispersive AFS. Since our non-dispersive AFS instrumentation is assembled from individual components, a detailed optimization and fine tuning of individual parts influencing the measured atomic fluorescence intensity as well as the atomization process in two flame atomizers, *i.e.*, MDF and FIGS, is possible. This is a significant advantage over commercial AFS instruments that were developed to be user-friendly, utilizing compromise conditions for the determination of several hydride forming elements (*e.g.*, the same optical path) but with the minimum possibility of fine adjustment or any further modification.⁴⁰ Thus, the potential of ultrasensitive detection of Cd²⁺ in AFS could be fully exploited here.

While both flame atomizers exhibited similar resistance to interferences from hydride forming elements, an overall better performance was in the end obtained with the FIGS atomizer, wherein the sensitivity was almost 2-fold higher compared to the MDF atomizer, which is considered to be the standard atomizer used in AFS. The exceptionally low LOD of 0.42 ng L⁻¹ (63 fg absolute) achieved without any preconcentration step may be attributed to the high CVG efficiency and high intensity of the EDL. Such sensitivity brings additional issues to be dealt with, especially significant contribution of analyte contamination in the reagents to the background intensity unless high purity reagents are used. Regarding the reagents, it should be mentioned that despite the significant reduction of KCN modifier consumption in comparison with previous studies,^{22,23,35,36} the use of this modifier still poses some risk and proper handling of the waste is advised. The methodology was validated by Cd determination in various certified reference materials of water and it was even found suitable for direct determination of low concentrations of Cd (without any dilution) in samples with a matrix as complex as seawater. Such a high concentration of dissolved salts is known to be an obstacle for conventional solution nebulization ICP-MS, typically regarded as a trademark of unparalleled sensitivity, requiring significant sample dilution prior to determination. Furthermore, Cd was successfully determined in rice and rice flour samples after microwave digestion in diluted acid and the results were cross-checked with the results obtained by ICP-MS. The highest concentration of Cd in rice corresponded to 33.5 µg kg⁻¹, which is well below the maximum limit established by the European Commission.⁶²

Author contributions

Barbora Štádlarová: formal analysis, investigation, methodology, supervision, validation, visualization, writing – original draft; Linda Sagapova: formal analysis, funding acquisition,

investigation, visualization; Stanislav Musil: conceptualization, formal analysis, funding acquisition, investigation, project administration, supervision, visualization, writing – review & editing.

Conflicts of interest

There are no conflicts of interest to declare.

Acknowledgements

The work was supported by the Czech Science Foundation (Project no. 19-17604Y), the Czech Academy of Sciences (Institutional Research Plan no. RVO: 68081715) and Charles University (Project GAUK 377321 and SVV260690).

References

- 1 J. M. Moulis and F. Thévenod, *Biometals*, 2010, **23**, 763–768.
- 2 H. Zhang and M. Reynolds, *Sci. Total Environ.*, 2019, **678**, 761–767.
- 3 N. Johri, G. Jacquillet and R. Unwin, *Biometals*, 2010, **23**, 783–792.
- 4 M. P. Waalkes, *J. Inorg. Biochem.*, 2000, **79**, 241–244.
- 5 L. Järup and A. Åkesson, *Toxicol. Appl. Pharmacol.*, 2009, **238**, 201–208.
- 6 P. Wu, C. Li, J. Chen, C. Zheng and X. Hou, *Appl. Spectrosc. Rev.*, 2012, **47**, 327–370.
- 7 K. Pyrzyńska and K. Kilian, *Water Res.*, 2007, **41**, 2839–2851.
- 8 V. A. Lemos and A. L. de Carvalho, *Environ. Monit. Assess.*, 2010, **171**, 255–265.
- 9 A. Pires Santos, M. das Graças Andrade Korn and V. Azevedo Lemos, *Environ. Monit. Assess.*, 2017, **189**, 1–16.
- 10 A. D'Ulivo and R. Sturgeon, *Vapor Generation Techniques for Trace Element Analysis: Fundamental Aspects*, Elsevier, 2022.
- 11 J. Dědina and D. L. Tsalev, *Hydride generation atomic absorption spectrometry*, Wiley, 1995.
- 12 Z. Long, Y. Luo, C. Zheng, P. Deng and X. Hou, *Appl. Spectrosc. Rev.*, 2012, **47**, 382–413.
- 13 A. D'Ulivo, J. Dědina, Z. Mester, R. E. Sturgeon, Q. Wang and B. Welz, *Pure Appl. Chem.*, 2011, **83**, 1283–1340.
- 14 S. Musil and T. Matoušek, in *Vapor Generation Techniques for Trace Element Analysis: Fundamental Aspects*, ed. A. D'Ulivo and R. E. Sturgeon, Elsevier, 2022, pp. 91–128.
- 15 L. Lampugnani, C. Salvetti and D. L. Tsalev, *Talanta*, 2003, **61**, 683–698.
- 16 E. Pitzalis, D. Angelini, M. C. Mascherpa and A. D'Ulivo, *J. Anal. At. Spectrom.*, 2018, **33**, 2160–2171.
- 17 Y. L. Feng, R. E. Sturgeon and J. W. Lam, *Anal. Chim. Acta.*, 2003, **75**, 635–640.
- 18 X. Yuan, L. Yang, S. Liu, H. Yang, Y. Tang, K. Huang and M. Zhang, *Anal. Methods*, 2018, **10**, 4821–4826.
- 19 M. Valdés-Hevia y Temprano, M. Fernández de la Campa and A. Sanz-Medel, *J. Anal. At. Spectrom.*, 1993, **8**, 847–852.
- 20 A. Sanz-Medel, M. Valdés-Hevia y Temprano, N. Bordel García and M. Fernández de la Campa, *Anal. Chem.*, 1995, **67**, 2216–2223.

- 21 X. Yang, M. Chi, Q. Wang and W. Zhang, *Anal. Chim. Acta*, 2015, **869**, 11–20.
- 22 V. Yilmaz, L. Rose, Z. Arslan and M. D. Little, *J. Anal. At. Spectrom.*, 2012, **27**, 1895–1902.
- 23 V. Yilmaz, Z. Arslan, L. Rose and M. D. Little, *Talanta*, 2013, **115**, 681–687.
- 24 G. Li, L. Wu, J. Xin and X. Hou, *J. Anal. At. Spectrom.*, 2004, **19**, 1010–1013.
- 25 N. A. Kasa, D. S. Chormey, Ç. Büyükpınar, F. Turak, T. B. Budak and S. Bakırdere, *Microchem. J.*, 2017, **133**, 144–148.
- 26 J. L. Manzoori, H. Abdolmohammad-Zadeh and M. Amjadi, *Talanta*, 2007, **71**, 582–587.
- 27 H. Luo, X. Wang, R. Dai, Y. Liu, X. Jiang, X. Xiong and K. Huang, *Microchem. J.*, 2017, **133**, 518–523.
- 28 M. L. Chen, Y. Tian and J. H. Wang, *J. Anal. At. Spectrom.*, 2008, **23**, 876–880.
- 29 H. Matusiewicz and M. Krawczyk, *Microchem. J.*, 2006, **83**, 17–23.
- 30 D. Korkmaz, C. Demir, F. Aydın and O. Y. Ataman, *J. Anal. At. Spectrom.*, 2005, **20**, 46–52.
- 31 O. Cankur and O. Y. Ataman, *J. Anal. At. Spectrom.*, 2007, **22**, 791–799.
- 32 C. Vargas-Razo and J. F. Tyson, *Fresenius' J. Anal. Chem.*, 2000, **366**, 182–190.
- 33 X. Guo and X. Guo, *Anal. Chim. Acta*, 1995, **310**, 377–385.
- 34 Y. Lü, H. W. Sun, C. G. Yuan and X. P. Yan, *Anal. Chem.*, 2002, **74**, 1525–1529.
- 35 Z. Arslan, V. Yilmaz and L. Rose, *Microchem. J.*, 2015, **123**, 170–178.
- 36 L. Sagapova, S. Musil, B. Kodříková, M. Svoboda and J. Kratzer, *Anal. Chim. Acta*, 2021, **1168**, 338601.
- 37 V. Sychra, V. Svoboda and I. Rubeška, *Atomic Fluorescence Spectroscopy*, Van Nostrand Reinhold Company, 1975.
- 38 B. Welz, *Atomic absorption spectroscopy*, Verlag Chemie, Weinheim, New York, 2nd edn, 1986.
- 39 J. Dědina, *Spectrochim. Acta, Part B*, 2007, **62**, 846–872.
- 40 W. T. Corns, P. B. Stockwell, L. Ebdon and S. J. Hill, *J. Anal. At. Spectrom.*, 1993, **8**, 71–77.
- 41 J. Dědina, A. D'Ulivo, L. Lampugnani, T. Matoušek and R. Zamboni, *Spectrochim. Acta, Part B*, 1998, **53**, 1777–1790.
- 42 A. D'Ulivo, I. Paolicchi, M. Onor, R. Zamboni and L. Lampugnani, *Spectrochim. Acta, Part B*, 2009, **64**, 48–55.
- 43 S. Musil, T. Matoušek, J. M. Currier, M. Stýblo and J. Dědina, *Anal. Chem.*, 2014, **86**, 10422–10428.
- 44 K. Marschner, S. Musil and J. Dědina, *Spectrochim. Acta, Part B*, 2015, **109**, 16–23.
- 45 J. Dědina and A. D'Ulivo, *Spectrochim. Acta, Part B*, 1997, **52**, 1737–1746.
- 46 B. Štádlarová, M. Kolrosová, J. Dědina and S. Musil, *J. Anal. At. Spectrom.*, 2020, **35**, 993–1002.
- 47 <https://www-s.nist.gov/srmors/certificates/1568b.pdf>, accessed 10. 3. 2023.
- 48 K. Marschner, S. Musil and J. Dědina, *Anal. Chem.*, 2016, **88**, 4041–4047.
- 49 K. Marschner, S. Musil, I. Mikšík and J. Dědina, *Anal. Chim. Acta*, 2018, **1008**, 8–17.
- 50 K. Marschner, Á. H. Pétursdóttir, P. Bücker, A. Raab, J. Feldmann, Z. Mester, T. Matoušek and S. Musil, *Anal. Chim. Acta*, 2019, **1049**, 20–28.
- 51 M. Mrkvičková, P. Dvořák, M. Svoboda, J. Kratzer, J. Voráč and J. Dědina, *Combust. Flame*, 2022, **241**, 112100.
- 52 S. Musil, J. Kratzer, M. Vobecký, O. Benada and T. Matoušek, *J. Anal. At. Spectrom.*, 2010, **25**, 1618–1626.
- 53 Y. Arslan, T. Matoušek, J. Kratzer, S. Musil, O. Benada, M. Vobecký, O. Ataman and J. Dědina, *J. Anal. At. Spectrom.*, 2011, **26**, 828–837.
- 54 J. Šoukal, O. Benada, T. Matoušek, J. Dědina and S. Musil, *Anal. Chim. Acta*, 2017, **977**, 10–19.
- 55 J. Vyhnanovský, J. Kratzer, O. Benada, T. Matoušek, Z. Mester, R. E. Sturgeon, J. Dědina and S. Musil, *Anal. Chim. Acta*, 2018, **1005**, 16–26.
- 56 E. Nováková, K. Sembschová and S. Musil, *Spectrochim. Acta, Part B*, 2023, **202**, 106645.
- 57 E. Nováková, K. Horová, V. Červený, J. Hraníček and S. Musil, *J. Anal. At. Spectrom.*, 2020, **35**, 1380–1388.
- 58 S. Liu, X. Duan and J. Sun, *Anal. Sci.*, 2020, **36**, 419–423.
- 59 Z. Zhu, Q. Wu, Z. Liu, L. Liu, H. Zheng and S. Hu, *Anal. Chem.*, 2013, **85**, 4150–4156.
- 60 R. Sun, G. Ma, X. Duan and J. Sun, *Spectrochim. Acta, Part B*, 2018, **141**, 22–27.
- 61 M. Nishijo, H. Nakagawa, Y. Suwazono, K. Nogawa and T. Kido, *BMJ Open*, 2017, **7**, e015694.
- 62 Commission Regulation (EU) 2021/1323 Regulation (EC) No 1881/2006 as regards maximum levels of cadmium in certain foodstuffs.
- 63 G. C. L. Araújo, M. H. Gonzalez, A. G. Ferreira, A. R. A. Nogueira and J. A. Nóbrega, *Spectrochim. Acta, Part B*, 2002, **57**, 2121–2132.